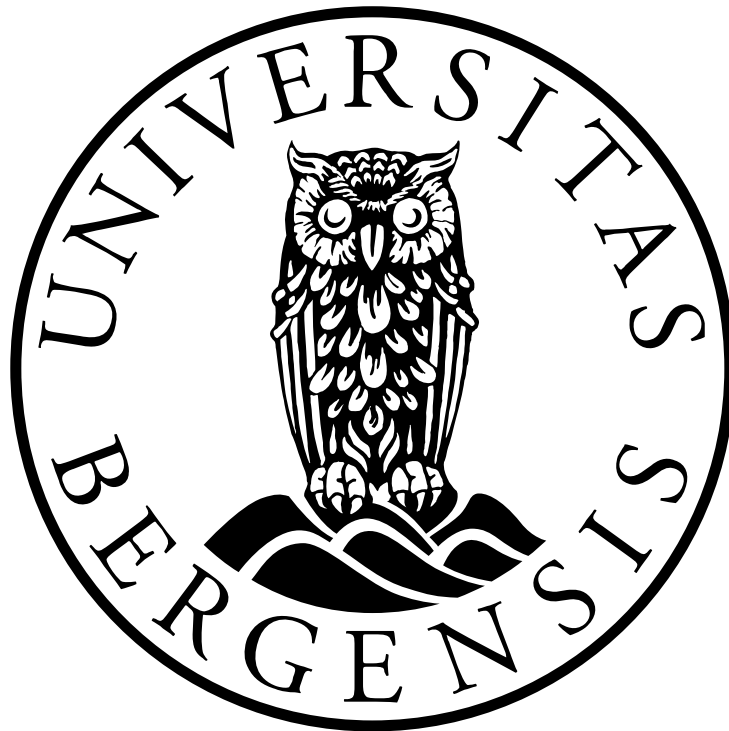


Controls on architecture and seismic imaging of
igneous intrusions: Examples from LIDAR outcrop data
on Traill Ø (East Greenland) and seismic data from the
conjugate Møre Margin

Malin Flesland



Master Thesis in Petroleum Geoscience

Department of Earth Science

University of Bergen

June 2017

Acknowledgement

First and foremost, I wish to express my sincere gratitude to my supervisor, Christian Haug Eide for all the feedback and the great help and guidance during the last two years. A special thanks to my co-supervisor Isabelle Lecomte for helping me with the seismic modelling and teaching me SeisRoX.

Thanks to NORSAR for the use of academic license to the program SeisRoX. The SAFARI group is thanked for the use of the outcrop data at Traill Ø, and the Centre for Integrated Petroleum Research (Uni Research CIPR) for providing the LIME software. I would also like to thank Tore Aadland for the python script and Kari Ringdal for help with converting images.

To my friends and family, thank you for the love and support during the work of this thesis. Especially I would like to thank Alexander for being there for me and always being supportive and encouraging.

Malin Flesland

Bergen, June 2016

Abstract

Intrusion of sills into sedimentary successions is a fundamental and widespread process in basins at volcanic rifted margins. Although intrusions emplaced at shallow paleodepths (<1.5 km) are relatively well understood, intrusions emplaced at deeper basinal levels (>1.5 km) are much less understood due to lack of large-scale outcrops and limitation in seismic illumination and resolution. This study makes an attempt to improve the understanding of emplacement mechanisms of deeply emplaced intrusions and how these are controlled by host rock structure and stratigraphy, by using a 25 km long digital outcrop LIDAR model from exceptionally well-exposed outcrops at Traill Ø, East Greenland. This is a world-class outcrop, exposing thick sill intrusions (up to 200 m) emplaced in a complex host rock with faults and variable stratigraphy. Traill Ø shares much of its history with the conjugate Møre Margin on the Norwegian continental shelf, and therefore provides an excellent analogue for understanding igneous sills seen in seismic data from the Møre Basin. Synthetic seismic is compared to seismic data from the Møre Margin to fill the gap between field observations and seismic data. Results show that the emplacement of deeply emplaced sill intrusions (c. 3-4 km) is controlled by host rock lithology, pre-existing structures and the strength of the host rock. Sills show brittle emplacement structures with little deformation around the sill margins despite the intrusions of large amount of sills into the host rock. Sill intrusions seems to prefer extensive mudstone units, thinly interbedded mudstone and sandstone and carbonate/evaporite units. Comparison between outcrop data, synthetic seismic and seismic data can improve the understanding of deeply emplaced sill complexes in the subsurface. Thin sills and steeply dipping intrusions are commonly not imaged in seismic, leading to underestimation of the volume of sills in basins. This study demonstrates the importance of host rock lithology, pre-existing structures and basin history, in order to predict emplacement mechanisms and expression in seismic data of deeply emplaced sill intrusions. Furthermore, it contributes to the understanding of deep sill complexes in sedimentary basins on volcanic margins worldwide.

Contents

Acknowledgement	I
Abstract	III
1 Introduction	1
2 Geological history	5
2.1 Tectonic history of the region	5
2.2 Sedimentological history	10
2.3 Igneous history	15
3 Theoretical background	17
3.1 General emplacement mechanisms for sills.....	17
3.2 Emplacement models.....	19
3.2.1 Linear Elastic Fracture Mechanism (LEFM)-Splitting Model.....	19
3.2.2 LEFM Barenblatt Cohesive Zone Model	19
3.2.3 Brittle and ductile faulting models	19
3.2.4 Fluidization Model.....	20
3.2.5 Viscous Indenter Model.....	20
4 Data and methods	21
4.1 LIDAR data	21
4.1.1 Interpretation of LIDAR data	22
4.2 Seismic modelling	27
4.2.1 Seismic modelling workflow: From outcrop model to seismic model	31
4.3 Seismic data and interpretation	35
5 Results	39
5.1 Virtual outcrop model	39
5.1.1 Large scale structures.....	39
5.1.2 Architecture and large scale intrusive geometries and relationship.....	42
5.2 Interpretation of seismic data	54
5.2.1 Stratigraphy and structural elements.....	55
5.2.2 Sill intrusions: geometry and expression in seismic data	57
5.3 Seismic modelling	60
5.3.1 Frequency	60
5.3.2 Maximum dip angle.....	63
5.3.3 Layered model	65
6 Discussion	69
6.1 Stratigraphic controls on sill emplacement.....	69
6.1.1 Emplacement model	69

6.1.2	Broken bridge deformation during large vertical inflation	70
6.1.3	Emplacement mechanism and preferred intervals	72
6.1.4	Connectivity of sill complexes	75
6.1.5	Effect of pre-magmatic faults on primary intrusive geometry.....	76
6.2	Comparison between outcrop and modelled seismic.....	78
6.3	Comparison between seismic modelling and real seismic	80
6.3.1	Resolution and detectability of sill intrusions	83
7	Conclusions and further work	85
7.1	Conclusions	85
7.2	Further work.....	86
	References	87

1 Introduction

Magmatic intrusions are common at rifted margins and in extensional basins (Magee et al. 2016). The magmatism is often associated with rifting and continental break up, often in the presence of large igneous provinces (Skogseid et al. 1992, Larsen et al. 2014), but it can also be associated with large igneous provinces away from rift zones (Bryan and Ferrari 2013).

Intrusive igneous systems in rifted margins are often a network of interconnected complexes that can cover large vertical and lateral distances (Cartwright and Hansen 2006, Magee et al. 2016). Sill complexes commonly form in mafic systems where magma flows easily, while intrusive in granitic systems are more viscous and more commonly form laccoliths and plutons (Bryan and Ferrari 2013). Studies of igneous intrusion in 3D seismic reflection data have shown that these interconnected sill networks, play a major role in transporting magma through the crust (Cartwright and Hansen 2006, Holford et al. 2013, Schofield et al. 2015), implying that existing models of vertically stacked systems are potentially oversimplified. Consequently, igneous intrusions in sedimentary successions can present a risk to hydrocarbon exploration, but can also be beneficial to hydrocarbon systems under some circumstances (e.g. Senger et al. in press). Magmatic sills may act as potential pathways for hydrocarbon migration, act as conducts, lead to compartmentalization of petroleum systems and influence reservoir properties (Holford et al. 2013, Schofield et al. 2015). Igneous intrusions are also important water reservoirs and barriers several places, e.g. in the arid Karoo Basin in South Africa (Chevallier and Woodford 1999), and they can be an important factor in CO₂ sequestration and underground repositories as they can act as barriers for CO₂ reservoirs and aquifers (Senger et al. 2013).

Interpretation of 3D seismic data and fieldwork have led to a good understanding of relatively shallow emplaced intrusions (<1,5km) (Cartwright and Hansen 2006, Hansen and Cartwright 2006, Schofield et al. 2015). These shallow intrusions have a saucer shaped geometry, and are easy to observe and image in seismic, because of the high impedance contrast between the sediments and the sills (Cartwright and Hansen 2006). As a consequence, shallow igneous intrusions are commonly seen as high amplitude reflections in the seismic (Magee et al. 2015).

However, sill intrusions that are emplaced at deeper depths (>1,5km), which have a more planar geometry, are generally much less understood than shallow intrusions.

There are several reasons for why deep intrusions are less understood than shallow intrusions. Lack of data is one of the problems. Only a few well exposed, large-scale outcrops that are comparable in scale to seismic datasets, have been studied (Hutton 2009, Eide et al. 2017). They are also challenging to study due to the inaccessibility of currently active subsurface systems, and general lack of exposures of ancient systems at the Earth's surface (Magee et al. 2016). Another reason is that deep intrusions are sometimes hard to image in seismic, because of the limitation in seismic resolution. They are often poorly imaged, since much of the energy can be reflected back from overlying shallower intrusions and lava flows. Comparison between seismic and well data has shown that a large proportion of sills in a basin are not identified from seismic data, because they are thinner than the seismic detectability. Even though each one of these unimagined intrusions may be thin, their total volume is large and combined they can have a huge impact in sedimentary systems (Schofield et al. 2015).

The fact that these deep intrusions are so poorly understood both because of poor imaging in seismic and lack of data, can lead to problems for reservoir forecasting, mainly in the petroleum industry, but also for other application such as CO₂ storage (Senger et al. 2013). Studies have shown that these deep intrusions are quite common towards the base of some basins along the NE Atlantic, that are important for hydrocarbon exploration (Planke et al. 2000, Skogseid et al. 2000, Skogseid 2001, Schofield et al. 2015). It is therefore important to understand the distribution and connectivity of these complexes to reduce exploration risks in the petroleum industry.

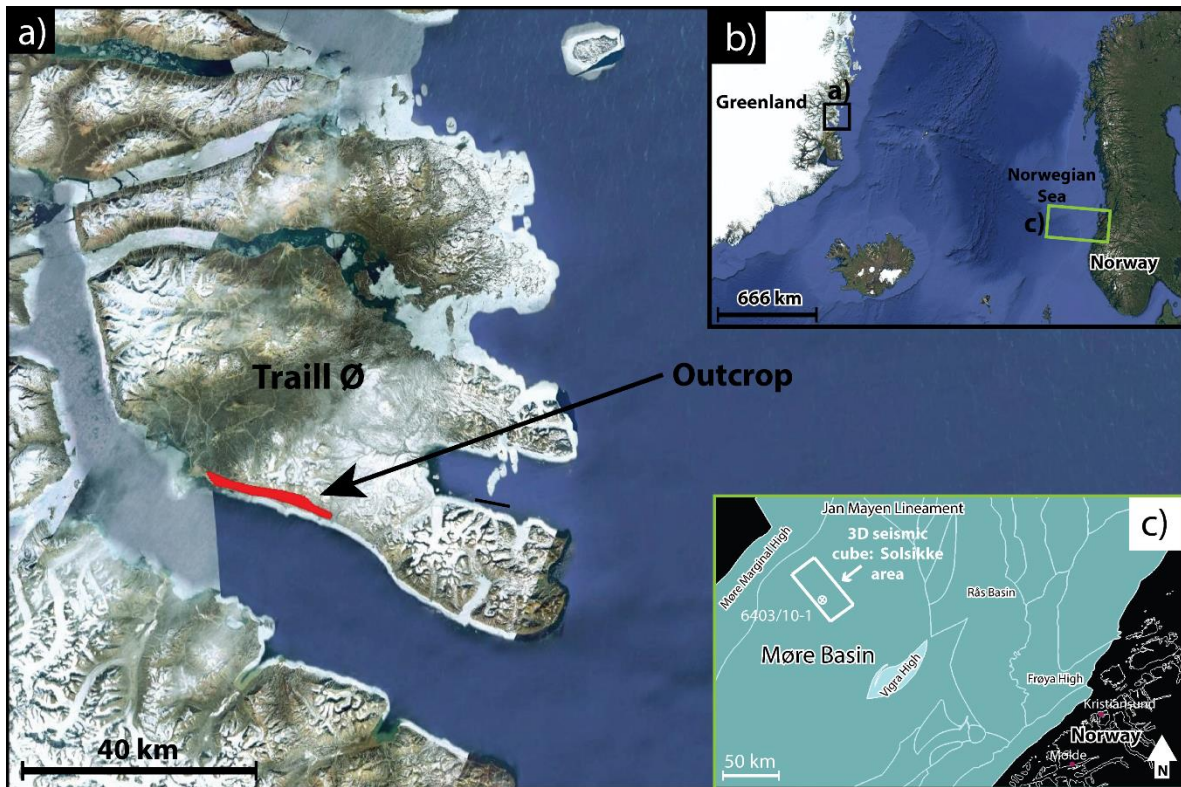


Figure 1.1: Maps of the study area. a) Map of Traill Ø and the outcrop at Svinhufvuds Bjerge shown in red. b) Overview of the NE Atlantic rift system and the conjugate margins. c) Overview of the Møre Basin and the 3D seismic dataset.

More studies are needed in both seismic and in the field to understand these intrusions better. Interpretation of deep intrusions in the field can be used as analogues for igneous sill intrusions in seismic. Using synthetic seismic modelling of intrusions in the field can offer insight that can be used to better understand these deep sills in seismic, and increase the understanding of interaction between igneous activity, sediments and faults in general.

In order to understand these deep intrusions better, this thesis presents the results of a 25 km long cliff section of intruded and faulted sedimentary rocks, located on the southwestern side of Traill Ø in East Greenland in the western part of the NE Atlantic Margin (Fig. 1.1a,b). The sill intrusions on Traill Ø are dolerites (Price et al. 1997), and they form large sill complexes in the study area. The Møre Margin in the Norwegian Sea (Fig. 1.1b,c) shares much of its history with the conjugate Traill Ø. Therefore, this outcrop on Traill Ø can be used as an analogue for the Møre Margin.

The aims of this thesis are: (1) to investigate large-scale architecture and controls on intrusions emplaced in a complex host rock with faults and variable stratigraphy in a world class outcrop

on the southwestern side of Traill Ø (East Greenland), (2) to use synthetic seismic modelling of the studied sill complex to investigate how thick (>100 m) sill complexes would be imaged in seismic data; and (3) compare the exposed intrusions on Traill Ø with equivalent intrusions from seismic data from the Møre Margin as an analogue to the Møre Basin.

2 Geological history

2.1 Tectonic history of the region

Since the Devonian and the collapse of the Caledonian orogeny, the NE Atlantic Rift System has experienced several rift events (Ziegler 1992, Surlyk 2003). The rifting culminated with the onset of seafloor spreading in the Norwegian-Greenland Sea around 55 million years ago (Price et al. 1997, Brekke and Nøttvedt 2000, Fig. 2.1c). The NE Atlantic region experienced a similar geological development, from the Caledonian orogeny and the breakup of Pangea in the Paleozoic, to the opening of the NE Atlantic Ocean in the Paleogene (Stoker et al. 2016). Before break up Traill Ø and East Greenland lay adjacent to the Norwegian Continental Shelf (Fig. 2.1a and b), however following the onset of seafloor spreading, the Norwegian and the Greenland Margin evolved separately (Price et al. 1997, Whitham and Price 1997).

The result of these pre-Paleogene rift events in East Greenland was west-dipping rotated fault blocks bounded by a series of east dipping normal faults with large displacement. In the studied area, the spacing between faults is around 5-30 km, and the maximum vertical throw up to several kilometers (Price et al. 1997, Whitham and Price 1997).

The formation of a series of north-south trending extensional basins, started during the Devonian along the Greenland-Norway Margin, after the collapse of the Caledonian orogeny (Surlyk 1990, Surlyk 2003). This basin initiation was a result of the first rift event in the Middle Devonian (Larsen and Bengaard 1991, Surlyk 2003). Since that time, the zone of major extension and subsidence in NE Greenland has migrated eastward in a stepwise manner (Schlindwein and Jokat 1999). The basin initiation in the Devonian was caused by extensional dip-slip faulting, and sinistral transpressional faulting, and was restricted to the west by the Fjord Region detachment (Larsen and Bengaard 1991). This rifting resulted in two major NNE-SSW trending normal faults that crops out in the inner fjord of East Greenland, west of Traill Ø. These faults separated N-S trending fault blocks around 90 km wide, and they had large displacements (Larsen and Bengaard 1991).

In the Late Devonian to Viséan (early Carboniferous) times, and during late Carboniferous, E-W extension occurred in East Greenland (Stemmerik et al. 1991). In the Traill Ø region,

Carboniferous strata have a low regional dip ($<20^\circ$) suggesting a low stretching factor for these rift events (Whitham and Price 1997). The next rift phase happened in Early Triassic, and is recognized by an increase in basement subsidence rate (Price et al. 1997). Several west-tilted half-grabens were formed in the Early Triassic in East Greenland, and a marine seaway was situated between Greenland and Norway (Ziegler 1992, Stoker et al. 2016).

The next rift phase is the rifting between Middle Jurassic (Bajocian) and Late Cretaceous (Valanginian) (Price et al. 1997, Whitham et al. 1999). On Traill Ø, the start of this rift event is recognized by increased basement subsidence. The fault evolution in this period can be divided into two stages. The first stage is characterized by Middle and Upper Jurassic sediments thickening towards the west towards the Månedal Fault on Traill Ø (Fig. 2.2). The thickening of the sediments had a greater extent than present-day fault spacing. This means that the extension happened on wider fault blocks than seen today (Price et al. 1997). The second stage of fault evolution in this period, happened in Early Cretaceous, and is characterized by the development of new faults and narrower fault blocks than what is seen today. During this rift event, the major faults within the study area, *Mols Bjerge*, *Laplace Bjerge* and *Vælddal faults* (Fig. 2.2) were formed in the Traill Ø region, followed by erosion of Jurassic strata on their uplifted footwall crest. After this rift event, fault block crests in Traill Ø were buried by Cretaceous marine mudstone (Whitham and Price 1997). These Cretaceous sediments were deposited during thermal subsidence of the NE Atlantic rift system (Price et al. 1997).

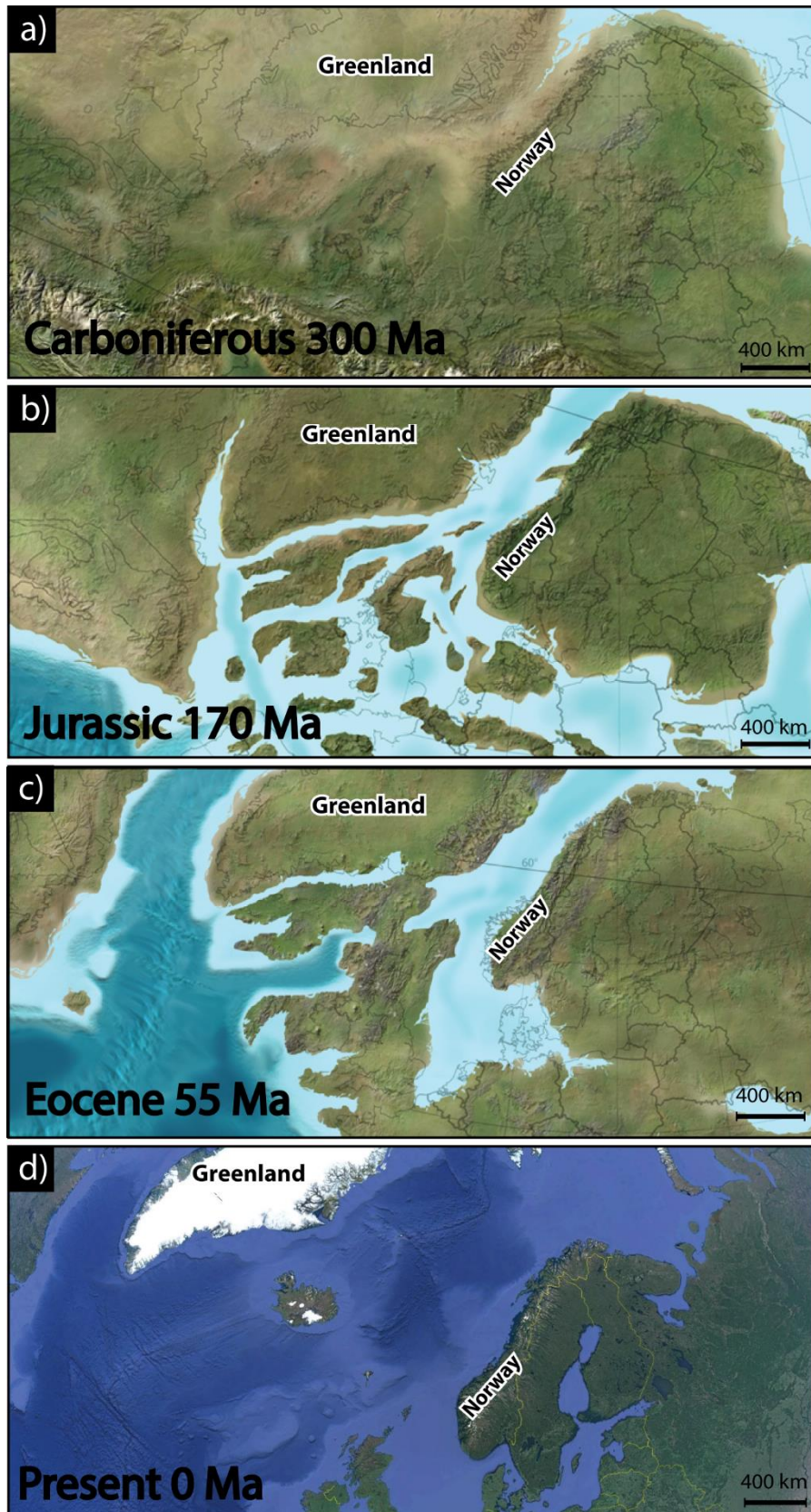


Figure 2.1: Paleogeographic map of the NE Atlantic during a) deposition of the Traill \emptyset Group, b) deposition of Jameson Land Group, c) main phase of rifting and emplacement of the Paleogene sill intrusions. d) Present-day setting. Modified from (Blakey 2012).

The most important phase of rifting in relation to structures and sedimentology in East Greenland, seen by normal faults and fault block rotation, was the rifting during the Cenozoic. The reason is that most of the faulting and fault block rotation in Traill Ø was a result of Paleogene rifting. Two periods of rifting happened in the Traill Ø region during the Cenozoic (Price et al. 1997). The first period of rifting may have been initiated in the latest Cretaceous as seen from the conjugate Norwegian Continental Shelf (Skogseid et al. 1992), and the rift event eventually led to development of oceanic crust. This rift phase is associated with voluminous igneous activity (Larsen et al. 1989, Brooks et al. 2011), which is treated in detail in Section 2.3 of this thesis. In Traill Ø, Cenozoic pre-breakup fault displacement was mostly shared between two faults, and therefore the stretching was accommodated on the two bounding faults of a 10 km wide fault block (Price et al. 1997).

The second rift event during the Paleogene was related to the westward shift of the spreading ridge, from the now extinct Ægir Ridge to the presently active Kolbeinsey Ridge (Talwani and Eldholm 1977, Mjelde et al. 2008). This resulted in the separation of the Jan Mayen microcontinent from the East Greenland Margin around 36 Ma (Price et al. 1997, Larsen et al. 2014).

This second Paleogene rift event was mostly associated with internal breakup of existing fault blocks in the Traill Ø region. In addition to new faults forming, almost all preexisting faults in this region were reactivated, indicated by the displacement of post-Cretaceous igneous intrusions. The post-magmatic extension led to internal break up of fault blocks, and the fault displacement was more evenly distributed between faults (Price et al. 1997). Extension in the Paleogene was greater in the crust east of the Månedal Faults (Fig. 2.2), relative to the region to the west (Parsons et al. 2017).

Uplift of the East Greenland Margin during the Cenozoic resulted in exhumation of deeply buried Mesozoic and Paleozoic stratigraphy. In the Traill Ø region, the amount of exhumation is 1.5-3.0 km from the Miocene to the present, and it increased towards the west (Price et al. 1997, Thomson et al. 1999).

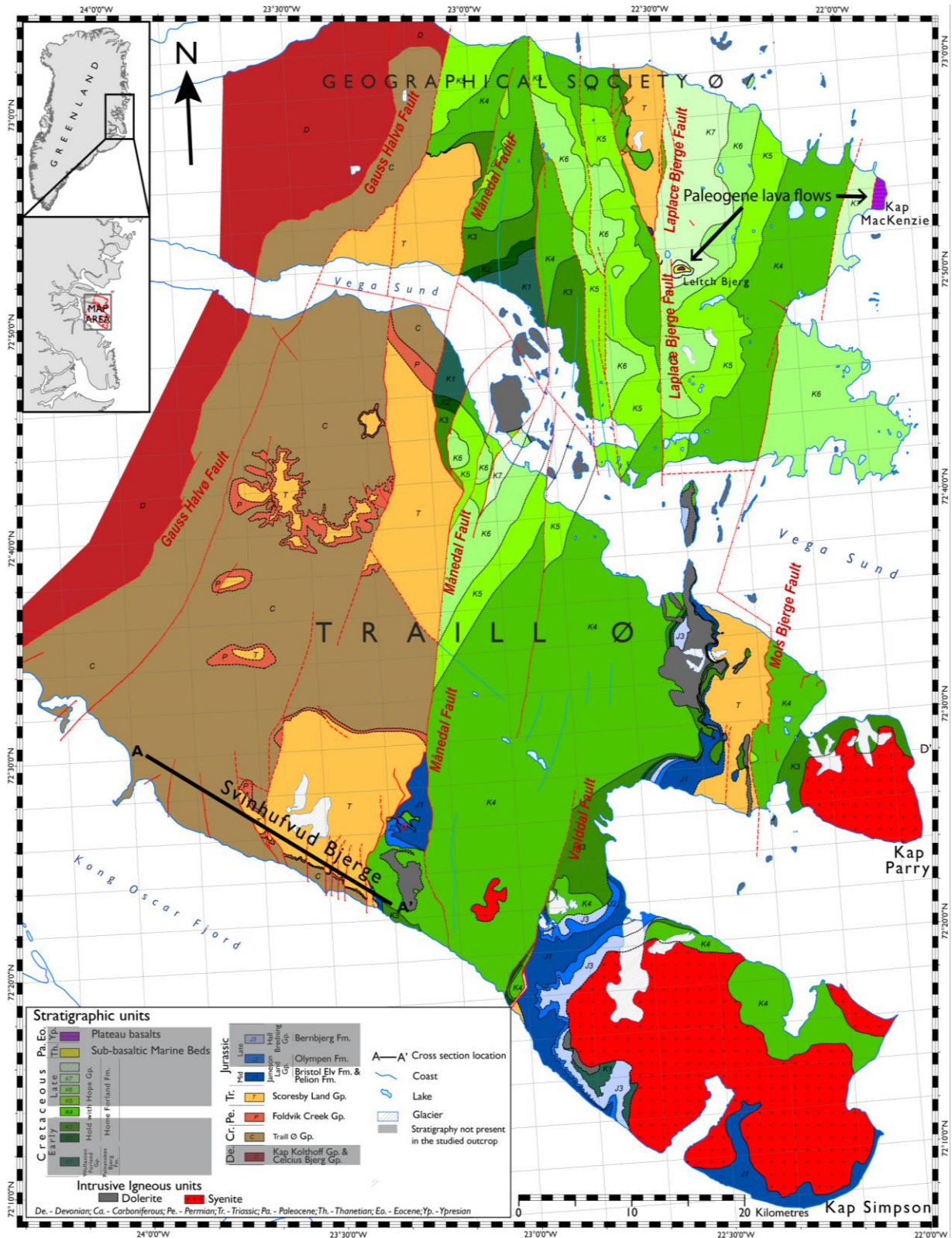


Figure 2.2: Geological map of Traill Ø. Modified from Parson et al. (2017). Location of studied outcrop is located at the profile A-A'.

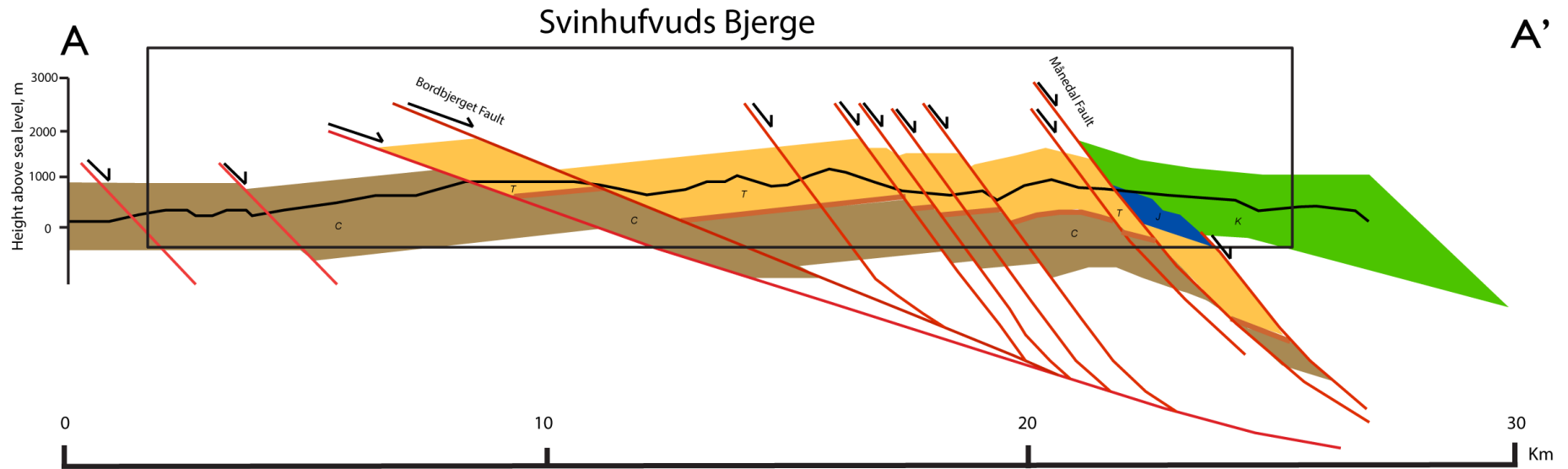
Three regional phases of post-breakup uplift and exhumation of Eastern Greenland have shaped the present-day topography (Japsen et al. 2014, Parsons et al. 2017). Post-breakup

subsidence and burial continued until the Eocene-Oligocene transition, and a major phase of uplift affected the margins along the NE Atlantic at this time. Apatite fission-track data from East Greenland also reveal a cooling event that started between 40 and 30 Ma (Thomson et al. 1999). This event is believed to be contemporaneous with the alkalic magmatic event (Thomson et al. 1999), which is further described in Section 2.3. Apatite fission track analyses suggest that the next phase of exhumation and uplift began in Late Miocene around 10 Ma (Thomson et al. 1999, Japsen et al. 2014). The last phase of uplift and exhumation started in the Early Pliocene around 5 Ma (Japsen et al. 2014). This event is widespread throughout the NE Atlantic region (Thomson et al. 1999, Japsen et al. 2014), and this cooling event is believed to be caused by the extinction of the spreading axis in the Labrador Sea, resulting in changes in the North Atlantic spreading direction and plate stress regimes (Thomson et al. 1999).

2.2 Sedimentological history

Traill Ø comprises a near complete record of Devonian to Late Cretaceous sediments (Whitham and Price 1997, Parsons et al. 2017, see Stratigraphic column Fig. 2.4). The rocks in the studied outcrop interval were deposited during the Carboniferous to the Cretaceous (Figs. 2.3 and 2.4). The stratigraphic record of Carboniferous to Eocene rocks preserved in the East Greenland Margin is one of the most important sources and analogues to understand the record within offshore basins on East Greenland and the Norwegian continental shelf (Surlyk 1990, Whitham et al. 1999).

Devonian strata are found in the western part of Traill Ø (Whitham and Price 1997), and is not a part of the studied outcrop (Fig. 2.2). This unit consists of continental deposits (Surlyk 1990, Fig. 2.4). Devonian continental deposits continued into the Carboniferous, with the deposition of the Traill Ø Group (Vigran et al. 1999, Fig. 2.1a). The Traill Ø Group mainly consists of sandstone, interbedded with mudstones and coals, deposited in a fluvial and lacustrine environment (Surlyk 1990, Fig. 2.4).



Scale 1:100,000








- | | | | | |
|-------------------|---|---|--|--------------|
| Cretaceous (K) |  | Hold with Hope Gp. |  | Normal fault |
| Jurassic (J) | Mid  | Jameson Land Gp.
Bristol Elv Fm. &
Pelion Fm. |  | Outcrop |
| Triassic (T) |  | Scoresby Land Gp. | | |
| Permian |  | Foldvik Creek Gp. | | |
| Carboniferous (C) |  | Traill Ø Gp. | | |

Figure 2.3: Geological cross section of the southwestern coast of Traill Ø showing stratigraphy and fault block geometry. See Fig. 2.2 for location. Modified from Parson et al. (2017).

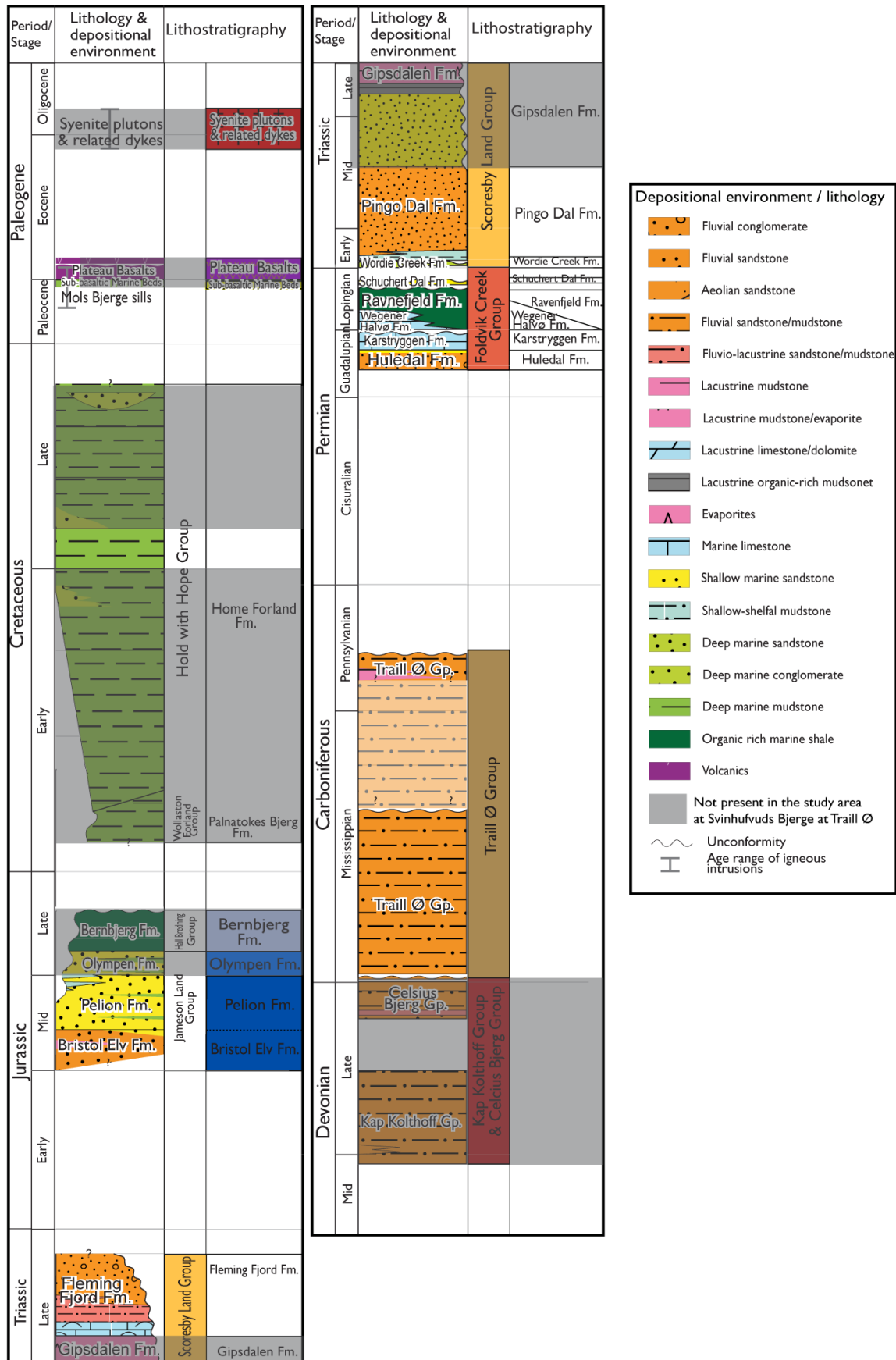


Figure 2.4: Stratigraphy in Traill Ø. Grey areas represent stratigraphy which is not present in the studied outcrop, but is present at Traill Ø. Modified from Parson et al. (2017).

The Carboniferous-Permian boundary is marked by a regionally extensive unconformity. This unconformity was caused by uplift and erosion of rift blocks in Late Carboniferous-Early Permian before deposition of Late Permian strata on top of this angular unconformity (Surlyk 1990). The structural setting during the Permian-Triassic period was a N-S trending rift basin along the NE Greenland Margin (Stoker et al. 2016). Permian record shows an overall development from fluvial deposits, followed by shallow marine, platform evaporites, basinal evaporites, carbonate and marine mudstone deposits of the Foldvik Creek Group (Surlyk 1990, Fig. 2.4).

Conglomerate, sandstone and mudstone of the Permian Huledal Formation were deposited by alluvial fans passing into fluvial braidplains and intermontane lakes, and they represent the initial phase of subsidence by thermal contraction after a long period of extension (Surlyk 1990). A major regional transgression took place in Middle-Upper Permian in East Greenland at the end of the deposition of Huledal Formation, and resulted in the formation of a shallow marine hypersaline deposits. These deposits are a part of the Karstryggen Formation (Surlyk 1990). Towards the top of the Permian sequence is the deposits consists of the largely contemporaneous carbonates and source rock prone interval of organic rich shale of the Wegener Halvø and Ravnefjeld Formations (Christiansen et al. 1993). The last deposits in Permian represent siliciclastic basin fill of the Schuchert Dal Formation, which was deposited during relative sea level fall, where subsidence could not keep up with the sediment supply (Surlyk 1990).

A major sea level fall during the Upper Permian marked the transition into the Triassic. In Traill Ø, Triassic deposits are dominated by marginal marine sediments and continental deposits of the Scoresby Land Group (Stoker et al. 2016). In the Early Triassic, the Permian succession was eroded along the basin margin, and the sea rapidly retreated over the Permian basin, leaving behind a thick succession of shallow marine deposits of the Wordie Creek Formation (Parsons et al. 2017). This Lower Triassic sequence is up to 1 km thick on Traill Ø, and consists of sandstone, conglomerates, shales and some minor carbonates. After the Early Triassic, the marine basin filled in, and the rest of the Triassic deposits are mostly characterized by continental deposits (Surlyk 1990, Stoker et al. 2016).

Table 2-1: Stratigraphy of Jurassic strata in the Traill Ø area. Only mid-Jurassic strata are present in the studied outcrop.

Jurassic strata

Group	Formation	Age	Lithology	Environment	Reference
Jameson Land Gp.	Bristol Elv Fm.	Mid-Jurassic	Sandstone, thin shales and coals	Braided rivers	Therkelsen and Surlyk (2004)
	Pelion Fm.		Sandstone and thin shales	Shallow marine	Parson et al. (2017)
	Olympen Fm.	Late - Jurassic	Sandstone	Shallow marine	Alsen and Surlyk (2004)
Hall Bredning Gp.	Bernbjerg Fm.		Micaceous organic rich shale with thin sandstone laminae	Anoxic and low energy shelf	Surlyk (1990), Stroger et al. (2005)

The lower boundary of the Jurassic is an erosional unconformity against the Triassic in the Traill Ø area (Stoker et al. 2016). The Middle-Upper Jurassic succession consists mainly of sandstone from the Jameson Land Group (Table 2-1), which represent a major northwestwards expansion of shallow marine facies (Parsons et al. 2017). The Bernbjerg Formation is poorly preserved in Traill Ø, and absent in the studied outcrop, because of the Middle Cretaceous unconformity (Surlyk 2003, Vosgerau et al. 2004, see Table 2-1 for detailed description of each formation).

Today Jurassic strata are exposed as scattered outcrops onshore along the East Greenland Margin (Fig. 2.2). The scattered outcrops are a result of deposition in the crest of partly eroded tilted fault blocks (see cross section Fig. 2.3), leading to wedge shape geometries of exposed units. Along the studied outcrop, Jurassic strata are exposed on the eastern side of the Svinhufvuds Bjerger on the hanging wall of the Månedal Fault. In this location, only the Pelion Formation and the Bristol Elv Formation are present (Whitham and Price 1997, Therkelsen 2016). Interestingly, sandstone of the Pelion Formation forms the reservoir rock of the exhumed hydrocarbon trap which is exposed in Svinhufvuds Bjerger within the study area (Whitham and Price 1997).

The Cretaceous succession is exposed on top of the Jurassic strata along the eastern part of the studied outcrop in Traill Ø, and the Månedal Fault forms the western limit of preserved Cretaceous deposits (Parsons et al. 2017, Figs. 2.2 and 2.3). Deposits of Cretaceous age occur along a system of narrow fault blocks. The succession is dominated by dark-grey marine silt and mudstones with intervals of coarse-clastic deep-water deposits, possibly related to rift related fault events, footwall uplift and erosion. On Traill Ø, this succession is up to about 2

km thick (Surlyk and Noe-Nygaard 2001).

In addition to these sedimentary rocks, Cenozoic igneous rocks are abundant in the Traill Ø area. These are described in Section 2.3 (Igneous history).

2.3 Igneous history

Continental breakup of the Northeast Atlantic led to extensive magmatism along 2000 km of the rifted margin (Brooks 2011). Along the East Greenland and Norwegian Margin, the plate started to separate during the Early Eocene, and resulted in extensive Paleogene igneous rocks (Brooks 2011).

There are two main periods of magmatism related to the continental break up in the NE Atlantic during the Paleogene, with ages of c. 62-58 Ma and c. 57-53 Ma (Hansen et al. 2009, Brooks 2011). Both of these magmatic periods are often implied to relate to the arrival of the Icelandic plume, and the main phase of rifting and continental breakup (Hansen et al. 2009, Larsen et al. 2014). The magmatism on Traill Ø corresponds to the second period (Price et al. 1997).

Around the time of break up, the NE Greenland Margin was located immediately west of the Norwegian Margin (Fig. 2.1c). Early Eocene magmatism in NE Greenland and in the Møre/Vøring Margin had a close spatial relationship (Upton et al. 1995), and there is an early Eocene igneous complex that link these two margins together during the early stage of seafloor spreading (Skogseid et al. 1992, Olesen et al. 2007).

Following the onset of seafloor spreading, the margins evolved separately. On the Norwegian Continental Margin, magmatism ceased, and went into compression (Price et al. 1997), while on East Greenland magmatism continued into Early Oligocene times (Upton et al. 1995, Price et al. 1997).

Magmatism on Traill Ø can be divided into two periods, one at c. 54 Ma and another at c. 36 Ma, based on dated specimens (Price et al. 1997, Larsen et al. 2014). Each of these periods is related to one of the periods of Paleogene rifting, described in Section 2.1 above. The first of

these periods happened in Early Eocene and gave rise to a large amount of tholeiitic sills and dykes (Upton et al. 1995, Price et al. 1997). A large number of Paleogene tholeiitic dykes and sills are intruded into the Late Paleozoic to Mesozoic succession on Traill Ø (Price et al. 1997). On Traill Ø, the average section intruded by igneous rock is about 1 km thick, and sill intrusions are quite common and some reach thicknesses of up to 200 meters (Price et al. 1997, Larsen et al. 2014).

The second period of magmatism was related to the formation of syenite plutons, and more alkaline basaltic intrusions (Price et al. 1997). Two of these large syenite complexes are exposed at Kap Parry and at Kap Simpson in the Eastern Traill Ø (Price et al. 1997, Fig. 2.2). No intrusives of this period have been documented to occur within the section studied in this work (Parsons et al. 2017). This event is dated to be of Late Eocene- Early Oligocene age (c. 35 Ma), which coincides with the separation of the Jan Mayen microcontinent from the East Greenland Margin (Price et al. 1997).

Igneous rocks in Traill Ø are part of a larger igneous province in East Greenland. Tholeiitic intrusions crop out in the entire area around Traill Ø. In addition to intrusions, large amount of flood basalts are found in the East Greenland area (Brooks 2011), and seaward dipping-reflectors are imaged on regional seismic lines (Berger and Jokat 2008). Up to 2 km thick flood basalts overflowed the East Greenland Margin during the Paleogene (Larsen and Marcussen 1992). Uplift and erosion have led to preservation of these Early Paleogene lava successions in Hold with Hope, Wollaston Foreland and South of Scoresby Sund (Larsen and Marcussen 1992, Hald and Tegner 2000). No lava is present in Jameson land and Traill Ø, but plateau basalts are found on Geographical Society Ø at Kap MacKenzie and Leitch Bjerg (Parsons et al. 2017, Fig. 2.2), and sills and dykes are quite abundant in all areas. Dating of the tholeiitic sills on Traill Ø, support the fact that they were intruded at the same time as the thick basaltic lavas were extruded elsewhere (Larsen et al. 2014).

3 Theoretical background

3.1 General emplacement mechanisms for sills

Host rock lithology has an important influence on the emplacement of sill intrusions into sedimentary successions. This results in a link between emplacement mechanisms and intrusion morphology (Schofield et al. 2012b, Eide et al. 2017, Fig. 3.1). An important control in respect to emplacement mechanism is the strength of the host rock at the time of intrusion and the ability to act brittle or non-brittle during intrusion. This brittle or non-brittle emplacement mechanism will be controlled to a large degree by the burial diagenesis and the cementation history of the host rock prior to the intrusion of magma (Schofield et al. 2012b). These two different emplacement mechanisms lead to distinctly different structures developing during magma intrusion, and these structures can in some cases be used to understand the magma flow direction (Schofield et al. 2012b).

Steps and bridges (Fig. 3.1a, b) are emplacement structures associated with brittle emplacement. Steps form from slightly offset or *en echelon* segmented intrusion tips that later coalesce as one sheet (Rickwood 1990, Fig. 3.1b). The offsets between the segments are preserved as steps on sill margins and each segment is therefore parallel to the direction of magma flow (Rickwood 1990, Schofield et al. 2012b). Bridges form when two separate overlapping sills propagate along horizons with slight offsets. Further inflation of the sills will bend the host rock strata between the sills, and create a structure called a bridge (Hutton 2009, Schofield et al. 2012b). On the outer bend of these bridges, tensile cross fractures may develop perpendicular to the bridge. If inflation of the sills continue the tensile stress will increase, and cross fractures may breach the bridge linking the two sills, creating a broken bridge (Hutton 2009, Schofield et al. 2012a, Fig. 3.1b). Bridges and broken bridges seen in cross sections indicate that magma flow direction was perpendicular to the outcrop (Hutton 2009).

Non-brittle/ductile propagation of magma leads to formation of magma fingers and magma lobes (Fig. 3.1c). These structures will often occur in host rock with low mechanical strength and cohesion. Magma emplacement in these cases leads to the development of a viscous-viscous interface between host rocks causing the magma to create magma fingers (Pollard

1973, Schofield et al. 2012b). Intrusion into poorly consolidated sediment can form a zone of incoherent and clast like mixture of sediment and igneous rock called 'peperite' (Fig. 3.1d,e), as a result of dynamic interaction between sediments and magma (Skilling et al. 2002). If several small-scale magma fingers coalescing, magma lobes can be constructed. The term lobe is often more used in seismic as lobes often are observed in seismic (Schofield et al. 2015).

The final intrusion morphology can be used to understand the magma emplacement mechanism and host rock properties during intrusion (Schofield et al. 2012b). Figure 3.1 shows brittle and non-brittle magma emplacement structures and their features.

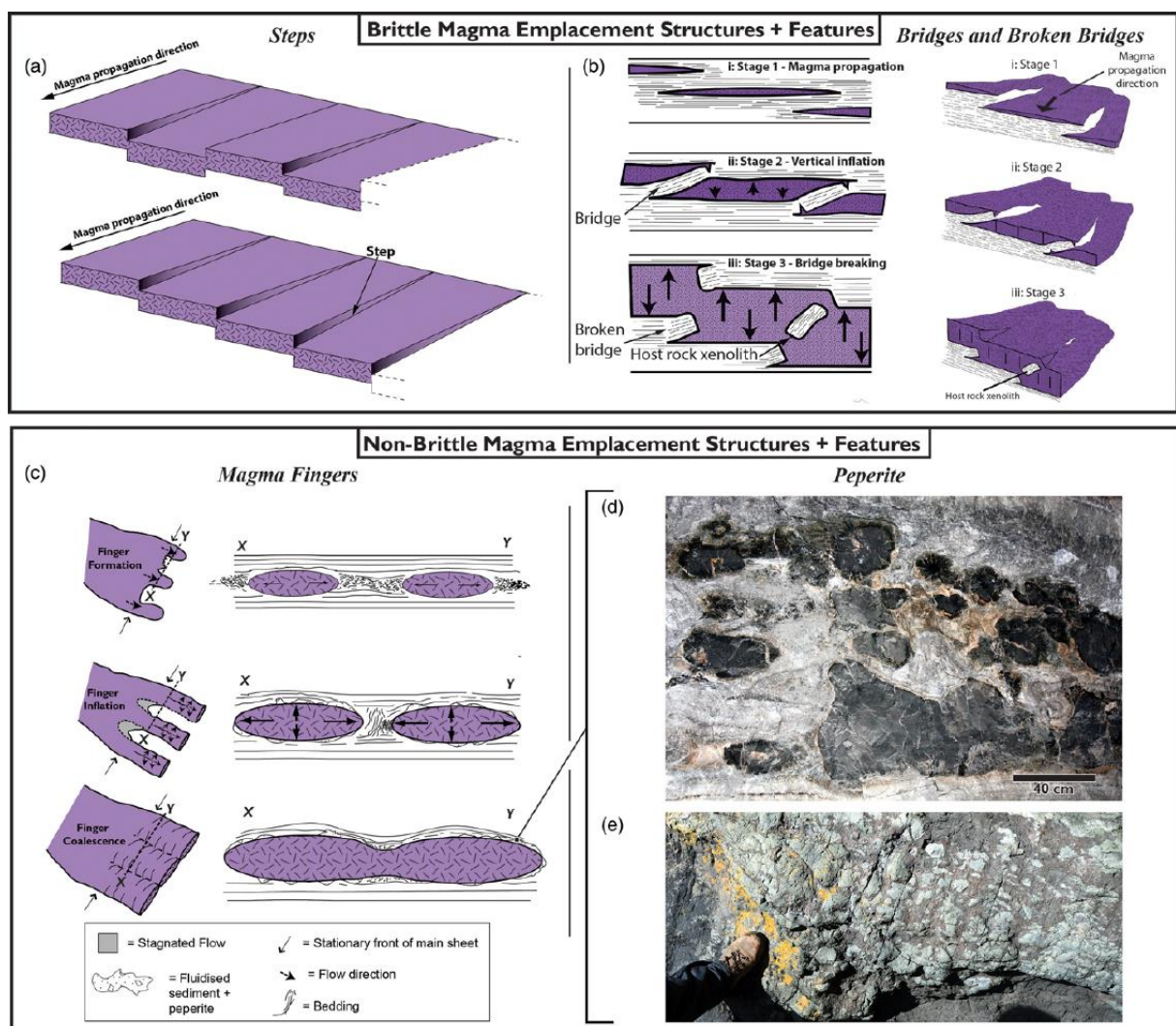


Figure 3.1: Overview of brittle a,b) and non-brittle c-e) emplacement structures and their features. From Eide et al. (2017). a) Steps on sill margin and how these relate to magma propagation direction. b) Development of broken bridges. c) Development of magma fingers. d, e) Example of peperite.

3.2 Emplacement models

Emplacement mechanisms of sill intrusions are still poorly understood, and a large range of various models exists. It is clear from the underlying assumptions that some models are more applicable in certain cases and in certain host rocks than others. These models are summarized briefly here and in Figure 3.2:

3.2.1 Linear Elastic Fracture Mechanism (LEFM)-Splitting Model

The LEFM-Splitting Model is the most commonly accepted model. It assumes that the host rock behaves purely elastic, and sills propagate by tensile fracturing of the surrounding rock (Fig. 3.2a) (Pollard 1973). This model is normally used for modelling of sheet intrusions (e.g. Kavanagh et al. 2013), and the displaced host rocks show little deformation ahead of the fracture tip.

3.2.2 LEFM Barenblatt Cohesive Zone Model

Rubin (1993) suggested that the LEFM-Splitting Model was too simplistic, and proposed a cohesive plastic zone at the intrusion tip. In this model, the intrusions will also propagate by tensile fracturing of the host rock, however suction induced by the tip cavity will lead to compression, and the host rock is expected to be pulled into the sill tip (Fig. 3.2b).

3.2.3 Brittle and ductile faulting models

Sill intrusions are known to commonly follow host rocks of certain lithologies, such as mudstone (Pollard et al. 1975, Thomson 2007, Schofield et al. 2010, Magee et al. 2014). Mudstones are easily deformed in an inelastic manner, which indicate that the LEFM models cannot explain these type of emplacement mechanisms. These emplacement mechanisms are better explained by inelastic deformation of the host rock.

Pollard (1973) came up with two models explaining the propagation of the magma, brittle or ductile faulting (Fig. 3.2c,d). The propagation of magma can lead to faulting ahead of the intrusion tip, and these faults will accommodate the compression of the propagating magma. The main difference between these models is that brittle faulting has a 30° shear plane, and the ductile has a 45° shear plane (Pollard 1973).

3.2.4 Fluidization Model

Propagation of magma can also be accommodated by fluidization of host rock (Schofield et al. 2010, Schofield et al. 2012b). As magma is emplaced into the host rock, it heats up the surrounding rock. This can lead to boiling of the pore fluids and the resulting pressure build-up in the rock, can trigger fluidization (Schofield et al. 2010, Fig 3.2e). This model can produce magma fingers and the so-called ‘perperite’ explained in Section 3.1 (Schofield et al. 2012b, Fig. 3.1d,e).

3.2.5 Viscous Indenter Model

The magma viscosity also plays a major role during magma emplacement, and magma propagation can form complex systems. In this model, the viscous shear stresses near the magma tip are higher than the host rock strength (Galland et al. 2014). This result in magma pushing rock ahead of the sill tip like an indenter with a blunt or rectangular tip (Abdelmalak et al. 2012, Fig. 3.2f).

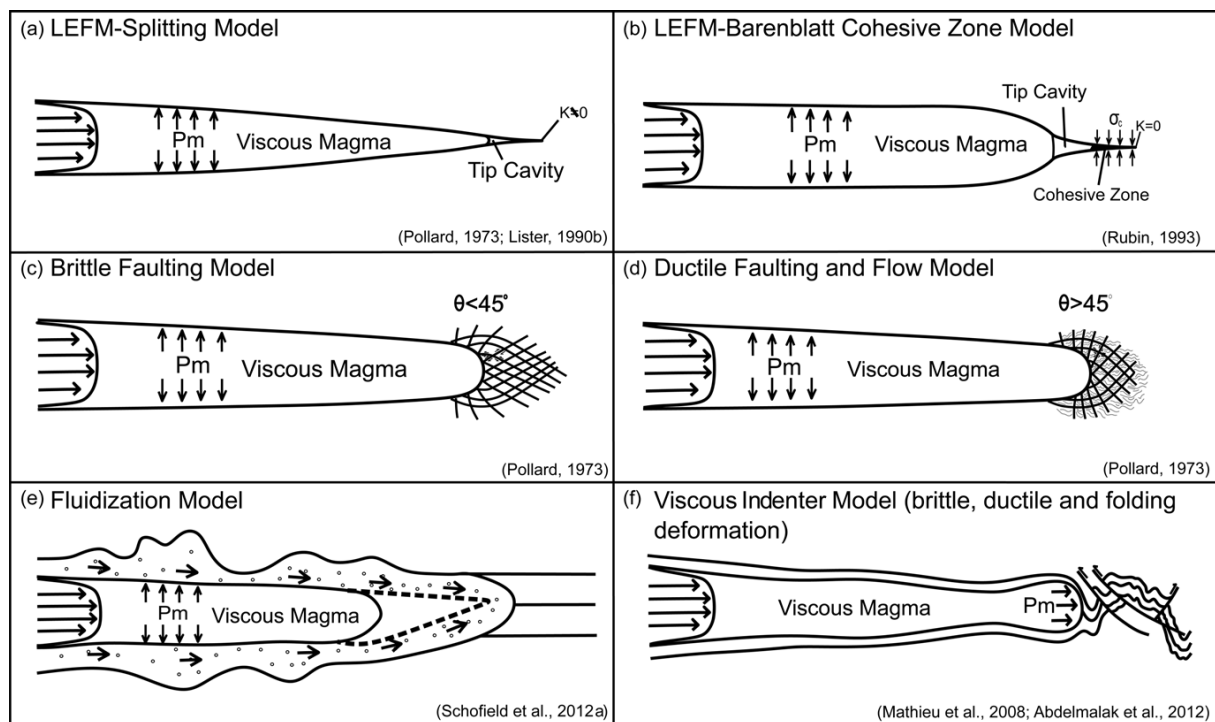


Figure 3.2: Sill emplacement models. P_m is the overpressure in the magma pushing on the sills. Elastic models: a) LEFM -Splitting Model and b) LEFM-Barenblatt Cohesive Zone Model. Inelastic models: c) and d) Brittle and Ductile Faulting Model, e) Fluidization Model and f) Viscous Indenter Model. From Spacapan et al. (2016).

4 Data and methods

In this chapter, the data and the methods used in this thesis will be presented. This includes digital LIDAR outcrop data from East Greenland (4.1), which was used for large-scale interpretation and study of the relationships between stratigraphy, faults and igneous intrusions. This LIDAR model is the basis for the seismic modelling, which will be presented in Section 4.2. Digital outcrop models allow for detailed interpretation of sub-seismic geometries and structural relationships. The use of synthetic seismic modelling illuminates what can and cannot be imaged in offshore seismic data. Comparing synthetic seismic to intrusions imaged in actual seismic data from the Møre Margin (Section 4.3) can inform seismic interpreters to create more confident interpretations and improve our understanding of sills observed in seismic data. The use of synthetic seismograms obtained from outcrop observations also provide valuable insight into the limitations of reflection seismic data, particularly illumination and resolution, and interpretation issues related to these limitations.

4.1 LIDAR data

The study area is located on the southwestern coast of Traill Ø in East Greenland (Fig. 1.1a). The area is called Svinhufvuds Bjerge, and the dataset consists of a 25 km long and 1 km thick, high-resolution virtual outcrop model (Fig. 4.1) acquired using oblique helicopter-mounted laser scanning, also known as LIDAR scanning. LIDAR data can be an easy and time efficient method for obtaining outcrop data, and it can be an useful tool for studying large-scale architecture and geometries. LIDAR (light detection and ranging) uses laser light to measure distances (Buckley et al. 2008). A laser is a very stable beam of light, which results in low divergence over long ranges. Laser travels at the speed of light, which means that large amount of measurements can be taken in a short period. Because of this rapid data acquisition, it is possible to cover large areas and high cliffs in a short period of time (Buckley et al. 2008).



Figure 4.1: LIDAR virtual outcrop model from Svinhufvuds Bjerge at Traill Ø, East Greenland. The entire outcrop is 25 km long and 1 km high.

Data collection was conducted using methods described by Buckley et al. (2008). The data were acquired using a laser scanner combined with a digital medium-format camera. Using a flying data acquisition platform is a great advantage as it provides good coverage of the outcrop as it can maneuver and can be positioned where images can be taken orthogonally to the outcrop, resulting in a detailed outcrop model (Buckley et al. 2013).

The LIDAR scanner collects a large number of 3D data points from the outcrop. Each of these points corresponds to a measurement of the shape of the outcrop, and the entire cloud of such points record the shape of the entire study area. The point-cloud is later processed into a 3D model of the outcrop. Digital images are also captured in the field at the same time as the laser scanning, and these images have been used to texture the 3D model. This yields a photorealistic 3D model of the outcrop, which has been used to interpret sedimentary, structural and igneous features. The distance from the helicopter to the outcrop during data acquisition was c. 350 m, resulting in a point spacing of 50 cm and a pixel resolution in the finished models of 7 cm.

4.1.1 Interpretation of LIDAR data

The interpretation was done by visually inspecting features in the LIDAR outcrop model focusing on intrusions, emplacement structures, sedimentary beds and structural elements such as faults. The software LIME was used to do this interpretation.

The magmatic intrusions are seen as dark brown bodies in the outcrop. The strong color contrast between the intrusions and the stratigraphy makes them relatively easy to recognize (Fig. 4.2). However, there are some difficulties in places where the LIDAR model has limited resolution or in areas where the intrusions are covered by scree. In order to improve the

interpretation in some of these areas where the resolution is low, the unprocessed images taken of the outcrop during the data acquisition have been used to pick the intrusions margins more confidently, as these have slightly higher resolution.

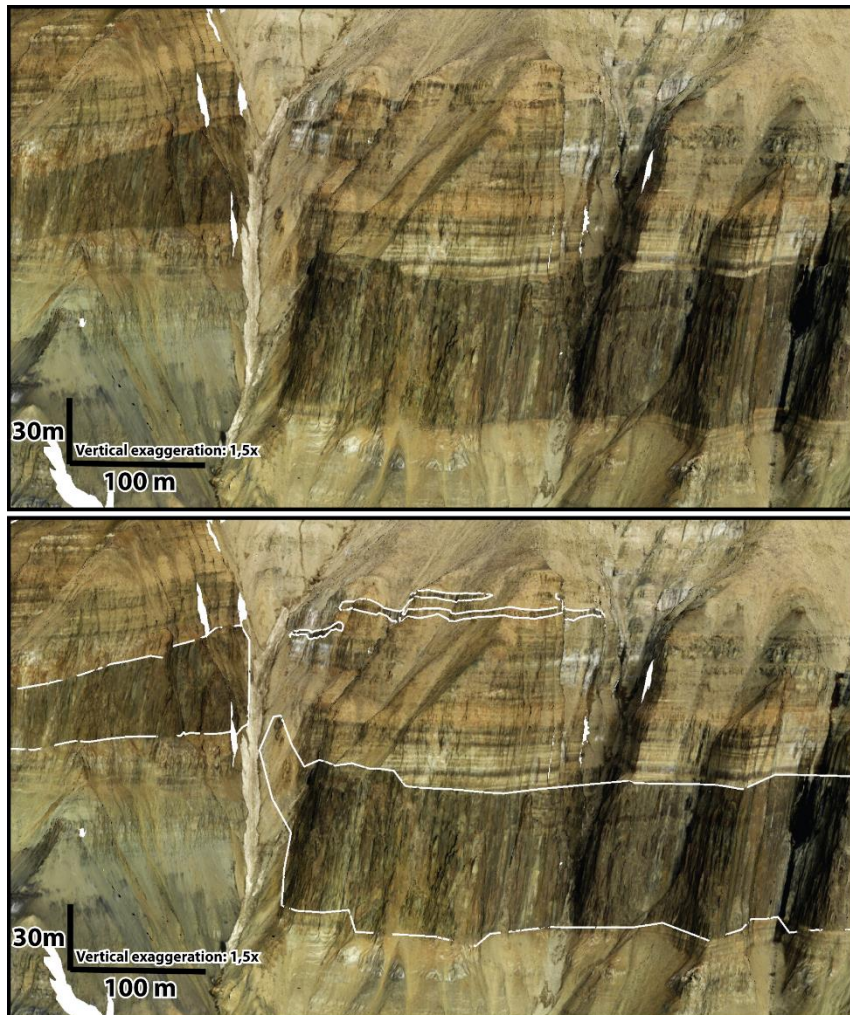


Figure 4.2: Interpretation of intrusions (outlined). Strong color contrast between the dark brown intrusions and the stratigraphy makes the intrusions easy to interpret.

The stratigraphy of the outcrop includes sedimentary succession from the Carboniferous to the Cretaceous. Some of the boundaries between these units have been difficult to define confidently because sedimentary logs from the outcrop have not been available to me during the study, and because no fieldwork was conducted as part of this thesis work. Comparison to previous work has therefore been critical in order to reliably define the stratigraphy (Table 4-1).

The stratigraphy of the area is complex, and consists of several relatively thin units. For this study, the stratigraphy has been grouped into seven units, which can be confidently

recognized across the entire outcrop (Table 2-1). In the outcrop, the base of the upper Permian succession is an angular unconformity with the underlying Carboniferous Traill \emptyset Group (Parsons et al. 2017). In some exceptionally well-exposed locations, this angular unconformity is obvious (Fig. 4.3). In the LIDAR data, the Permian succession, which consists of the Foldvik Creek Group, two units have been interpreted: The first consists of the Huledal Fm (sandstone and conglomerate), Karstryggen Fm (evaporites, carbonates and mudstone) and the Wegener Halv \emptyset Fm (carbonates), and the second unit is the Ravnefjeld Formation (organic rich shale). The boundaries between all of the Permian units are hard to correlate throughout the outcrop, however at some places you can observe the contacts (Fig. 4.3).

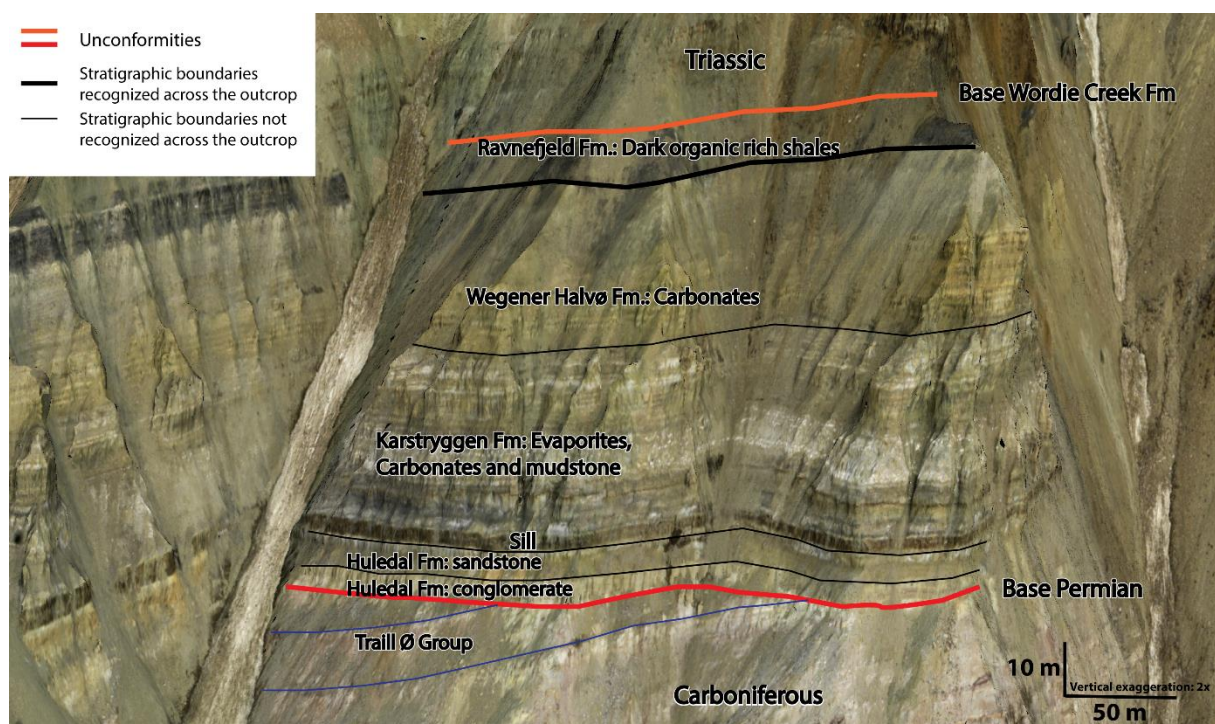


Figure 4.3: Showing detailed interpretation of the Permian Foldvik Creek Group. In the LIDAR data, the Permian succession has been interpreted as two units. Notice that the Carboniferous succession has been interpreted as one unit.

In Traill \emptyset , the Triassic succession is almost entirely made up of the Wordie Creek Formation (Bjerager et al. 2006). However, the Pingo Dal Formation and the Fleming Fjord Formation are also present, but they have been interpreted as one unit since they show similar lithologies. In addition, it is difficult to pick the boundaries between these units across the outcrop. However, red colored strata indicate Triassic Pingo Dal Formation on the left side of the fault (Månedal Fault in Fig. 4.4), while red colored strata at the right side of the fault is interpreted as the Fleming Fjord Formation (Therkelsen and Surlyk 2004).

Table 4-1: Interpreted units along the outcrop.

Interpreted unit	Age	Nature in literature	Defining characteristics used to interpret (base)	Any particular issues	Figure showing interpretation	Key references
Traill Ø Group	Carboniferous	Coarse to medium grained sandstone, interbedded with minor mudstone and coals	Base Carboniferous is not seen along the outcrop		Figure 4.3	Parson et al. 2017
Foldvik Creek Group: Huledal Fm., Karstryggen Fm., Wegener Halvø Fm.	Upper Permian	Conglomerates, sandstones, carbonates and evaporites (gypsum)	Angular unconformity with underlying Traill Ø Gp. Picked under the resistant Huledal conglomerate layer	Correlation of the different formations within this group is challenging	Figure 4.3	Bugge et al. 2002
Foldvik Creek Group: Ravnefjeld Fm.	Upper Permian	Black organic rich shale	Color change to black		Figure 4.3	Bugge et al. 2002 Christiansen et al. 1993
Scoresby Land Group: Wordie Creek Fm./Pingo Dal Fm./Fleming Fjord Fm.	Early Triassic	Gray-green mudstones and sandstone overlain by red mudstone and sandstone	Picked at Ravnefjeld Fm. upper boundary		Figure 4.4	Bjeranger et al. 2006 Parson et al. 2017
Jameson Land Group: Bristol Elv Fm.	Mid Jurassic	Yellow /whitish sandstone with a few mudstone layers	Slight colour change from the underlying Triassic deposits	Difficult to pick base Jurassic	Figure 4.4	Therkelsen 2016
Jameson Land Group: Pelion Fm	Mid Jurassic	Yellow homogenous sandstone	Contrast between sandstone with mudstone layers and homogenous sandstone	Difficult to see transition from Bristol Elv to Pelion Fm.	Figure 4.4	Therkelsen 2016
Hold with Hope Group	Late Cretaceous	Dark mudstone	Color contrast between Cretaceous mudstone and light Jurassic sandstone		Figure 4.4	Parson et al. 2017

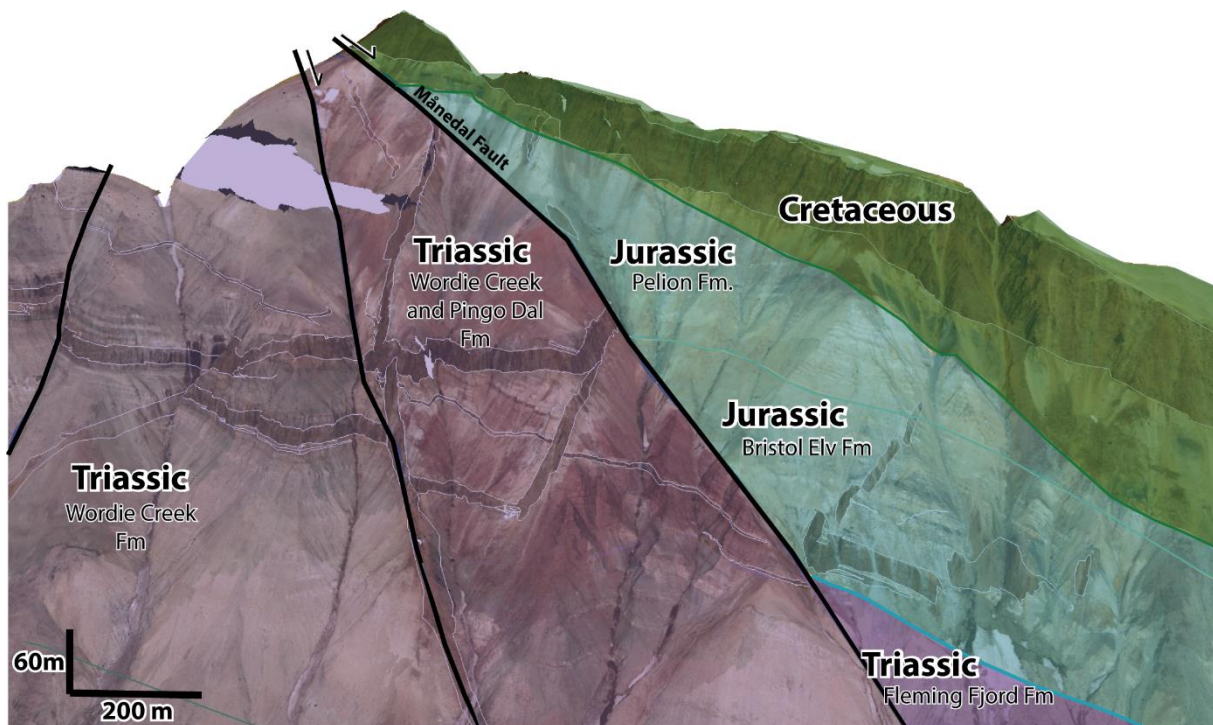


Figure 4.4: Interpretation of Triassic, Jurassic and Cretaceous strata. In the LIDAR data, the Triassic succession has been interpreted as one unit as it is hard to pick the boundaries between the Wordie Creek Formation and Pingo Dal Formation.

The basal contact of the Cretaceous is an angular unconformity (Parsons et al. 2017). The angularity of this contact is not evident in the outcrop data, but the boundary is interpreted at an upwards color change from yellow sandstone to dark mudstone.

Faults have been interpreted where there either is an offset in the stratigraphy or in the intrusions. Most intrusions have been cut by faults, and only a small number are not.

The final interpretation of the LIDAR outcrop was exported as an image file and then made into a geological model. The model consists of a number of colors, where different colors represent intrusions and different stratigraphic units. For detailed description, see Section 4.2.1.

4.2 Seismic modelling

Seismic modelling is a necessity to understand wave propagation in the subsurface, and modelling can guide geological interpretation of real seismic data. In addition, digital outcrop models with large amount of details can lead to more realistic geological models, and these models can thus be used to do more adequate seismic modelling, in order to get insight into complex geometry in real seismic data (Lecomte et al. 2016).

Seismic modelling can be done in a number of ways, including full-wavefield methods like finite-difference modelling, and ray-based approaches such as 1D convolution and 2D convolution (Lecomte et al. 2015). These methods vary in their complexity and their accuracy. A 2D ray-based convolution modelling has been chosen here because it provides suitable results with a method that is sufficiently easy to use. Another advantage is that the method may be run within a short enough timeframe (Lecomte et al. 2016) considering the scope of work that must be done in this thesis.

The selected 2D ray-based convolution method simulates pre-stack depth migrated (PSDM) seismic sections. This method builds a filter function in the wavenumber domain (PSDM filter), which is equivalent to a point spread function (PSF) in the space domain, i.e., PSF and PSDM filters are related by the Fourier Transform. The PSF is actually the response of a point scatterer through seismic imaging and corresponds to the convolution operator applied to the input geological model in the 2D convolution modelling (Lecomte et al. 2003). This method provides cost-effective modelling for geological interpretations, and gives more reliable results than the standard 1D convolution method geologist tends to depend on when more advanced modelling is not affordable (Lecomte 2008, Lecomte et al. 2015, Magee et al. 2015).

In 1D convolution modelling, each seismic trace of a section is generated individually by convolving the vertical reflectivity log with a given wavelet. The method is used to generate post-stack time-migrated seismic sections by gathering each modelled trace side by side. This gives a good estimate of the vertical resolution and is extensively used to study, e.g., tuning effects at wedges. However, the concept derives from a very simple geological model, i.e., homogenous horizontal layers, and no lateral resolution effect from seismic imaging or lack of illumination is accounted for. This method is therefore too simplistic to aid interpretation of

complex geological models, such as igneous intrusions, which exhibits extremely complex architectures. On the contrary, the 2D ray-based convolution derived from a PSDM imaging approach takes also into account lateral resolution and illumination effects.

Theoretically, the vertical resolution is defined as a quarter wavelength, $\lambda/4$, and defines the tuning thickness (Herron 2011, Simm et al. 2014). Lateral resolution is defined by the Fresnel zone, which is defined by constructive interference over an area along the wavefront and is larger than $\lambda/2$ (Fig. 4.5). However, seismic migration collapses this zone to a lateral resolution of $\lambda/2$ in standard imaging (Herron 2011, Simm et al. 2014), and in an ideal case, lateral resolution should be $\lambda/4$ (perfect illumination). In the 2D convolution modelling, the PSF shows us numerically how a diffraction points appear after (PSDM) migration. As even reflectors can be decomposed into dense set of point scatterers (Huygens' principle), the PSF provides a tool for analyzing both resolution and illumination issues, as will be discussed in the following section.

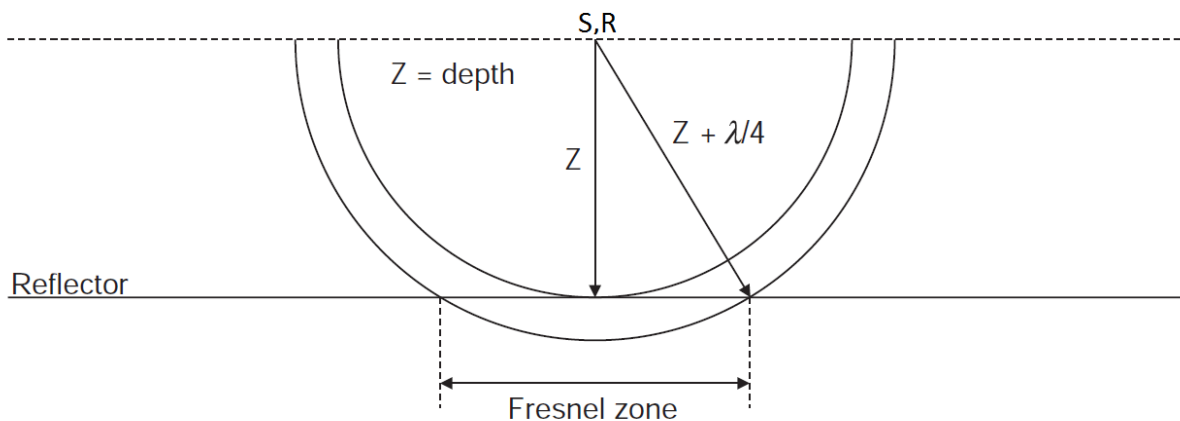


Figure 4.5: Illustration of the Fresnel zone. The Fresnel zone is defined by constructive interference over an area along the wavefront. Modified from Herron (2011).

Figure 4.6 illustrates the key elements of the modelling process, which is described in detail in Lecomte (2008). The first step is to calculate the illumination vector I_{SR} at a given reference point in the target (Fig. 4.6a). This vector is the difference between two slowness vectors (inverse of velocity) P_S (from a shot S) and P_R (towards a receiver R) at the reference point (Fig. 4.6b). Ray tracing in a background velocity model down to the reference point (Fig. 4.6a) gives P_S and P_R . Their length is proportional to the slowness at the reference point and their orientation depends on ray bending in the velocity model.

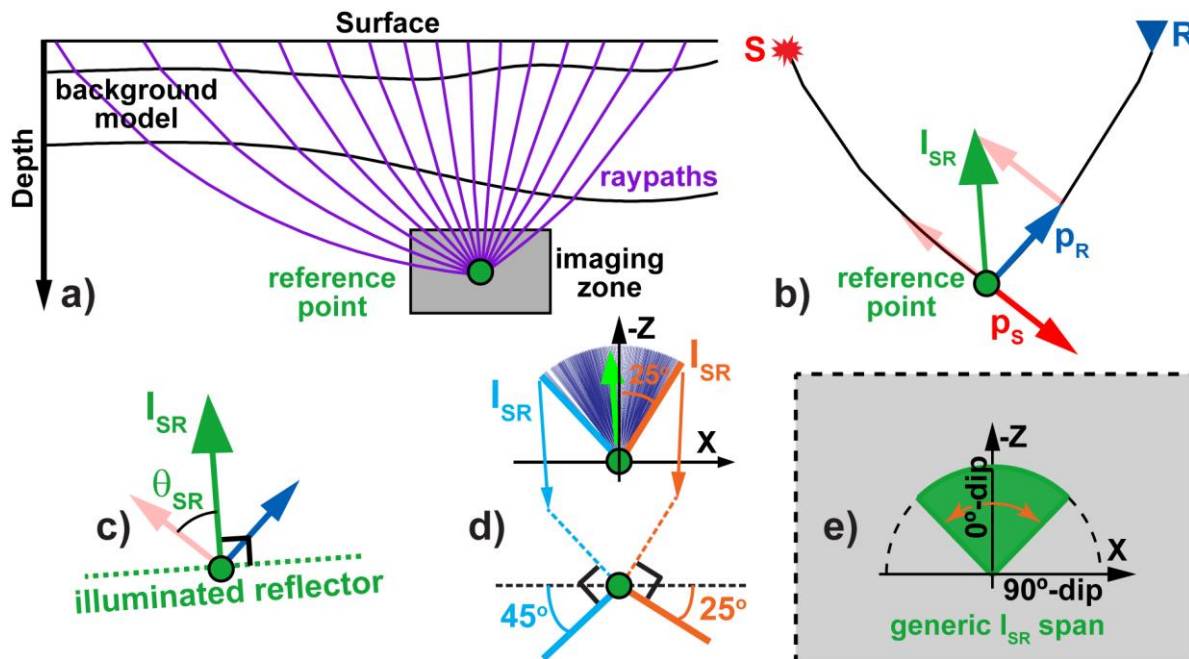


Figure 4.6: a) Raypaths towards a reference point. Background model are used to calculate I_{SR} b) The illumination vector (I_{SR}), calculated from the slowness vectors P_R, P_S . c) I_{SR} shows one illuminated reflector. θ_{SR} is the incident angle. d) A I_{SR} span with a range of different illuminated reflector dips. e) Unknown background model: use a generic I_{SR} span. From Lecomte et al. (2016).

I_{SR} is characterized by its length and orientation, but the length is not only defined as a function of velocity (V), due to the length of P_S and P_R , but also by the opening angle between the 2 slowness vectors (opening angle = $2 \times \theta_{SR}$ in Fig. 4.6c). The larger the velocity V , the shorter I_{SR} is. Similarly, the wider the angle θ_{SR} , the shorter I_{SR} is. Note that θ_{SR} increases with the offset (distance) between S and R , so a large offset means a short I_{SR} . The orientation of I_{SR} results from the combination of P_S and P_R (Lecomte et al. 2016). Both length and orientation of I_{SR} are key controlling factors of the resolution and illumination effects in seismic imaging. In particular, the orientation of I_{SR} indicates which reflector dips can be illuminated: reflectors in the vicinity of the reference point and perpendicular to I_{SR} will be seen as primary reflections for the considered (S, R) pair, this according to Snell's law; θ_{SR} (Fig. 4.6c) is the incident angle in that case.

Different set of (S, R) pairs from a given acquisition survey will give a span of I_{SR} at the reference point. The span will thus give us a range of reflector dips that can be illuminated nearby that point. The I_{SR} span of Figure 4.6d shows for instance that reflectors dipping more than 45° to the left or more than 25° to the right will not be imaged. If there is no available background velocity model and survey geometry, generic I_{SR} spans can be created by just

defining an average velocity (V), an incident angle (θ_{SR}) and the maximum reflector dip to illuminate (Fig. 4.6e). V and θ_{SR} will control the “height” of that span, while its “lateral opening” is controlled by the maximum reflector dip.

When the illumination vectors have been calculated, the next step is to generate scattering wavenumbers $K_{SR}(f)=f \cdot I_{SR}$, where f is frequency. Multiplying all the I_{SR} with the transmitted wavelet (given frequency spectrum) will generate PSDM filters in the wavenumber domain (Lecomte 2008). A Fourier Transform (FT) is applied to the PSDM filter to produce the PSF in the spatial domain. PSDM simulated images will be created by convolution between an input reflectivity model at the target and the PSF (Lecomte et al. 2015).

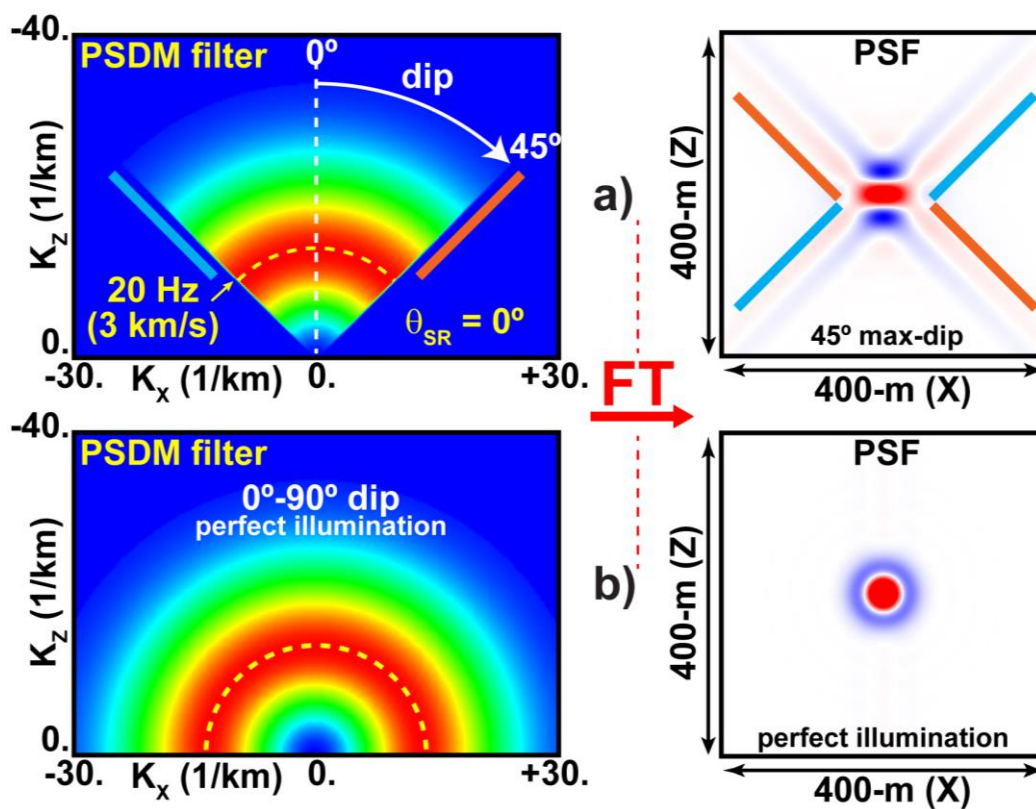


Figure 4.7: PSDM filter with corresponding PSF after Fourier-transformation of the PSDM filter for respectively a) PSDM filter with $V=3 \text{ km/s}$, $\theta_{SR}=0^\circ$, wavelet with $f=20 \text{ Hz}$ and max dip angle of $\pm 45^\circ$, and b) PSDM filter with perfect illumination ($\pm 90^\circ$). From Lecomte et al. (2016).

Figure 4.7a illustrates a generic frequency-dependent I_{SR} span with a symmetric maximum illuminated dip ($\pm 45^\circ$), a 20-Hz Ricker wavelet, an average velocity of 3 km/s and an incident angle of 0° . It is also possible to do modelling with perfect illumination (I_{SR} span $\pm 90^\circ$) (Fig. 4.7b). Both cases (Figs. 4.7a and b) will correspond to a vertical resolution of $\lambda/4$, while the

lateral resolution of Figure 4.7a will be $\lambda/2$ (as often quoted in literature), in opposition to the perfect case of Figure 4.7b with a lateral resolution of $\lambda/4$ (the PSF is a perfect sphere in the latter case).

In this thesis, neither a background velocity model nor detailed survey information are available. Therefore, only PSFs calculated from generic I_{SR} spans are used. By using these PSFs, it is however possible to investigate how illumination and resolution react to changes in parameters. The 2D convolution modelling is used to investigate how intrusions are imaged in PSDM seismic images by using interpretations from the virtual outcrop model. The process going from outcrop model to seismic modelling is described in detail in the next section.

4.2.1 Seismic modelling workflow: From outcrop model to seismic model

Interpretations of intrusions, faults and sedimentary units were transferred to the seismic modelling and modelled using the following five steps (Fig. 4.8):

1. Interpretations were projected onto a vertical section parallel to the outcrop. In this process, distortion of the interpretation can happen in areas where the outcrop is far from parallel to the vertical plane, for example in valleys. The outcrop is slightly bent, and in order to accurately reproduce the interpretation of the outcrop, three panels parallel to the outcrop have been used.
2. The projections of the geological interpretations in (1) were exported as three graphic files (PNG format), and each of the recognized stratigraphic units (later referred to as “blocks”), including the intrusions, were assigned a distinct color using a bitmap editing program. Resolution of 1 m horizontally and 40 cm vertically was chosen, as this faithfully reproduces the interpreted geometries, while yielding files that are small enough to be handled efficiently by the modelling method. The exported files had the following sizes in pixels: 12539x2750, 8312x2750 and 4047x2750. The first panel is mostly used for seismic modelling throughout this thesis.
3. The colored graphic files were turned into 8-bit greyscale graphic files where each stratigraphic unit corresponds to a single color value to ease the link between colors and block properties.
4. The graphic files were converted to a SEG-Y file (standard seismic format used by the

modelling software) using a python script, and then imported into the 2D convolution software. Each grey color from the model now corresponds to a specific stratigraphic unit (block) in the new target model. A total of 7 different blocks are defined and each block is assigned with homogeneous properties, i.e., constant values all across zones with same block index. In order to do the seismic modelling, each of these layers/blocks is assigned with different elastic-wave properties as required for seismic modelling.

5. Populating the target model with properties results in a reflectivity model of the outcrop. Convolution between the reflectivity model and the PSF results in PSDM seismic images.

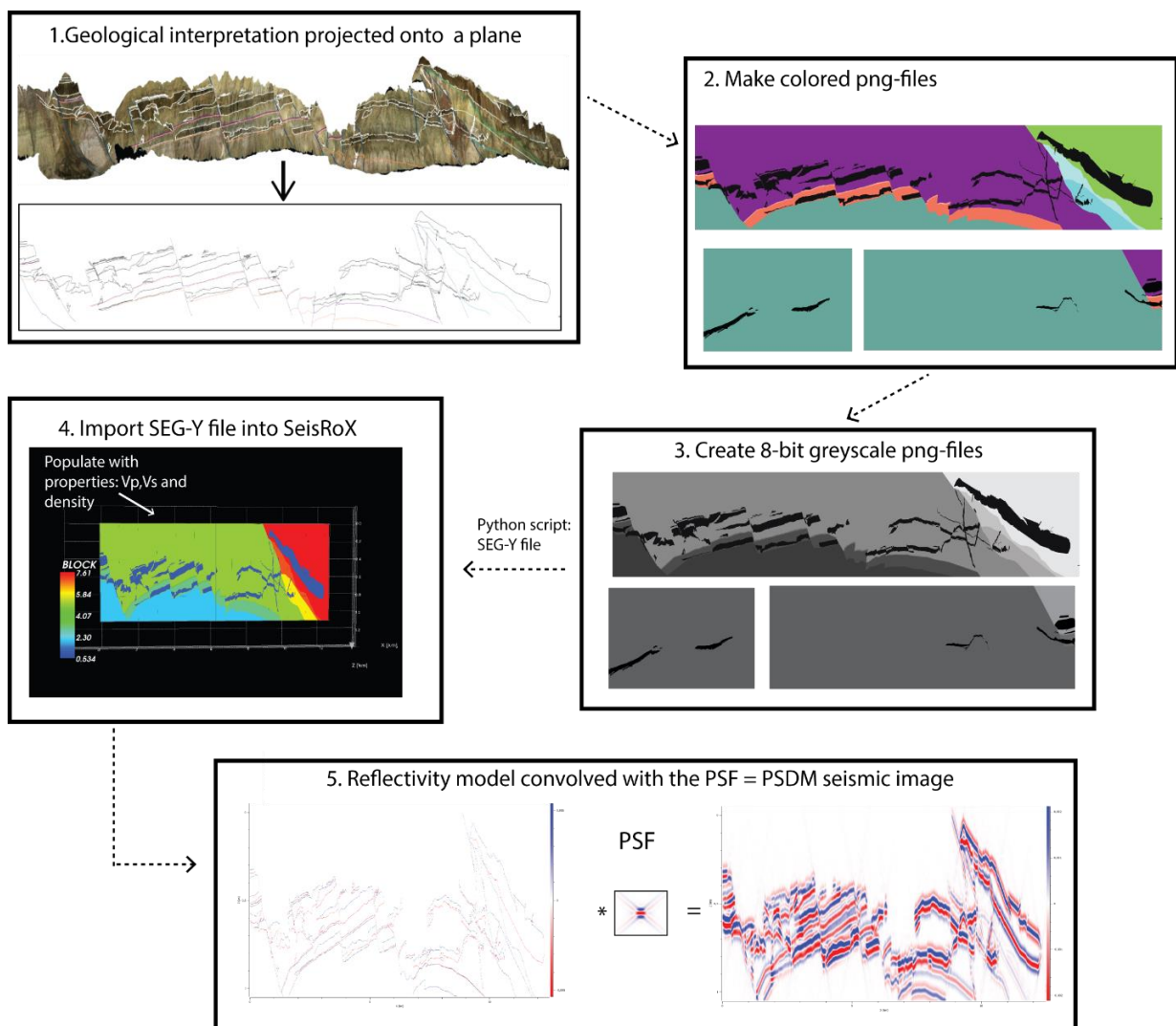


Figure 4.8: Seismic modelling workflow: showing steps from the interpretation of the LIDAR data to the resulting seismic modelling.

The elastic properties required in the 2D convolution modelling are P-wave velocity (V_p), S-wave velocity (V_s) and density (ρ). Values from the Norwegian Sea have been used in order to make the comparison between synthetic seismic data and real seismic data more reliable. The values are mostly found from stratigraphy that correspond to or are similar in composition to the stratigraphy in Trill Ø. The regional correlations presented by Stoker et al. (2016) have been used to identify equivalent stratigraphy across the North Atlantic. Cretaceous, Jurassic, Triassic and the Permian Foldvik Creek Group have all equivalents that are similar in composition and age in the Norwegian Sea (Table 4-2). However, the Permian Ravnefjeld Formation and the Carboniferous Trill Ø Group do not have any clear equivalents. The organic rich Spekk Fm from the Jurassic in the Norwegian Sea is similar to the Ravnefjeld Fm as both of them are organic rich mudstone, and values from this formation are used as input to the Ravnefjeld Formation. The Carboniferous Trill Ø Group corresponds to a braided river system. Since there are no similar drilled deposits of braided river systems in the Norwegian Sea, values from The Billefjorden Group from the Barents Sea have been used, since both the Trill Ø Group and the Billefjorden Group are of similar age (Carboniferous), and represent braided river systems dominated by sandstone, conglomeratic sandstone with interbedded beds of mudstone and coal. All the information are taken from well data at a depth of around 3 kilometer, if possible and present, since the purpose of this study is to image how deep intrusions behave at this depth.

Host rock V_p velocities used for the seismic modelling lie between 2,4 - 4,4 km/s (see Table 4-2 for more details). P-wave velocity for sills are set to 6,0 km/s, as the dolerite intrusions in East Greenland (Price et al. 1997) have values comparable to well-studied intrusions from West of Shetland by Smallwood et al. (2002). The rock density lie between 2,20 - 2,75 g/cm³ (Table 4-2). Sills have a higher density than the sedimentary host rock, 3,0 g/cm³ are used in the seismic modelling.

V_s have been calculated from the V_p velocities by using V_p/V_s ratios from relevant literature. V_p/V_s ratio for the intrusions has been set to 1,86 (Smallwood et al. 2002). The connection between V_p/V_s and lithology is quite well established. A low V_p/V_s is associated with sandstone (1,6-1,75) and limestone (1,84-1,99), while shales typically have higher values (1,7-3) (Domenico 1984, Mjelde et al. 2003). Another important thing to remember is that the V_p/V_s

ratio is influenced by other rock parameter such as porosity, pore fluid, and degree of consolidation (Mjelde et al. 2003). The V_p/V_s ratio are proven to decrease with depth, which correspond to an increase in compaction and consolidation of the rocks (Mjelde et al. 2003). At a depth of around 3-4 kilometers the V_p/V_s ratios have been set to be 1,7 for sandstone, 1,75 for shale, and 1,8 for limestone.

Table 4-2: Summary of properties V_p , V_s and ρ used for seismic modelling including units interpreted on Traill \emptyset and their equivalent stratigraphy in the Norwegian sea, well and depth at which the property is collected and additional references.

Unit Greenland	Unit Norwegian Sea	Depth (m)	Well	References	V_p (km/s)	V_s (km/s)	ρ (g/cm ³)
Dolerite intrusions		4400	219/20-1	Smallwood and Maresch 2002	6,0	3,2	3,00
Carboniferous- Traill \emptyset Gp.	Similar to Billefjorden Gp, Soldogg Fm. in the Barent Sea	2490	7128/6-1	npd.no factpages	4,4	2,6	2,35
Permian- Foldvik Creek Gp.	Zechstein Gp.	1880	6609/7-1	npd.no factpages, Bugge et al. 2002	2,8	1,6	2,75
Permian- Ravnefjeld Fm.	Spekk Fm.	2900	6407/2-1	npd.no factpages	2,5	1,4	2,25
Triassic- Wordie Creek Fm.	Grey Beds	2930	6204/11-1	npd.no factpages	3,8	2,2	2,70
Jurassic- Bristol Elv Fm.	Fangst Gp, Ile Fm.	3450	6507/3-3	npd.no factpages, Stemmerik et al. 1998	3,6	2,1	2,35
Jurassic- Pelion Fm.	Fangst Gp, Garn Fm.	3370	6507/3-3	npd.no factpages, Stemmerik et al. 1998	3,4	2,0	2,20
Creatceous- Hold with Hope Gp.	Cromer Knoll Gp.	3200	6506/12-4	npd.no factpages	3,0	1,7	2,35

In the base case model, the seismic properties within each of the stratigraphic units are homogenous and identical throughout the layer and there is no internal reflectors. However, an alternative model with a more complex layered geological model has also been created to investigate the influence of internal stratigraphic heterogeneity on seismic imaging. This model includes internal heterogeneities which corresponds to the bedding observed in the outcrop. For instance, the Triassic succession predominantly consists of sandstone, interbedded with planar mudstone layers. This lamination was modelled as 4 meters thin layers placed within the otherwise homogeneous units, and these layers were modelled with a 10% decrease in p-wave velocity and density.

In this thesis, the goal is to model something simple and general, and it is therefore not needed to use complicated survey geometries and parameters that will vary from case to case. PSF was generated from user-defined parameters: frequency, average velocity and maximum

illuminated dip. The average velocity was found by taking the average of the P-wave velocity from the lithologies and is set to be 3,2 km/s. The seismic modelling was performed with different dominant frequencies, i.e. 10 Hz, 20 Hz, 30 Hz and 40 Hz, in order to observe how the different frequencies influence the seismic resolution and imaging. The chosen wavelet was of zero-phase Ricker type. In addition, seismic modelling was done by varying the maximum illuminated dip, which is also a way of changing the lateral resolution in addition to control the illumination of the steeper structures. The PSDM filter, described in Section 4.2, not only determines the vertical resolution, but also the lateral resolution by varying max illumination dip. The max dip was initially set to 45°, which typically represents a good standard seismic acquisition in a rather horizontally layered overburden, thus resulting in the standard $\lambda/2$ lateral resolution and no illumination of reflectors steeper than 45°.

4.3 Seismic data and interpretation

Detailed interpretation of the sill complexes, host rock, and their interaction in the 3D seismic dataset is beyond the scope of this work. Rather, the 3D seismic dataset has been used for comparison between real seismic data and seismic modelling, since the seismic data give good examples of imaging of similar intrusions to those at Traill Ø. Examination of sill intrusion geometries in seismic is important, in order to get a better understand of the seismic expression of intrusions. The seismic data can also give insight to the resolvability and illumination of deeply emplaced sill intrusions by comparing this to well imaged sills in synthetic seismic. Some seismic interpretation of the large-scale geometry of the sills has been done to get a better visual image of the deep intruded sills.

The seismic data used in this work are from the Norwegian Sea on the Norwegian Continental Shelf. This area shares much of its history with the conjugate East Greenland Margin, since they are at the opposite sides of the NE Atlantic rift system. East Greenland and the conjugate Mid-Norwegian Margin have equivalent sedimentary succession, and a large number of sill intrusions have intruded both margins. One of the differences is that these sedimentary successions are exposed on land in East Greenland. This is a huge advantage since East Greenland can be used as a good analogue for better understanding sill intrusions in seismic

data. Another important difference is the fact that intrusions in the seismic data are emplaced mainly into the Cretaceous mudstone, while on East Greenland intrusions are emplaced into different stratigraphy from Carboniferous to the Cretaceous.

A 3D seismic cube from the Solsikke area located in the northern part of the Møre Basin (Figs. 1.1b,c and 4.9) is used to compare to the seismic modelling results. The Møre Basin is limited by the Jan Mayen lineament to the north, and this lineament divides the Møre Basin from the Vøring Basin (Brekke 2000, Fig. 4.9). The basin have a thick Cretaceous succession (Brekke 2000) and is an example of a rifted volcanic margin. Extensive sill complexes are present in large parts of both the Møre and the Vøring Basin.

This seismic cube covers an area of c. 1050 km², and the data are zero phase time migrated (Hansen and Cartwright 2006). Blue in the seismic data denotes an impedance increase. The focus of this study have been the most northwestern side of the cube as intrusions are present in this part. Only one well is present in the study area, exploration well 6403/10-1 (Fig. 4.9). The exploration well reached a total depth of 3400 m (1700 m below the sea surface, water depth 1700 m) and reached Upper Cretaceous sediments.

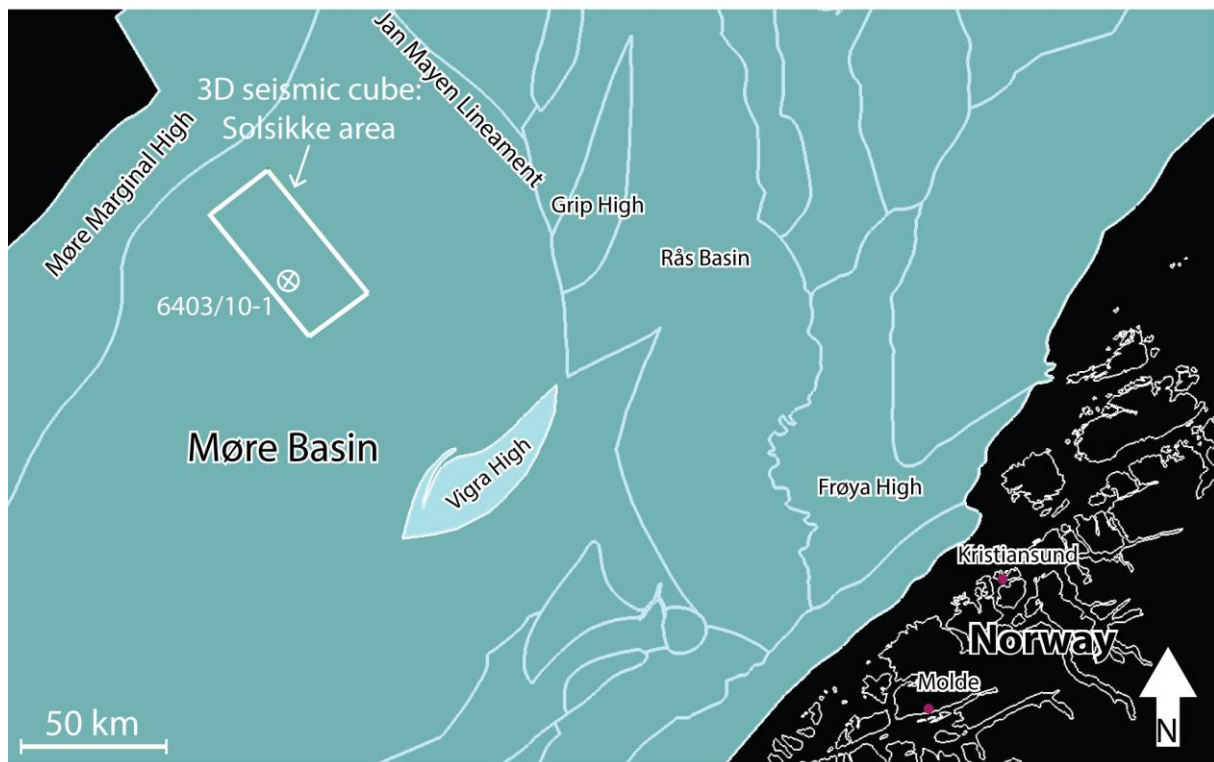


Figure 4.9: Seismic cube from the Solsikke area. The Solsikke area located south of the Jan Mayen Lineament in the Møre Basin.

Intrusions imaged in 3D seismic data are characterized by their very strong reflectivity/high seismic amplitudes compared to the surrounding host rocks, their lateral discontinuity and the tendency to crosscut stratigraphy (Smallwood et al. 2002). They may also exhibit concordant relationship with the host rock (Hansen and Cartwright 2006). Sills in seismic data are referred to as continuous sheet, which is either concordant or discordant with the stratal reflections. It may be hard to interpret sills, because they can split into several units or several units can merge into one unit. Sills can also transgress (move up and down in the stratigraphy), and sill intrusions may contain holes (Planke et al. 2005).

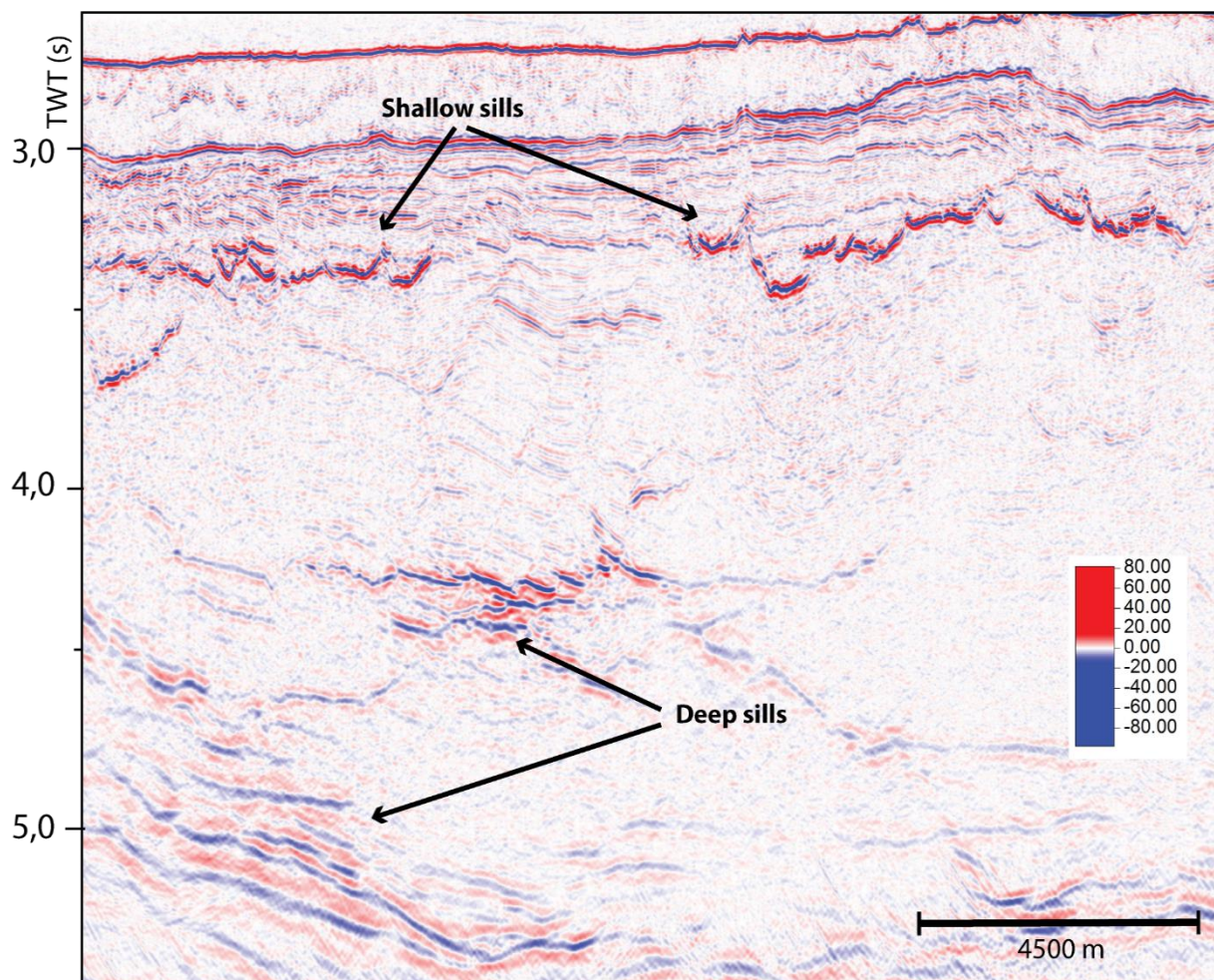


Figure 4.10: Seismic section showing shallow and deep sill intrusions in the seismic data.

On the northwestern side of this cube, there are prominent high amplitude reflections. There are both high amplitude reflectors at shallow (c. 3,5 s TWT) and deep depths (4-5,5 s TWT). The focus will be at the deep intrusions. Shallow emplaced sills are often saucer shaped in the seismic (Fig. 4.10), and have a concave upward geometry, which cross cut the surrounding

stratal reflections. Deeply emplaced intrusions may be hard to see in the seismic due to poor quality data at depth, and shallow intrusion can mask deeper intrusion by reflecting all the seismic energy.

5 Results

This section first presents the results from the analysis of the virtual outcrop model (5.1), focusing on large-scale structures (5.1.1) and architecture and large-scale intrusive geometry and relationships (5.1.2). Secondly the seismic data from the Solsikke Survey are presented (5.2) with a summary of the stratigraphy and intrusion geometry of deeply emplaced sill intrusions. The seismic modelling results are presented in Section 5.3 with focus on different expressions in the modelled seismic as frequency (5.3.1) and maximum dip angle (5.3.2) are changed. Finally, the effect of internal layering in the sedimentary sections on imaging of deeply emplaced intrusions is investigated (5.3.2).

5.1 Virtual outcrop model

5.1.1 Large scale structures

The outcrop consists of 11 rotated fault blocks cut by both post- and pre-magmatic normal faults (Fig. 5.1). The Månedal Fault and the Bordbjerget Fault are two of the pre-magmatic faults with the largest pre-magmatic displacement (Faults 2 and 13, Fig. 5.2). Around 80% of the total pre-magmatic extension is shared between the Månedal Fault and the Bordbjerget Fault. The pre-magmatic extension was accommodated on these faults, which then bounded a 10 km wide fault block (Price et al. 1997). These two faults have also experienced some reactivation, and thus have a minor amount of post-magmatic displacement (Price et al. 1997). The Månedal Fault has a displacement of over 1 km (Price et al. 1997), and Cretaceous, Jurassic and Triassic strata are down thrown against Triassic strata in the footwall. Pre-magmatic deformation of one of the splays to the Månedal Fault (Fault 12, Fig. 5.2) is evidenced by undeformed sills and dykes cutting through and following the fault. Carboniferous, Permian and Triassic strata are downthrown against Carboniferous strata in the Bordbjerget Fault (Fault 2, Fig. 5.2), and the fault has a displacement of around 1 km if both pre- and post-magmatic displacement are taken into account (Price et al. 1997).

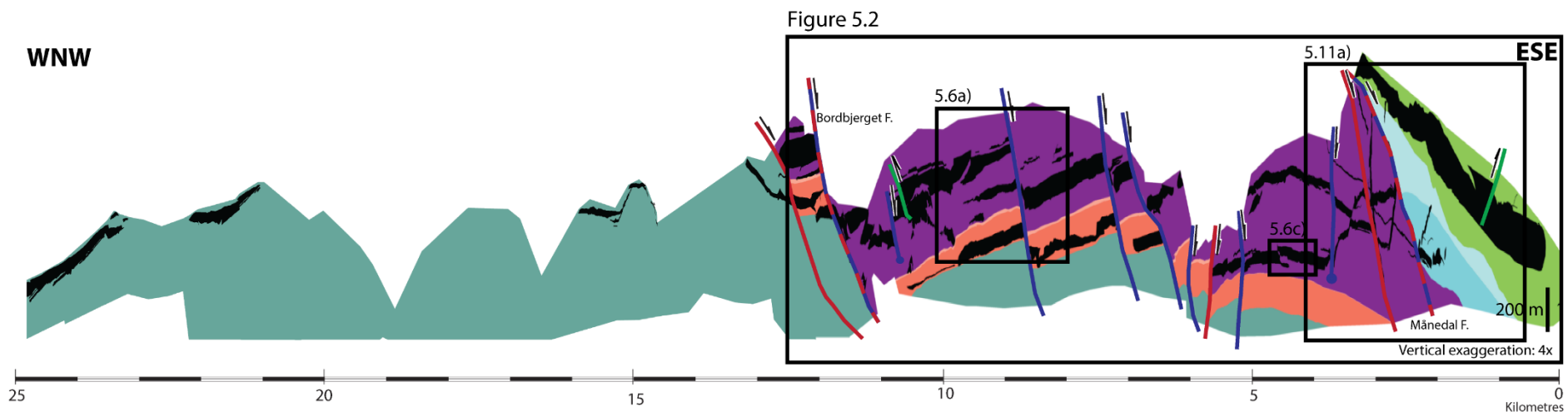


Figure 5.1: Overview of the entire outcrop at Svinhufvudsberge at Traill Ø showing dolerite intrusions, faults and stratigraphy. Note absence of large faults west of the Bordbjerget Fault

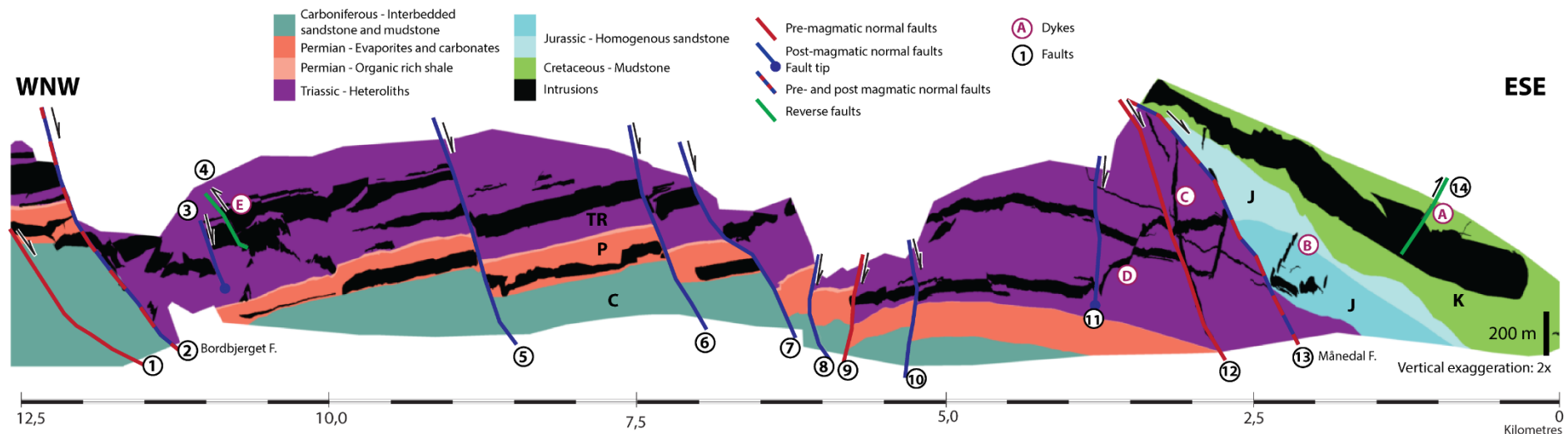


Figure 5.2: Overview of the eastern side of the outcrop showing faults, dolerite intrusion geometry and stratigraphy. The outcrop is shown with a vertical exaggeration of 2x. Faults are labeled from 1-14, red faults are pre-magmatic, blue faults are post-magmatic ones and green faults are reverse faults. Dykes are labeled A-E.

The post-magmatic faults are a result of internal break-up of these earlier formed fault blocks with only minor reactivation along the bounding faults (Price et al. 1997). Several post-magmatic faults are interpreted along the outcrop (Fig. 5.2). They mostly show displacement of a couple of meters to around 150 meters, which is minor compared to the kilometer-scale displacement on pre-magmatic faults. The intrusions do not show any evidence of interaction with these faults, and the architecture of the faults are easily reconstructed by cutting sections of images along faults and restoring the sections (Fig. 5.3). This indicates that the faults have not formed prior to intrusion, and that they are fully post-magmatic. Some of the faults have been reconstructed in Figure 5.3 in order to study stratigraphy and intrusions before the faulting, and this shows that the intrusions seems to follow the stratigraphy before they were influenced by the post-magmatic faulting.

Original image



Reconstructed faults

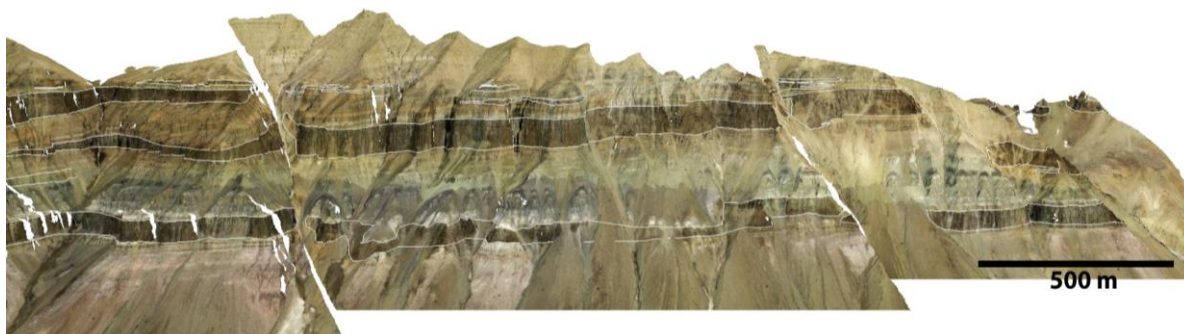


Figure 5.3: Planar parallel intrusions are easily reconstructed back to their original position by reconstructing the post-magmatic normal faults. Reconstructed image obtained by cutting along the faults. There is no visible deformation of the intrusions or stratigraphy after the reconstruction, indicating that the faults have not influenced the intrusions.

As seen from Figure 5.1, the distribution of faults is densest at the eastern part of the outcrop. Most of the faults are normal faults, however Fault 4 and 14 on Figure 5.2 seem to be reverse

faults. These two faults have small displacement and they cut through the intrusions. In addition to large pre- and post-magmatic normal faults, there is some evidence of small-scale faults and deformation close to the intrusions margins. However, this is at the limit of the resolution of the data, and therefore beyond the focus of this study.

5.1.2 Architecture and large scale intrusive geometries and relationship

Figure 5.1 shows all the intrusions along the studied outcrop. The sill intrusions show a wide range of thicknesses, and vary between 1 meter and 200 meters thick. The average thickness is 56 meters. Sill splays, which are much thinner sills which originate from the main sill and often develop parallel to the main sills, are from around a meter to a couple of meters in thickness. These splays are found along the entire outcrop, and they commonly originate from irregularities on the sill margins.

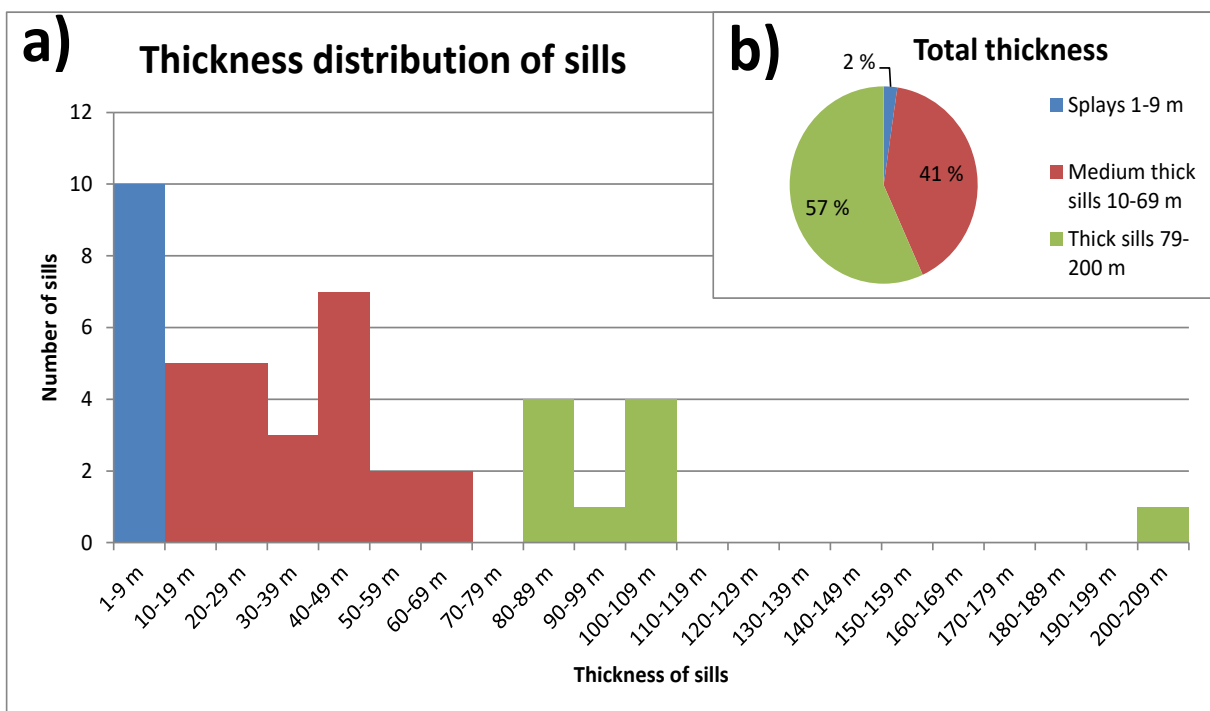


Figure 5.4: a) Thickness distribution of sills along the outcrop. Sills are measured in vertical lines every kilometer. Sill intrusions are divided into three groups: splays in blue, medium thick sills in red and thick sills in green. b) Pie diagram illustrating how much each of these groups constitute of the total thickness of sill intrusions in the outcrop.

The thickness distribution of sills are shown in Figure 5.4a. This histogram shows that there is a large range of sill thicknesses along the outcrop. Most of the sills are from 1-9 meters thick. There is also a number of intrusions in the 40-49 meters range, which seems to be a common

thickness for some of the main sills in the area. Some of intrusions are more than 100 meters, and most of them are located on the eastern side of the outcrop (see Fig. 5.5). The intrusions can be divided into three groups based on their thickness, splays or thin sills from 1-9 meters thick, medium thick intrusions (10-69 meters) and thick intrusions (70-200 meters). As the histogram shows (Fig. 5.4a), a large number of splays and thin sills are observed along the outcrop, but they only constitute 2 % of the total thickness of the intrusions (see Pie diagram Fig. 5.4b), while the thickest sills are making up 57 % of the intrusions along the outcrop.

Sill intrusions are emplaced into the stratigraphy along the entire outcrop, but the amount of intrusions shows significant variation along the outcrop. This is visualized in Figure 5.5, which shows the total thickness of intrusions measured on vertical lines every 1 kilometer along the outcrop. On the western half of the outcrop, the total thickness of the sills is small. This is due to presence of only Carboniferous deposits on this western half of the outcrop. Only four sill intrusions, in addition to splays, are emplaced into the Carboniferous succession along the outcrop, and none of these is thicker than 50 meters. From 12 to 18 kilometer on Figure 5.5, the total thickness of the intrusions are almost constant. This is due to the presence of the same stratigraphic interval along this area, and the thickness of the intrusion are constant since they follow the same stratigraphic layers throughout this section. At 19-21 kilometers on the curve in Figure 5.5, there is a drop, corresponding to the presence of only intrusions within the Triassic interval. The total thickness is largest in the Cretaceous succession at the easternmost side of the outcrop. The total thickness of intrusions are also highest at the eastern side of the outcrop, reaching total thicknesses of around 250 m.

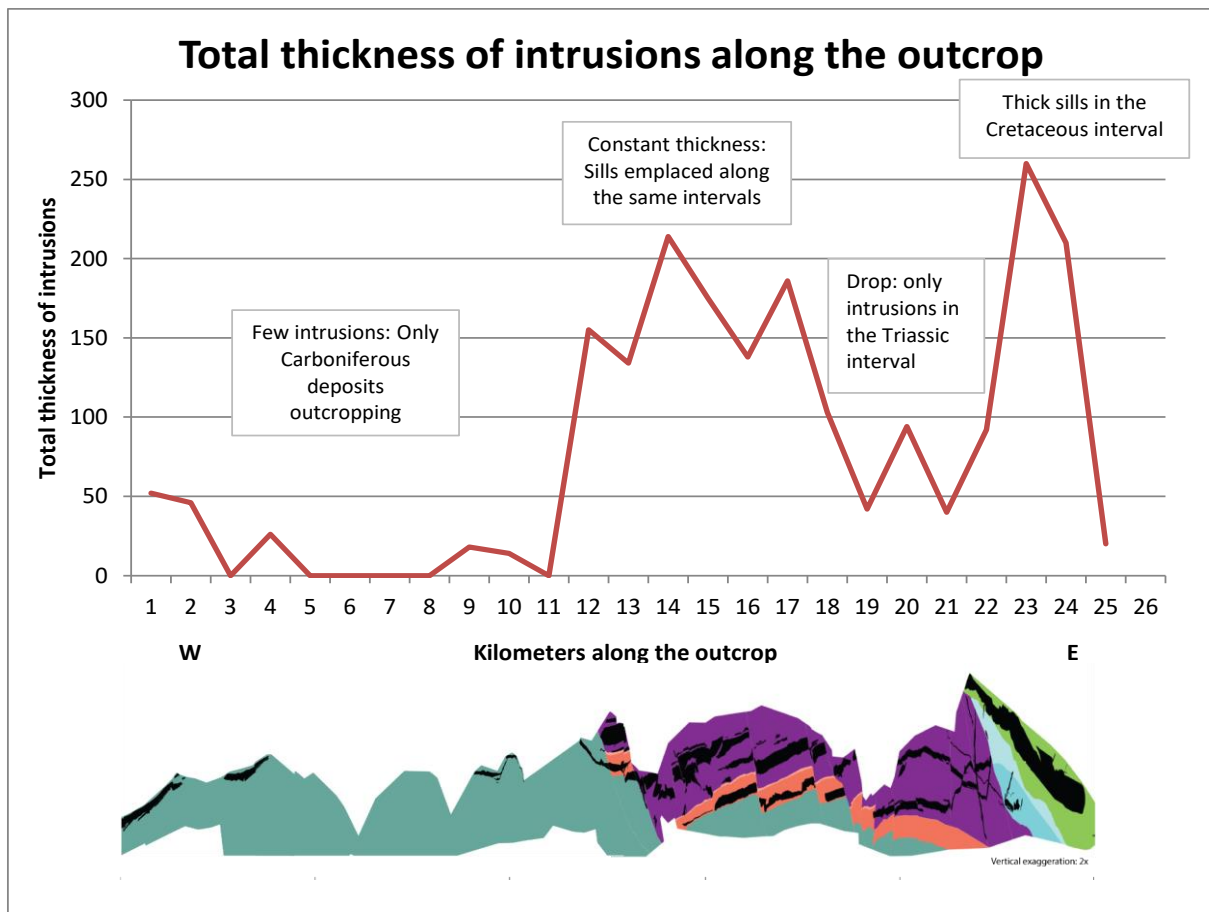


Figure 5.5: Graph showing variation in the total thickness of sill intrusions along the outcrop.

The sill intrusions on Traill Ø exhibit a layer parallel geometry, and the presence of structures such as broken bridges and steps (Fig. 3.1a and b) can indicate that the sill intrusions were emplaced into a brittle host rock (Schofield et al. 2012b, Fig. 3.1). Two well defined broken bridges are observed in the outcrop. One of them is particularly well exposed (c.f. Fig. 5.6b). Unbroken bridges (Fig. 3.1) are not observed in the study area. Features typical for sills propagating in non-brittle rocks (Schofield et al. 2012b, Fig. 3.1c-e), such as fingers and lobes, have not been observed.

Both broken bridges seen in Figure 5.6b and c are slightly deformed. They show a rectangular geometry, which means that the layering and bedding of the actual bridge is preserved parallel to each other, without being curved (Fig. 5.6c). The broken bridges are bent up as two separate magma flows have propagate with a slight offset. They are sometimes modified in shape by deformation where the bridge is bent (see Fig. 5.6b, d and e). Bridges are dominated by interbedded lithologies, and the bedding is always parallel to the longest dimension of the bridge (Fig. 5.6c). The bridges are 190 m and 250 m in length.

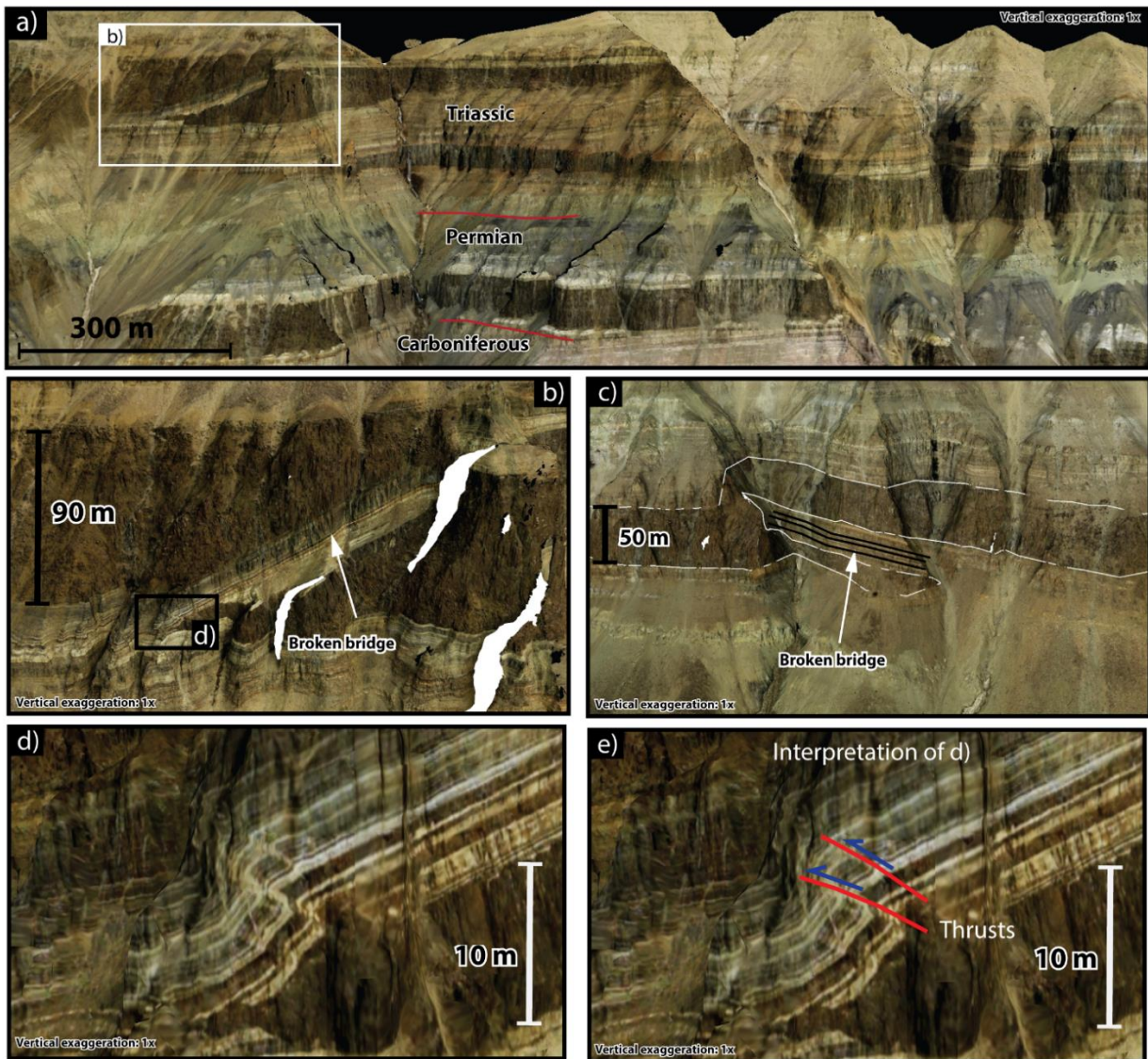


Figure 5.6: Broken bridges in the outcrop. a) Overview of the most well exposed bridge along the outcrop. Note the two sills on each side of the bridge that propagated as two separate sills before the broken bridge was made. See Fig. 5.1 for location. b) Well exposed broken bridge clearly showing the rectangular shape and the interbedded lithologies. c) A smaller broken bridge. Interbedded layers are indicated, and observe that the layering is parallel to the longest dimension of the bridge. See Fig. 5.1 for location. d) Fold and minor thrust faults at the outer bend of the bridge e) with interpretation.

5 dykes are observed along the outcrop (Fig. 5.2, marked from A to E), and these are 10-60 meters wide. In addition, there are some intrusions along the outcrop that can be defined as either dykes or just as climbing sills. These intrusions originates from a horizontal sill, then climbing to a higher level before resulting in a new horizontal sill. Dyke D is a good example of this (Fig. 5.7a), and in addition there are two other examples of climbing sills along the outcrop that are not defined as dykes. All dykes are oblique with dips varying from 30 to 70 degrees, and no vertical dykes are observed. Most dykes cut sedimentary layering, but one obviously follows one of the major faults for around 750 meters before continuing into the Jurassic

strata in the hanging wall of the fault (Dyke C in Figs. 5.2 and 5.7a) before being offset by the Månedal Fault. Dyke C has a dip of 35° and an average width of around 35 meters. This dyke is present at almost the entire height of the outcrop and it has a small horizontal offset by one of the sill it cuts through (Fig. 5.7a).

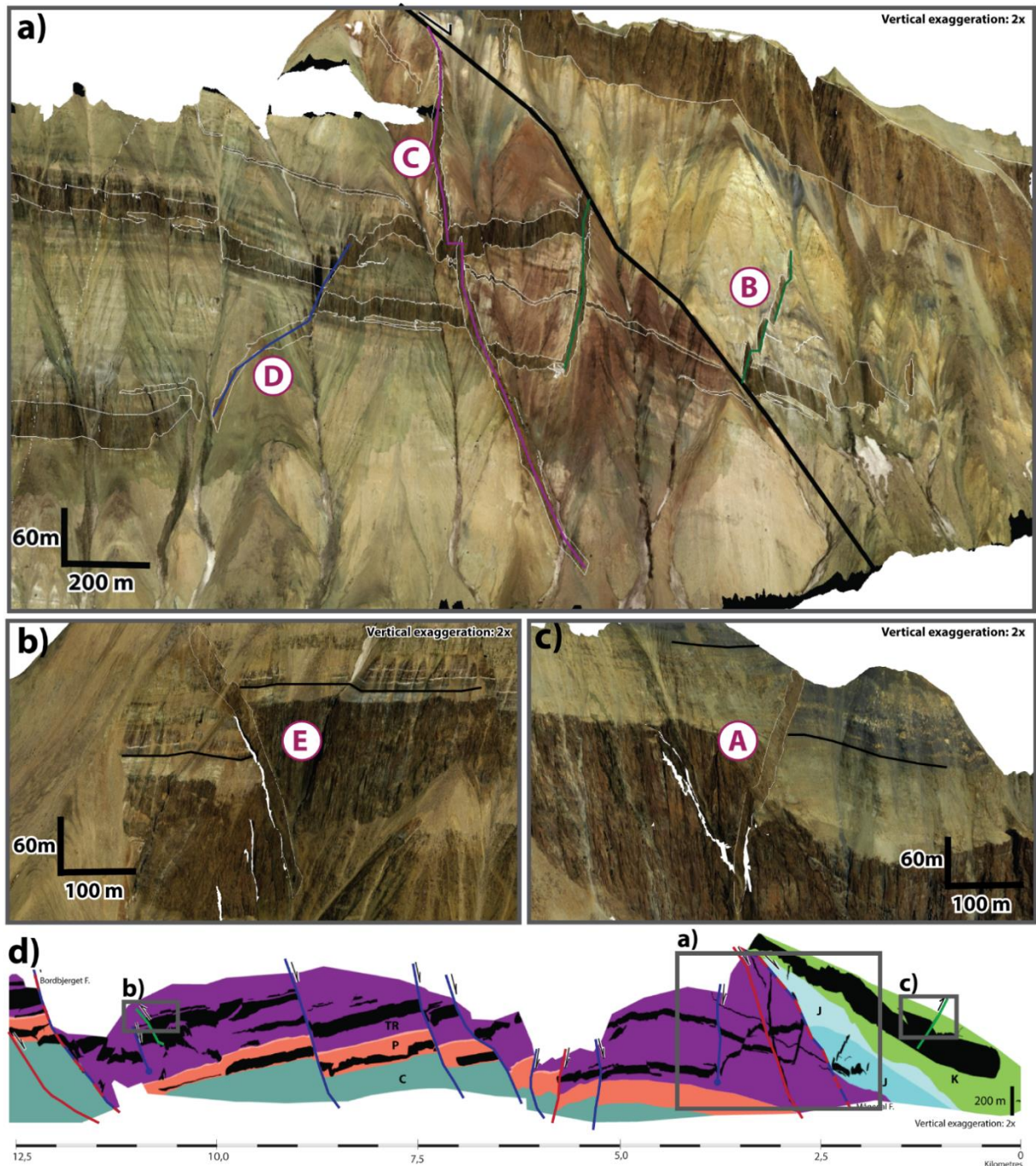


Figure 5.7: Dykes in the study area. a) Oblique dykes: Dyke C (purple) interacts with two other sills in addition to following a fault, Dyke B (green) abruptly originates from a sill and is cut by the Månedal Fault and Dyke D in blue is linking two sills from different levels. b) and c) Thinner dykes cross-cutting sills and exploiting reverse faults. d) Overview of the outcrop and location of the dykes.

Two of the dykes seem to have exploited small reverse faults that cut through intrusions below the dykes (Dyke A and E Fig. 5.2 and Fig. 5.7b,c). These two dykes have a dip of around 70°. There is also evidence that the dykes have crosscut through the faulted sills as well. This indicates that these dykes were not emplaced contemporaneous with the rest of the intrusions.

Dyke B shown in green in Figure 5.7a is cut by the Månedal Fault and has a dip of around 60°. This dyke seems to stop in the middle of the Jurassic succession and it starts abruptly as it bends away from a planar parallel sill intrusion. On the eastern side of the fault, the dyke seems to be cut by a number of small-scale faults since the dyke has small offsets. The last dyke is shown in blue in Figure 5.7. It is also reasonable to call this a climbing sill as it originates from a layer parallel sill and cut the stratigraphy for 500 meters before resulting in another layer parallel sill. This dyke has a dip of 52°.

Sills make up c. 13 % of the outcrop, and are most common on the eastern side of the outcrop. Magmatic sill intrusions are emplaced into the stratigraphy along the entire outcrop, but some stratigraphic intervals contain a systematically greater proportion of intrusions than others, indicating that intrusions prefer some intervals more than others. The highest proportion of intrusions found within one interval is intrusions in the Cretaceous mudstone interval (Fig. 5.8b). Intrusions make up 45 % of the Cretaceous interval and the thickest sill is found within this interval. The Triassic interval, which consists of interbedded sand and mudstone, contains the largest volume of intrusions (Fig. 5.8a). Over half of the intrusions along the outcrop are found within this interval. As seen from Figure 5.8a, only a low proportion of the sills occur in the homogenous sandstone of the Jurassic. All interpreted intervals contain intrusions except the Permian organic rich mudstone of the Ravnefjeld Formation.

If the proportion of intrusions in each stratigraphic interval is normalized to the area of each stratigraphic interval (Fig. 5.8b), it becomes clear that intrusions are preferentially emplaced within the Cretaceous mudstone, and intrusions are rarely emplaced into the Jurassic homogenous sandstone and the interbedded sandstone and mudstone dominated Carboniferous. Figure 5.8b largely gives an expression on how easy it is for the intrusions to intrude into each of the different intervals. It shows how much of the interval consist of intrusions, and this indicates the extent to which it is easy to enter into each unit.

Figure 5.8a however, is a function of how the intrusions in this exact outcrop are distributed, and it shows the proportion of sills that are present in each interval. This distribution will strongly depend on the size of the different intervals, and this percentage distribution could have been very different if the outcrop for example was placed 2 km further north.

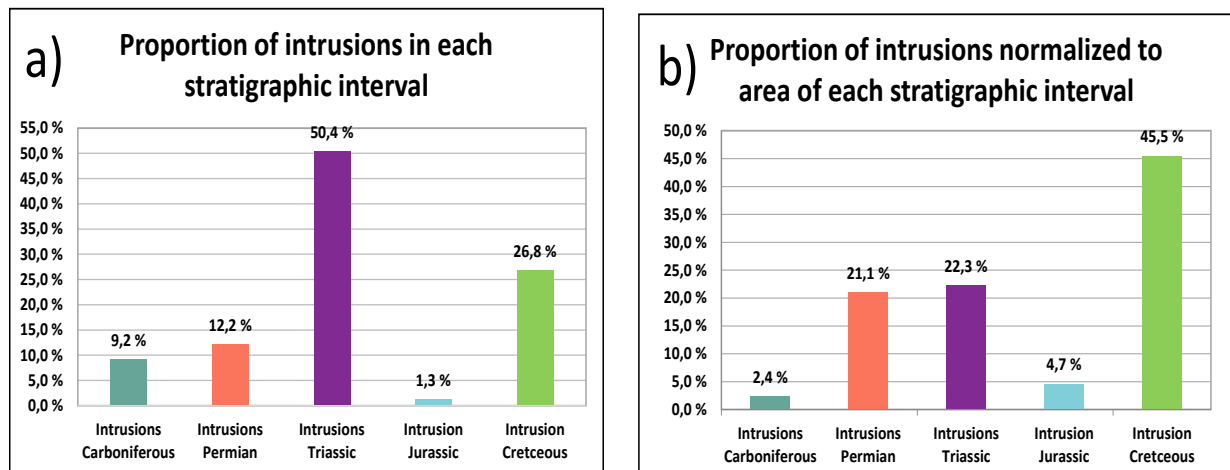


Figure 5.8: a) Histogram showing proportion of intrusions in each stratigraphic interval along the outcrop. Most of the intrusions are found within the Triassic heteroliths. b) Histogram showing the proportion of intrusions normalized to area of each stratigraphic interval. Example: 2,4 % of the Carboniferous succession is intrusions.

There is a large variety in the lithology of the different host rock intervals within the study area. A majority of the sedimentary rocks consist of brittle, layered sandstone interbedded with mudstone from the Carboniferous Traill Ø Group and the Triassic Wordie Creek Formation (Parsons et al. 2017, Bjerager et al. 2006). There are also intervals with more homogenous sandstone with only minor amount of mudstone within the Jurassic Jameson Land Group and the Triassic Pingo Dal Formation (Therkelsen and Surlyk 2004, Parsons et al. 2017). The Cretaceous consists of mudstone (Parsons et al. 2017), and the Permian Ravnefjeld Formation is dominated by organic rich shale (Christiansen et al. 1993). The rest of the Permian succession is dominated by carbonates and evaporites (Surlyk 1990). Sills propagating in these different lithologies show different morphologies and structures, and these are investigated below.

Sills emplaced within the Traill Ø Group in interbedded sandstone, mudstone and coal deposits

Very few sills are seen within the Traill Ø Group, and no intrusions are observed within the Traill Ø Group east of the Bordbjerget fault zone (Fault 2, Fig. 5.2). Only 2,4 % of the Carboniferous interval consists of sill intrusions (Fig. 5.8b), which is the lowest amount of intrusions within any of the intervals along the entire outcrop. Generally, the sills emplaced in this interval follow the bedding, but in a few instances sills are observed to crosscut stratigraphy and ascend obliquely through the stratigraphy (see 15 km in Fig. 5.1 and Fig. 5.9a), most likely indicating that the sills have tried to exploit overlying, more mudstone-rich horizons.

Splays are quite common parallel to the sill margins in the Carboniferous interval (Fig. 5.9c). In this interval, there are more irregularity on the sill margins than in any other interval. Splays in this interval usually originate from the irregularities along the margins, such as steps. All splays occur close to the main sills. One of the intrusions has caused a fold, indicating vertical inflation of the sill in the directly overlying mudstone rich host rock (see 23,5 km in Fig. 5.1 and Fig. 5.9d).

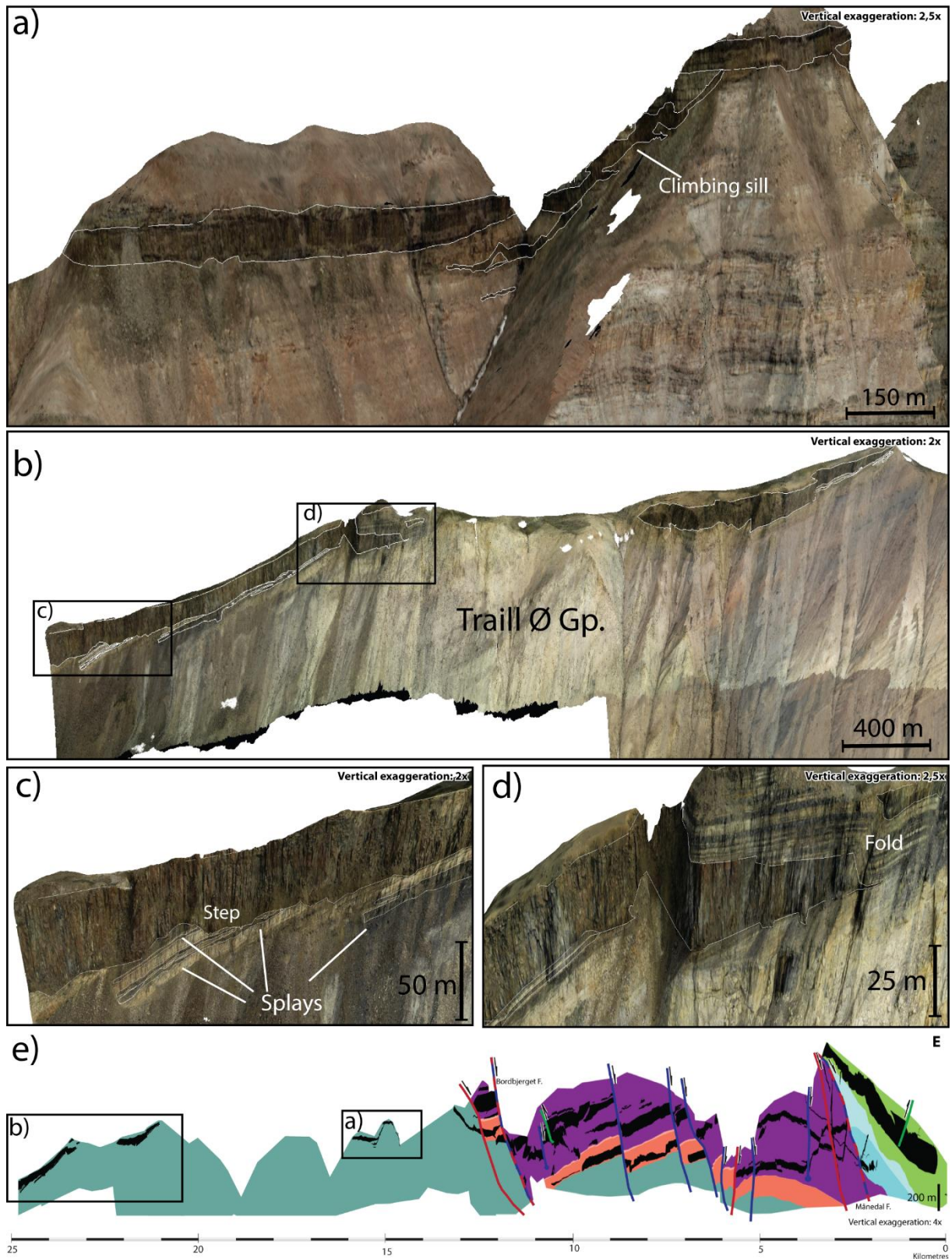


Figure 5.9: Intrusion geometries and features within brittle interbedded heteroliths of the Traill Ø Group. a) Climbing sill b) Overview image of the westernmost intrusions in the Traill Ø Group. c) Splays originate from irregularities along the sill margins and d) Emplacement of magma into the host rock has caused a fold, as the host rock was inflated and uplifted. e) Overview of the outcrop and location of sills in the Carboniferous.

Sills emplaced within the Permian strata dominated by carbonates and evaporites (Foldvik Creek Group)

The intrusions in this interval make up around 21 % of the Permian interval, and within this interval, the sills exhibit two quite different morphologies. Sills mainly show planar parallel geometries without clear steps along their length, and there are only few irregularities along their margins (Fig. 5.10a). However, in a small interval between two normal faults (at 5 km Fig. 5.2) the sill does not exhibit geometries parallel to the bedding. The sill seems to be emplaced in different levels in the host rock within the same interval, causing it to look different from the other sills (Fig. 5.10b). The sill exhibits an unusual geometry and the sill seems to change level within the interval and transgress up and down, and some places there seem to be large steps. This interval is partly covered in scree and it is therefore hard to observe detailed changes along the margins. No intrusions are emplaced within the Permian succession on the eastern side of the outcrop (Fig. 5.2, east of Fault 7).

Sill emplacement in Triassic strata (Wordie Creek Group) mainly consisting of brittle sandstone interbedded with mudstone

Around half of the intrusions along the outcrop are found within the Triassic interval, and around 20 % of the interval consists of intrusions. The intrusions commonly show steps along their length. The steps have vertical offsets of around 1 m. Broken bridges are also present in this interval. These bridges have developed between separated sills (Fig. 5.6b,c). Some splays are also observed in this interval. Sills that have propagated in this interval show many structures related to emplacement mechanisms commonly seen in brittle rocks, along the entire outcrop. This interval also shows individual thinner sills that are isolated from the main sill, but are still parallel to the main sill (Fig. 5.10a). This can indicate that these have exploited other horizons than the main sill or splays from the main sills that are connected outside the outcrop.

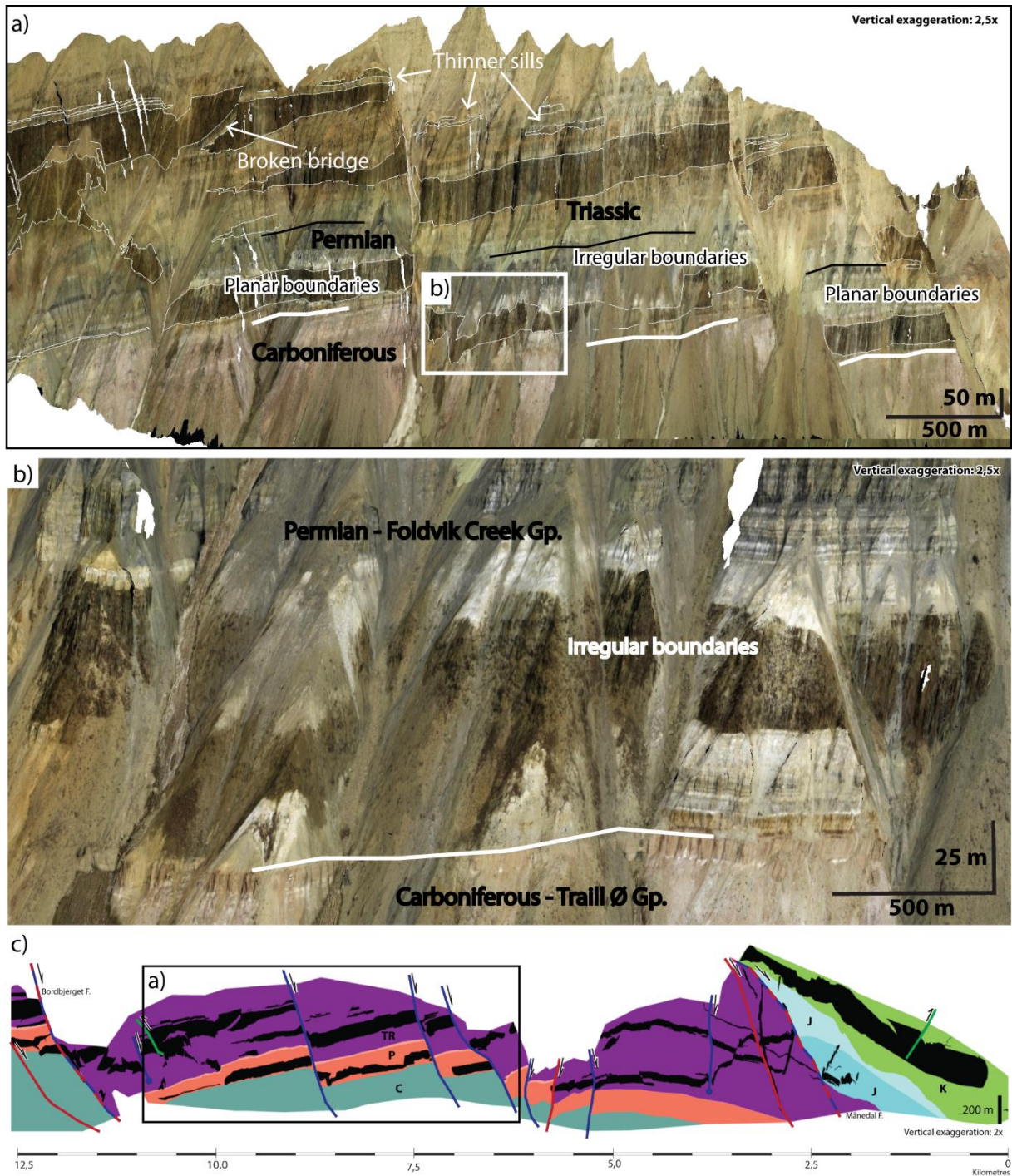


Figure 5.10: a) Overview showing sills emplaced into the Triassic and Permian interval. Note the difference in the expression of the Permian sill. b) Unusual expression of the sill's boundaries. c) Overview of the western side of the outcrop, and location of Fig. 5.10a.

Sill emplacement in Jurassic strata (Jameson Land Group) and Triassic strata (Pingo Dal Group) mainly consisting of brittle homogenous sandstone interbedded with small amounts of mudstone:

Sills that have propagated in more homogenous sandstone show different morphologies than

sills intruded into the other intervals. Intrusions seem to not follow stratigraphic layering to the same degree as in the Permian, and sills seem to transgress out of the Jurassic and Triassic homogenous sandstone interval over short distances (At 3 km in Fig. 5.2 and Fig. 5.11a,b).

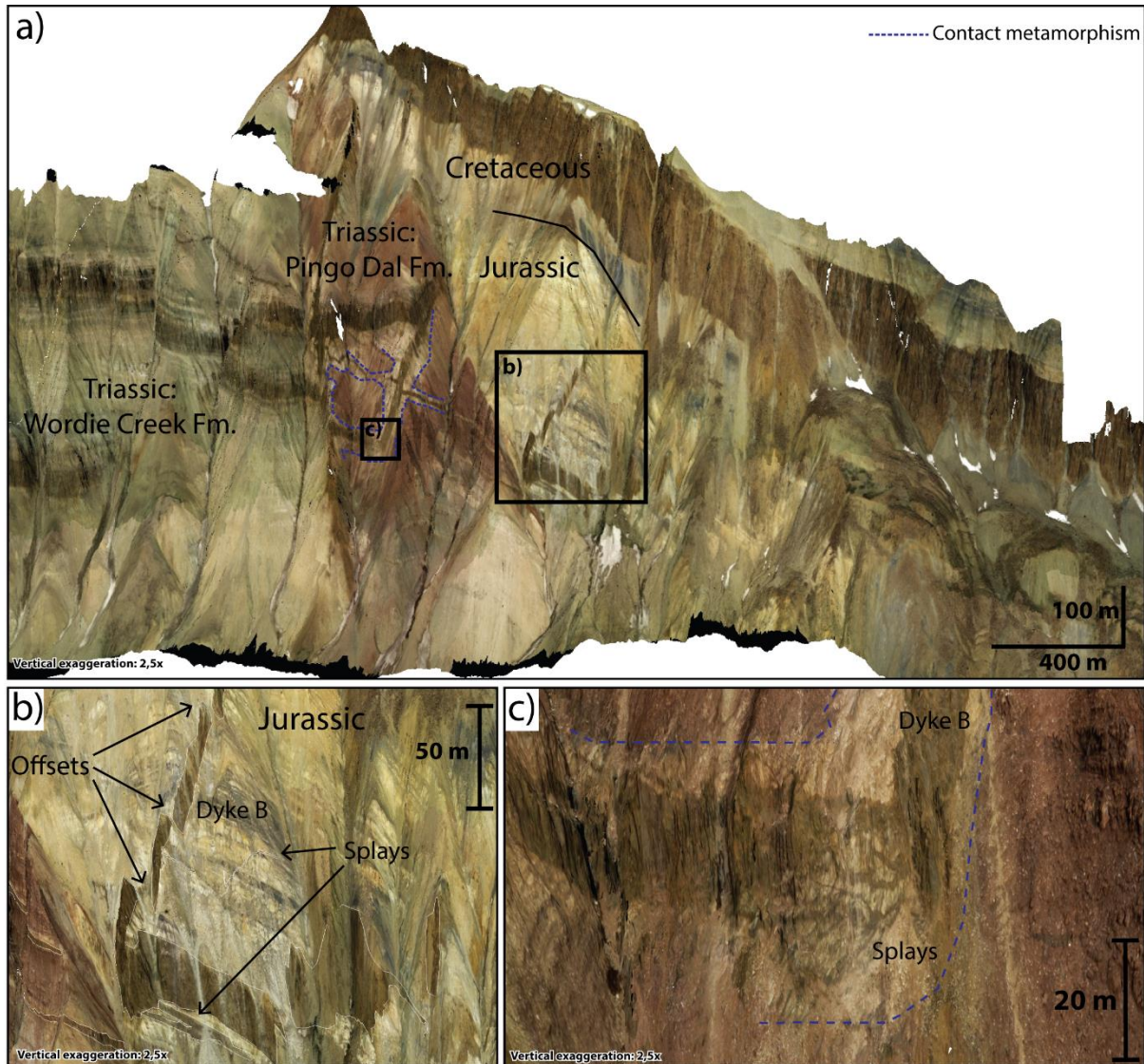


Figure 5.11: a) Overview of intrusions emplaced into Triassic, Jurassic and Cretaceous strata. Note the thick Cretaceous sill. See Fig. 5.1 for location. b) Sill in Jurassic homogenous sandstone transgress. The dyke has several small offsets. c) Several splays in the Triassic Pingo Dal Formation.

Zones of visible contact metamorphism (shown in a blue stippled line in Fig. 5.11a,c) around the intrusions are observed as a paler zone in the otherwise red-colored Pingo Dal Formation. This zone varies in thickness from almost zero to around 40 meters, away from the main sill margins.

The sill in the Jurassic sandstone does not follow the bedding for more than 250 meters, and

then the intrusion continues to propagate as a dyke crosscutting the strata (Fig. 5.11b). There are a number of small splays propagating in all directions. Only a low proportion of the sills occur in this Jurassic succession, which indicates that propagating sills do not prefer sandstone intervals.

The Triassic Pingo Dal succession is situated between two large faults (Fig. 5.11a), and it seems that the intrusions are not follow the bedding. Instead, they are propagating in a stepwise manner through the stratigraphy. There are two sills propagating in different levels, before merging into a common dyke (Dyke C, Fig. 5.7a). The lowermost of these sills propagates as small splays instead of a sill close to the dyke (Fig. 5.11c). This behavior is not observed anywhere else along the outcrop.

Sill emplacement in the Cretaceous mudstone interval:

The sill observed in the Cretaceous mudstone is the thickest sill in the study area, and attains a thickness of c. 200 meters, and is also highest in the stratigraphy in the area (Fig. 5.11a). The sill shows step-like features on the margins and a few small sills/splays up to 3 m in thickness originating from the main sill. Almost 50 % of the Cretaceous interval is occupied by intrusions (Fig. 5.8b), and even though there are only one main sill in this interval, it makes up 25 % of all the intrusions along the entire outcrop (Fig. 5.8a).

5.2 Interpretation of seismic data

A number of seismic surveys and a number of studies from the Norwegian Sea have shown that there are large amounts of igneous intrusions in the subsurface, and the Norwegian Continental Margin shows evidence of a classic volcanic rifted margin (Skogseid et al. 1992, Planke et al. 2005, Mjelde et al. 2008, Peron-Pinvidic et al. 2013, Schmiedel et al. 2017).

The dataset from the Solsikke area, that is used in this thesis, shows well-imaged deeply emplaced sill intrusions (e.g. Hansen and Cartwright 2006). The seismic interpretation in this study focuses on the interval where the deep intrusions are emplaced. This interval is between 4 s and down to 5,5 s two way travel time (TWT). Below this depth, which corresponds c. 4,5

km, the seismic quality is very poor and noisy, making it hard to do observations.

A previous study of the seismic data from the Solsikke area by Hansen and Cartwright (2006) is available and consulted for interpretations of the stratigraphy and the shallow sills, which were the focus in their study. Correlation to the geological setting and structural evolution of the Mid-Norwegian Margin also provides useful information when proceeding to understand the local geological succession and intrusions (Brekke 2000).

5.2.1 Stratigraphy and structural elements

The recognition of the stratigraphy in the area has not been in focus in this study, and no interpretation of the stratigraphy has been done in the seismic data. Therefore, correlation to previous work done by Hansen and Cartwright (2006) has been used, to ensure some information regarding the stratigraphy. Borehole data from well 6403/10-1, which is present in the Solsikke area, was used in their study to identify the lithology of the upper 1700 meters of the seismic data. All maps and seismic sections shown here, display depth in two-way travel time (TWT). Two of the units recognized by Hansen and Cartwright (2006) are shown in Figure 5.12. Horizon 1 is Upper Cretaceous, and horizon 2 represents the Base Paleocene.

The exploration well 6403/10-1 reached a total depth of 3400 m and reached Upper Cretaceous sediments. The well is positioned at the southern side of the 3D-seismic dataset and has therefore avoided all the shallow intrusions (Fig. 4.9). It does not reach the studied interval with the deep intrusions. The well penetrated the Cenozoic Nordland, Hordaland and Rogaland groups, and the Cretaceous Shetland Group (Dalland et al. 1988). All of these groups mainly consist of mudstone and siltstone. The Base Paleocene boundary (Horizon 2 in Fig. 5.12) corresponds to the upper boundary of the Shetland Group, and the Base of the Rogaland Group.

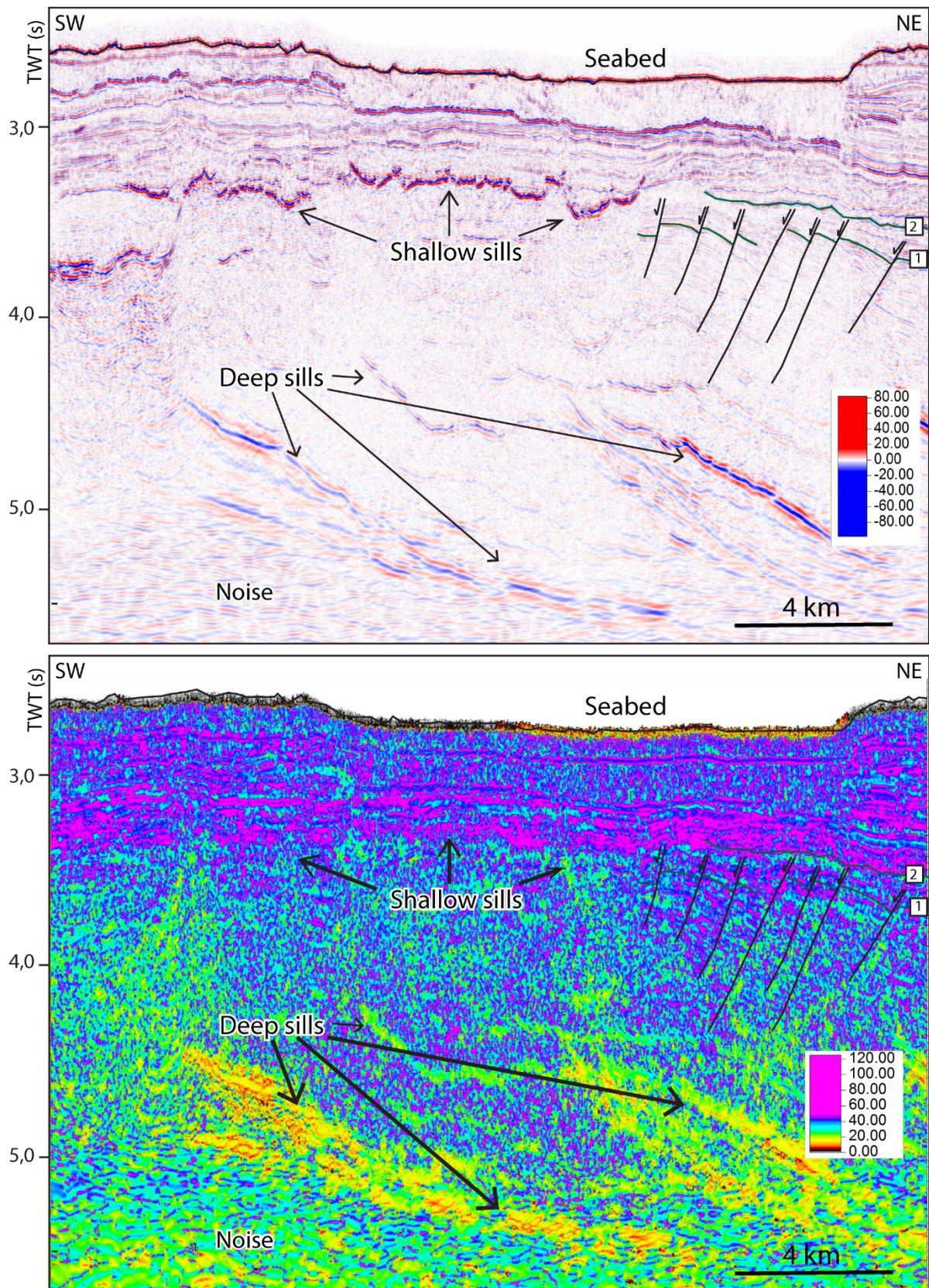


Figure 5.12: Seismic section showing faults, stratigraphy and shallow and deep intrusions. Lower figure show frequency distribution. The reflections interpreted as deep intrusions have a frequency of c. 12,5 Hz. Horizon 1 is Upper Cretaceous, and horizon 2 represents the Base Paleocene.

Below this depth, information about the general basin fill in the area is relied upon for information about the stratigraphy. The Cretaceous Cromer Knoll and the Jurassic Viking Group are present below this well. The Møre Basin is characterized by thick Cretaceous basins, and it is therefore reasonable to believe that the deep intrusions imaged in the seismic are emplaced into the Cretaceous Shetland Group and the Cromer Knoll Group. These Cretaceous sediments are dominated by mudstones and siltstones. The deeper Jurassic Viking Group is also dominated by mud- and siltstones, with the exception of locally developed sands (Dalland et al. 1988).

Structural elements in this area include a number of NNW-SSE trending normal fault starting below the Paleocene surface, mainly dipping towards the northwest, but there are also faults dipping towards the southeast. The lower fault tips are not easy to recognize and often ends where the deep intrusions start. This is likely caused by the high reflectivity of the intrusions masking the offsets of the faults.

5.2.2 Sill intrusions: geometry and expression in seismic data

Throughout the northwestern Solsikke area, several high-amplitude reflections are observed to crosscut the more laterally continuous, low-amplitude reflections from sedimentary strata. These are interpreted as igneous sill intrusions. At a TWT of around 3.5 s (c. 700-1100 m below the present-day sea bed), shallow sills are observed (Hansen and Cartwright 2006). These shallow sills are most dense at the northwestern corner of the seismic cube. The focus of this study is however, the deep sills occurring at lower depths in the seismic data, present in the TWT interval between 4-5.5 s (Fig 5.12).

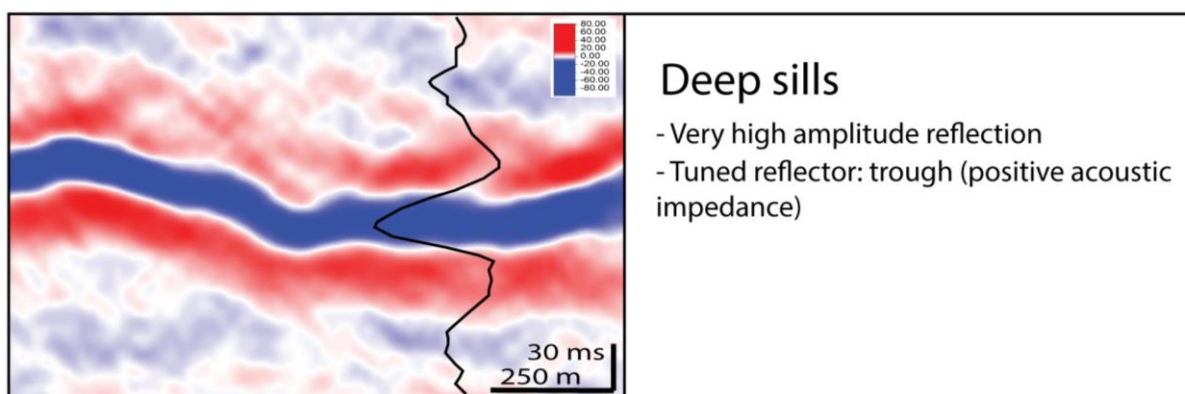


Figure 5.13: Seismic expression of the deep sills in the Solsikke area.

In the 3D seismic cube, deep igneous intrusions are expressed as packages of high amplitude reflections. The tops of the intrusions are positive, and represent an abrupt downward increase in acoustic impedance (Fig. 5.13). There is a large network of deep sills in the seismic data, and many of these are masked by shallower saucer shaped intrusions making it hard to study them. Shallow sills are present throughout the NW part of the cube, leading to poor imaging of underlying deeper sills. Therefore, it is hard to image deep sills in particular this area (Fig. 5.14).

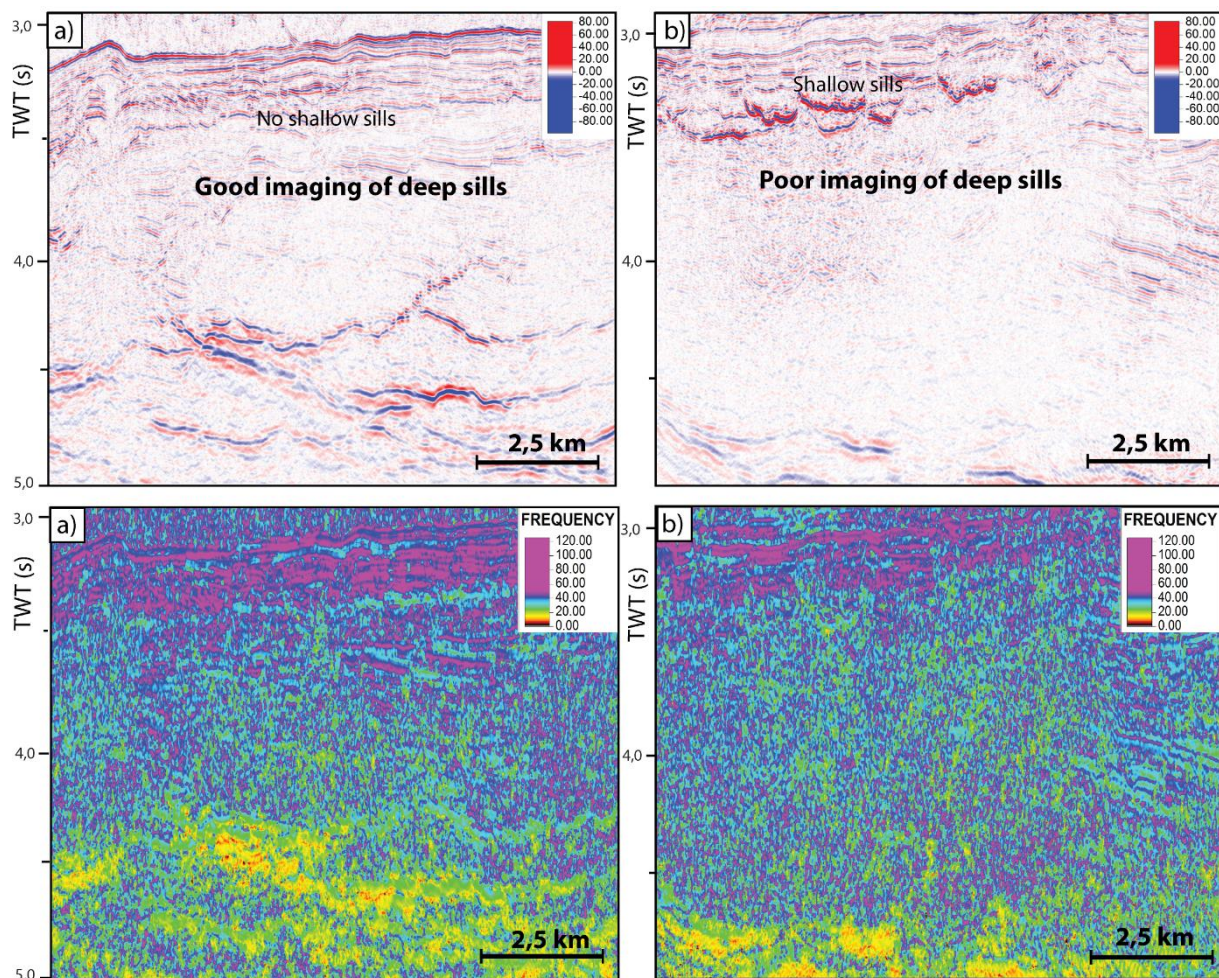


Figure 5.14: Showing the effect of how shallow intrusions influence the imaging of deep sills. a) With no shallow sills, the imaging of deep sills are relatively good. Note the gradual decrease in seismic frequency. b) With shallow sills present, the imaging below will be quite poor and noisy.

Most of the sill reflections are single reflectors (tuned reflectors), indicating that the resolution is not high enough to image both top and base reflector of the sills without interference between the reflectors. The thickness of the sills in the seismic data are below the vertical resolution, since the tuning thickness can be an indication of the vertical

resolution (Simm et al. 2014). In the time interval of interest (4-5,5 s TWT), the intrusions in the seismic data have a dominant frequency of 12,5 Hz (see Fig. 5.12b). Since it is not possible to clearly separate top and base of the sills, the sill thickness are defined to be between the limit of detection and the limit of resolution. The range of the thicknesses of the sill intrusions were calculated using the dominant frequencies in the area of the sills intrusions which is 12,5 Hz, and V_p of 6000m/s (also used in seismic modelling). By calculating, the wavelength ($\lambda=v/f$) will be 480 m and by calculating the resolution, intrusions below a thickness of 120 meters will appear as tuned reflection packages ($\lambda/4$), whereas those below the detection limit of 48 meters ($\lambda/10$) will not be identified in the seismic (Planke et al. 2005).

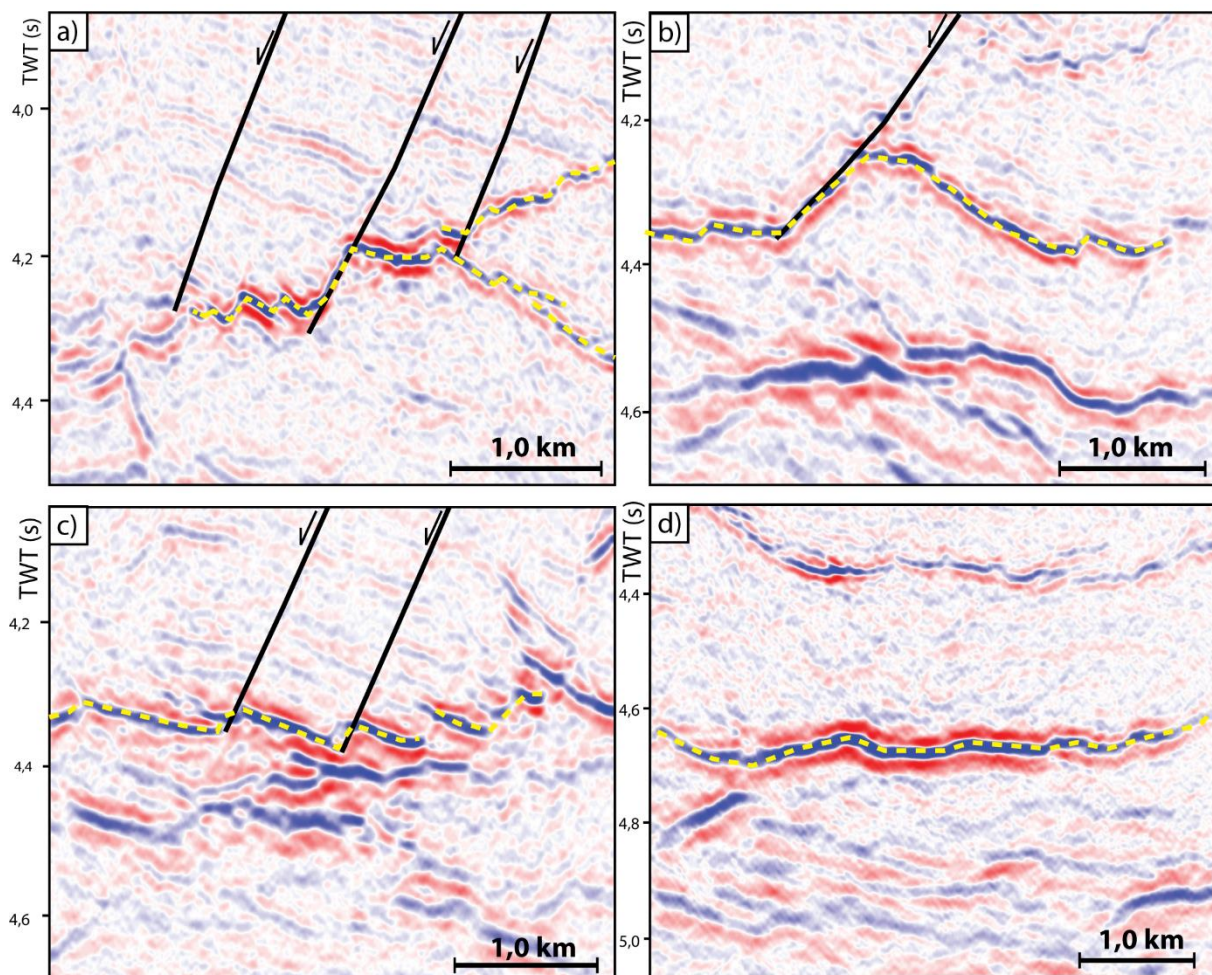


Figure 5.15: Different geometry of the deeply emplaced sill intrusions. a) This sill seems to be climbing the stratigraphy, and the sill clearly follows one of the faults. b) Sills follow layering in the stratigraphy and the fault plane. c) Same expression as sill in Fig. b, with more intrusions close to the main sill. d) Horizontal sill that most likely follow the stratigraphic layering. No faults are observed in close proximity to this sill.

Figure 5.15 shows the expression of some of the deep sills. Deep sill intrusions in the seismic data have different geometry. The sills display either a strata concordant geometry, or sills transgress upwards following faults. Where shallow intrusions mask the deeper intervals, only the deepest intrusions are imaged (from 4,5-5,5 s TWT, see Fig. 5.14b). These seem to display a flat geometry without much influence of faults (Fig. 5.15d). The deep intrusions in the interval between 4,0 – 4,5s TWT are more influenced by the faults. Some of them transgress up the stratigraphy by using fault planes (Fig. 5.15a-c).

5.3 Seismic modelling

The results of the seismic modelling are presented here. The modelling study has been carried out by varying parameters such as frequency and illumination angle (max dip angle), in order to study the effect of these parameters on the modelled seismic section. Various models have been run with frequencies between 10-40 Hz and illumination angles of 30°, 45° and 90° (perfect illumination), in addition to traditional 1D convolution. As explained in Section 3.2.1 the point spread function (PSF) is important to take into account when looking at seismic resolution limitation. The PSF is therefore used in this chapter to explain different resolution limitation in relation to both frequency and max dip angle. In the modelled images, blue corresponds to an increase in acoustic impedance.

5.3.1 Frequency

In real seismic data, frequency decrease with depth, and since deep intrusions are modelled, modelling was performed with both low and high frequencies in order to better compare the synthetic seismic to real seismic with low frequencies. Figure 5.16 shows seismic images with different seismic signal frequencies and the effect on the seismic resolution. Frequencies are in the range from 10-40 Hz. By comparison, the deep intrusions in the real seismic data from the Solsikke cube have a dominant frequency of c. 12,5 Hz. By varying the seismic signal frequency and comparing the resulting images demonstrate that the amount of geological detail resolved in the seismic can vary significantly. Figure 5.16 shows example of how sills will be imaged in 10, 20, 30 and 40 Hz respectively. The PSF for each model is plotted in each model, to give a sense of how the PSF influences resolution and illumination.

At 10Hz, none of the single sills are clearly resolved, except the 200 m thick sill emplaced into the Cretaceous succession, which is imaged with both top and base reflector. Sills are mostly tuned reflectors, and are therefore below the seismic resolvability. Sills are interfering with each other and the stratigraphy, which makes it hard to tell different sills and stratigraphy apart. Broken bridges are barely resolved or not resolved at all (Fig. 5.16b). The PSF at 10 Hz gives a lateral resolution of around 200 meters and a vertical resolution of 69 meters.

The 20 Hz modelled image shows more details than the 10 Hz image (Fig. 5.16c). The broken bridges are recognized, but there are still some interference between the different sills and stratigraphy. Most intrusions are still tuned reflectors, however the stratigraphy is imaged better.

Above 30 Hz (Fig. 5.16d), many of the details along the outcrop can be observed in the modelled seismic. Top and base reflection of the sills are mostly recognized, which mean that the modelled seismic is above the seismic resolvability. Broken bridges and single stratigraphic layers are clearly imaged. The PSF gives a vertical resolution of 23 m and a lateral resolution of 60 m. Thin sills are imaged as tuned reflectors. The 40 Hz seismic image (Fig. 5.16e) gives a detailed model that clearly resemble the input model. Steeply dipping intrusions are however not well images (Fig. 5.16e). These high frequencies modelled images are however not realistic, since it is very rare that real seismic data have these high frequencies at depths below 3 kilometers.

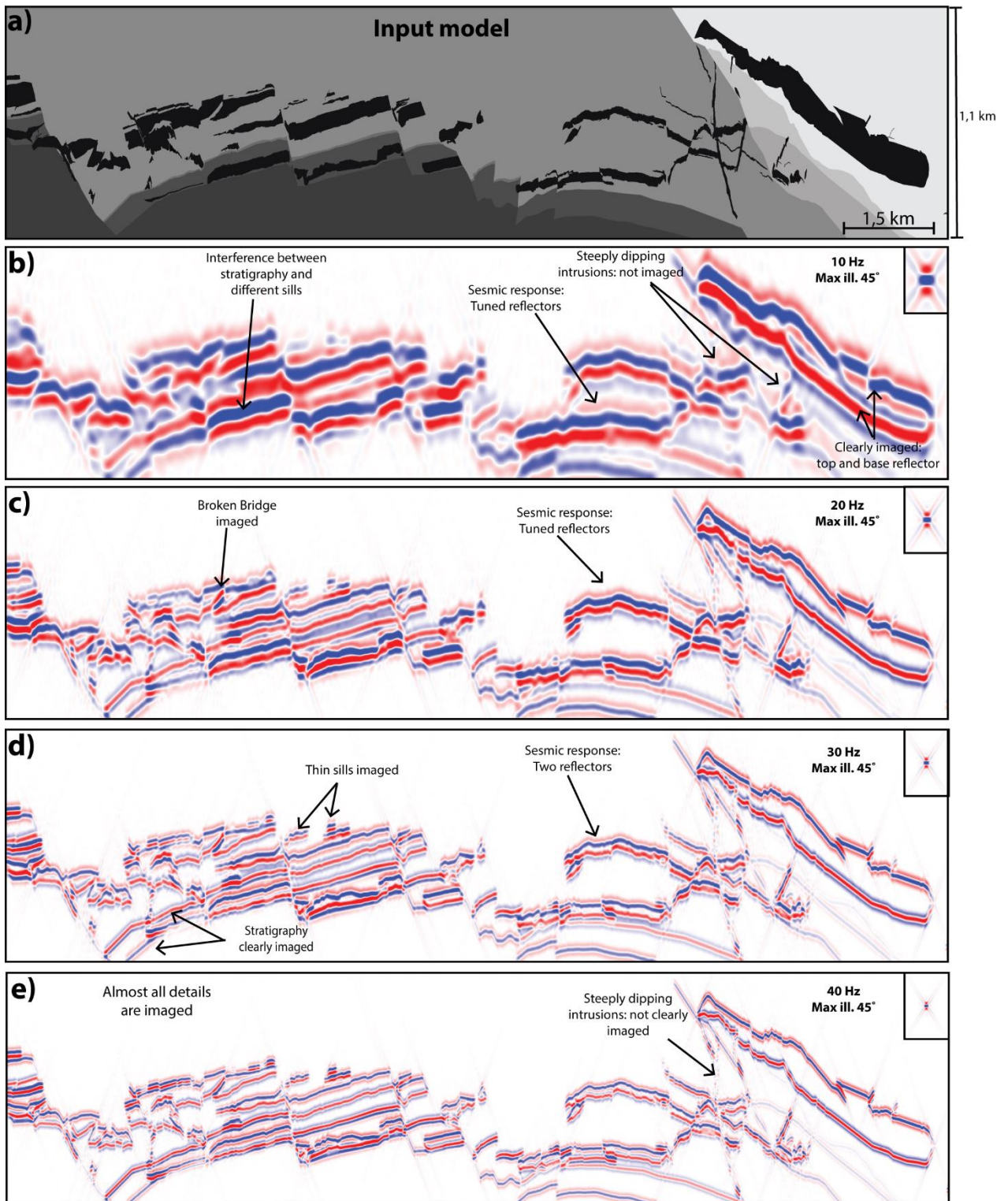


Figure 5.16: a) Overview of the Traill Ø outcrop model. b-e) Seismic images showing the effect of varying frequencies on seismic resolution. Each point spread function (PSF) is plotted in the top right corner to provide information of the seismic resolution. Maximum dip angle is set to 45°.

The post-magmatic normal faults are clearly seen in all the modelled images. These faults are recognized by clear offsets in the stratigraphy and the intrusions. On the contrary, it is hard to recognize the pre-magmatic faults with both high and low frequencies, especially the one fault with a dyke cutting across the fault. There can be several reasons for why the faults are not imaged. Firstly, the strong reflection from the intrusions might mask reflector stratigraphy. Limitation in lateral resolution when it comes to steeply dipping features are also an issue.

5.3.2 Maximum dip angle

Illumination angles of 30° , 45° and 90° are considered in Figure 5.17. A 1D convolution seismic section is also considered. The 2D convolution images obtained by varying the illumination (maximum dip angle) are showing significant differences in resolution and illuminated structures. The variable lateral resolution is here entirely due to variable illumination angle, since the frequency is set to 20 Hz in each of the modelled images.

Figure 5.17b illustrates the modelling result with perfect illumination. Note the lateral resolution of the PSF modelling compared to the 1D convolution in Figure 5.17a. Lateral reflectors are more continuous in the perfect illumination case, since no lateral resolution effects are taken into account in the 1D convolution

Figure 5.17c and d illustrate the modelling result with a max dip angle of 45° and 30° respectively. 30° max dip angle leads to lower lateral resolution (see PSF in Fig. 5.17d), and many of the steeply dipping layers are not imaged and are harder to observe than in the 45° modelled image.

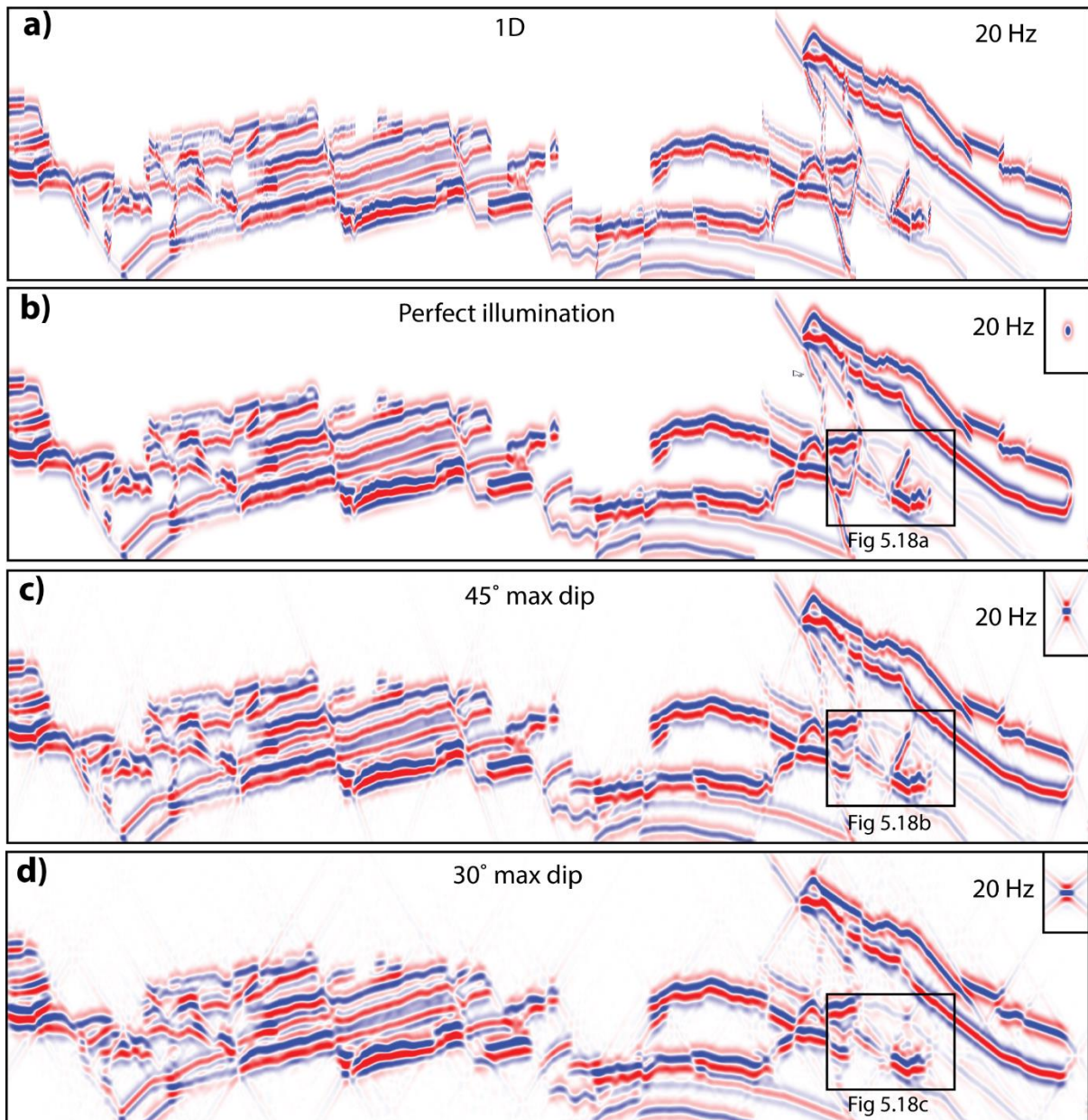


Figure 5.17 Synthetic seismic images demonstrate the influence of different max dip angle on the seismic resolution. a) Traditional 1D convolution. b) Perfect illumination case. The modelled images c) and d) show the effect by varying the max dip angle from 45° to 30°.

Figure 5.18 shows an example of one of the steep dipping dykes in the outcrop. Resolution of the dipping reflectors will be influenced by the degree of maximum dip angle, as the lateral resolution will be lower with a smaller max dip angle. In the perfect illumination case, the lateral resolution will be $\lambda/4$ and the lateral resolution for maximum dip angles of 45° and 30° will be larger than $\lambda/2$. The PSF shows how the vertical resolution is the same in both cases, however the lateral resolution is poorer in the 30° max dip.

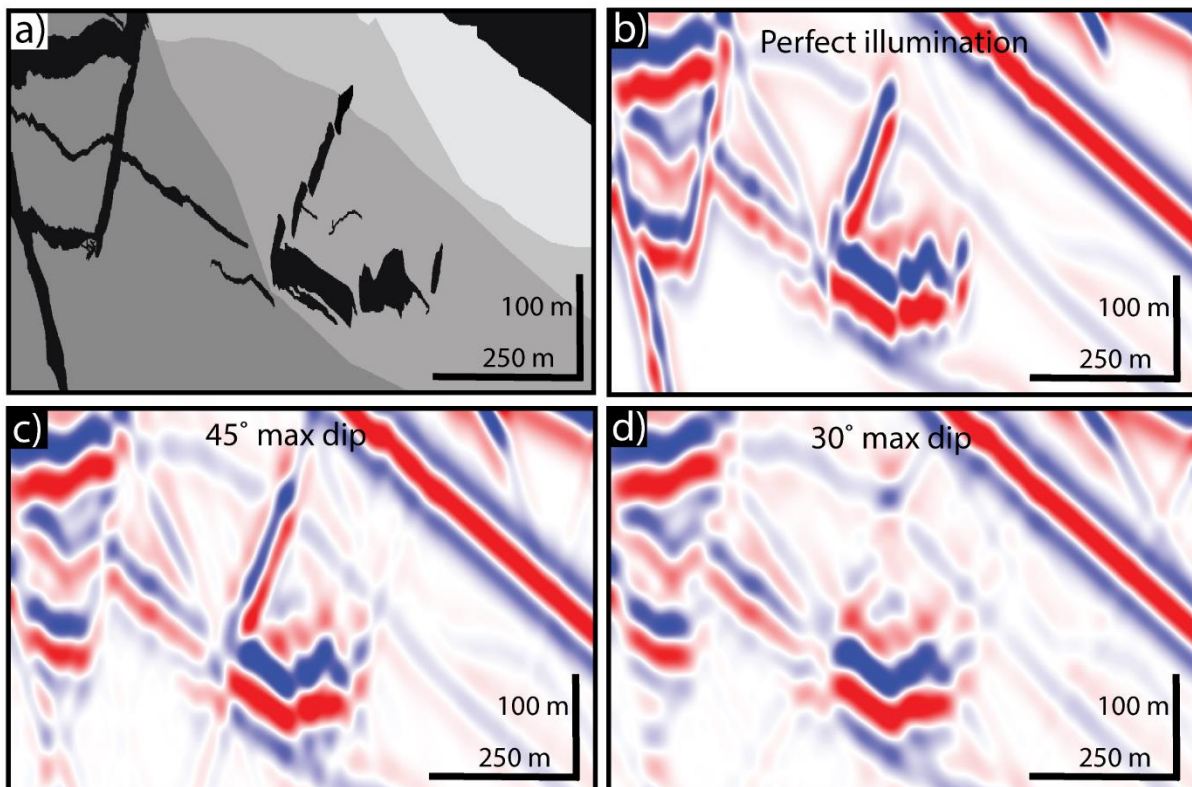


Figure 5.18: Effect on Dyke B (Fig. 5.7a) by varying the max dip angle. a) Input model. b) The perfect illumination replicates the dyke very well. c) 45° illumination image the dyke quite well. Note the poor imaging of the dyke with d) 30° max dip.

It is apparent that there is a significant improvement in resolution with higher max dip angles, and there is large limitation in resolution below a max dip angle of 30°. The perfect 90° angle of illumination creates the clearest images, but perfect illumination cases are not applicable in real seismic data.

5.3.3 Layered model

The two last models showing effects of frequency and maximum dip angle were created with homogenous host rocks. This is a simplification to make the modelling and the interpretation of the outcrop less time-consuming. However, in the real outcrop data the host rocks are heteroliths, which are taken into consideration in this last model. Layers of mudstone are included into the homogenous sandstone intervals, to observe how this affect the modelling of the intrusions.

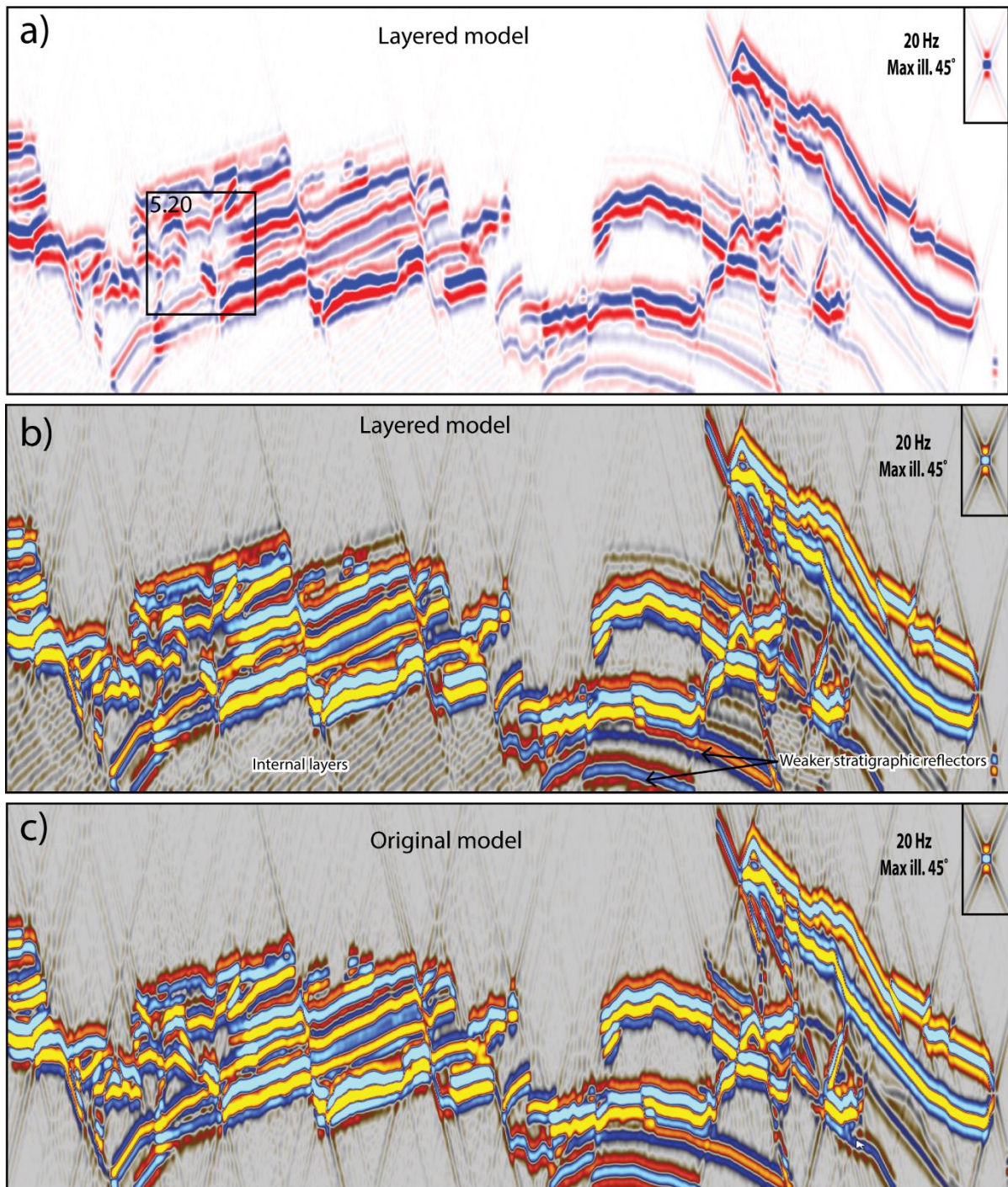


Figure 5.19: a) and b) Seismic modelling with layered host rocks with different color scale. The layered model is compared to c) a homogenous host rock model. No apparent changes are recognized, except the weaker stratigraphic reflections marked by the arrow. In a) the layers are poorly imaged, but when the color scale is changed b) the internal layers are much clearer.

No drastic changes are seen in the layered model (Fig. 5.19 a and b) compared to the model without layers (Fig. 5.19c). The reflections of the layers are clearly seen where there are no intrusions. By changing the color scale and amplify the amplitude, the internal layering is much clearer (Fig 5.19b). Some of the stratigraphic reflectors become weaker compared to the

model without internal layering (Fig. 5.19b). This can be due to interference between stratigraphic boundaries and internal layers. In this layered model, there also seem to be some interference between the layers and intrusions as well, which leads to different expression in the seismic (Fig. 5.20). The internal layers seem to interfere destructively with the intrusion, and making a gap in the reflection.

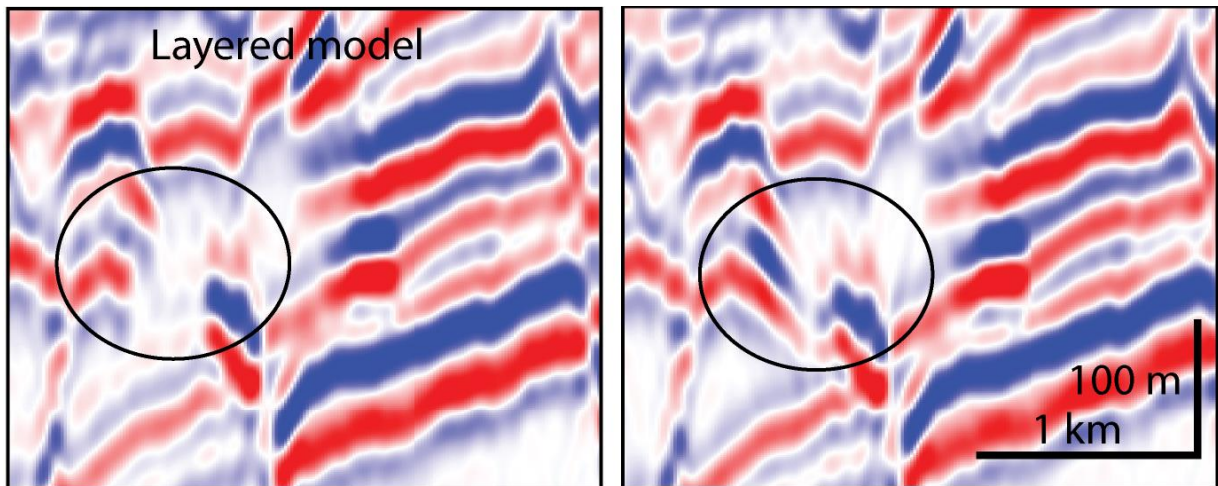


Figure 5.20: The effect of destructive interference between intrusions and stratigraphic layers.

6 Discussion

A number of questions arise from this large-scale study of igneous intrusions, and in this section, the evaluation and discussion of the results will be addressed. The stratigraphic controls on sill emplacement (6.1), the comparison between outcrop data, seismic modelling and real seismic data will be considered (6.2, 6.3).

6.1 Stratigraphic controls on sill emplacement

No other study has done work on deeply emplaced intrusions in the field, where a large number of normal faults influence the intrusions, and where there are intrusions that are emplaced into host rocks spanning a large age range. The intrusions on Traill Ø are exceptionally well exposed. It is therefore an excellent opportunity to investigate stratigraphic controls on sill emplacement, and how these are similar or different from other studies on deeply emplaced intrusions. The dolerite intrusions on Traill Ø show many similarities with the intrusions from Jameson Land, East Greenland, south of Traill Ø (Eide et al. 2017). They share the fact that intrusions seem to prefer to be emplaced in mudstone and heteroliths. The intrusions on Traill Ø however, are thicker than the ones in Jameson Land, and are influenced by faults. Sills from the Theron Mountains in Antarctica (Hutton 2009) also show similar geometries to the intrusions described in this thesis. They are planar parallel bodies, lateral continuous and show brittle emplacement structures such as steps and broken bridges.

6.1.1 Emplacement model

A number of emplacement models have been proposed for the emplacement of sills, largely based on outcrop observation supported by numerical and analogue modelling (e.g. Pollard 1973, Rubin 1993, Schofield et al. 2012b, Abdelmalak et al. 2012, Spacapan et al. 2016). The study of the intrusions and host rocks on Traill Ø allows us to compare to other studies and other existing magma emplacement models. The observations from this study are in agreement with the LEFM-Splitting Model (Pollard 1973, see Section 3.2.1). In this model, sill tips will propagate by tensile fracture of the host rock and the magma will inflate, causing the roof to be uplifted with no or minor deformation. In the Traill Ø outcrop, there is no discernible

deformation around the margins of the sills or ahead of the sill tips on the scale of the dataset in this study. The vertical thickness of the sills seems to have been accommodated by uplift of the overlying strata. A good example of the propagation of the sill tip and the vertical inflation of the sill along the outcrop is shown in Figure 5.9d. Magma has propagated into the fracture and later inflated vertically, causing the host rock (interbedded sandstone and mudstone) to be uplifted.

Previous studies on sills emplaced at depth comparable to those at Traill Ø, show similar behavior (Hutton 2009, Eide et al. 2017), where there is no or little deformation around the sill tips. These deeper sill intrusions are mostly emplaced into well-consolidated host rock, and at these depths, the high mechanical strength of the host rock, the low pore fluid volume and the low porosity can prohibit deformation. On the contrary, sill emplacement at shallow depth (0-1,5 km) is often explained by inelastic emplacement models as the propagation of magma is accommodated by host rock deformation (Schofield et al. 2010, Schofield et al. 2012b, Magee et al. 2016).

6.1.2 Broken bridge deformation during large vertical inflation

Broken bridges have been studied in a few different outcrops, for example the Theron Mountains in Antarctica, Isle of Skye in Scotland and Jameson Land in Greenland (Hutton 2009, Schofield et al. 2016, Eide et al. 2017). The sills at Traill Ø are significantly thicker than the sills in Jameson Land and Isle of Skye, and are of around the same thickness as the bridges from Theron Mountains.

The formation of broken bridges is described in Section 3.1 (c.f Hutton 2009, Schofield et al. 2012b, see Fig. 3.1b). However, further inflation of the magma than described in these and increased thickness of the bridge can result in an accommodation problem in the hinge zone. This can lead to deformation close to the hinge zone. The broken bridge (Fig. 5.6b) can develop thrust faults in the outer bend of the bridge in response to this accommodation problem (Fig. 6.1d). No previous work has shown this deformation feature. The broken bridge at Traill Ø has been bent up to c. 40° (Fig. 5.6b). In the studies done by Eide et al. (2017) and Schofield et al. (2016), the opening angle of the broken bridges are mostly small, in the order of c. 5-10°. There seem to be no accommodation problems associated with these low opening angles.

Hutton (2009) described large broken bridges, but these bridges seem to behave differently from the bridges at Trill Ø. Instead of thrusting in the hinge line, broken bridges are bent and folded. Many bridges also have melt trails and some bridges show evidence of partial melting, which could be a result of melting of host rock due to hot magma or abundant heat due to large magma-volumes. The sills in the Theron Mountains attain a thickness of 160 m (Hutton 2009), making the last hypothesis probable.

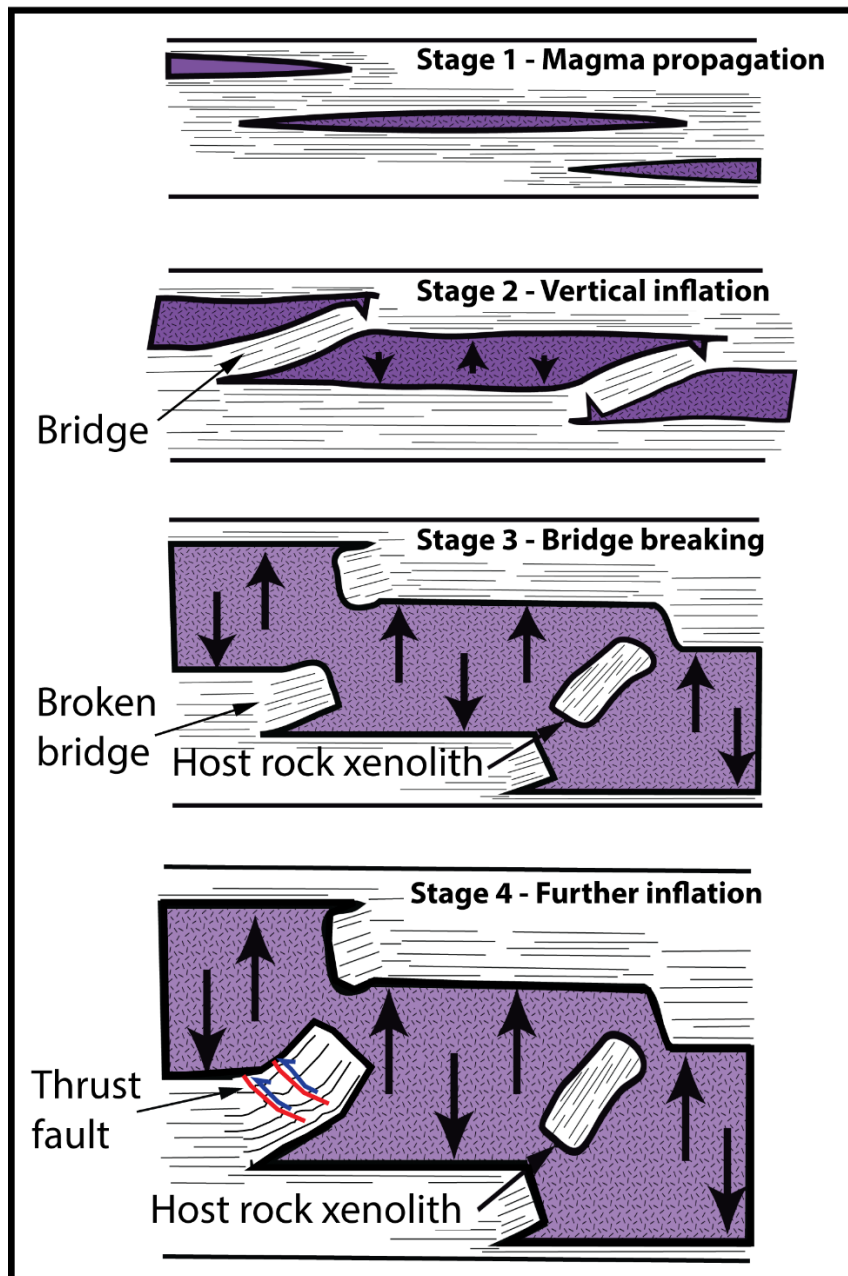


Figure 6.1: Broken bridge development. Stage 4: Lack of accommodation space in the hinge line of the host rock as the magma inflates, can lead to folding and thrust faults in the hinge line. Modified from Eide et al. (2017).

6.1.3 Emplacement mechanism and preferred intervals

Generally, the sills exhibit a layer parallel geometry along the studied outcrop on Traill Ø, which are expected for deeply intruded sills propagating in brittle host rock (Schofield et al. 2012b). The presence of morphological features such as steps and broken bridges, which are related to brittle fracture propagation in host rock, parallel to the outcrop (Fig. 3.1 and Fig. 5.6) indicate that the magma propagation direction was approximately perpendicular to the outcrop (Hutton 2009, Schofield et al. 2012b). According to Stemmerik et al. (1993), the host rock in this area has a burial depth of c. 1, 5 - 3 km at the time of magma emplacement. This study is based on the vitrinite reflectance data from the upper Permian Ravnefjeld Formation. However, by studying the cross sections from Parson et al. (2017), the burial depth of the Permian succession assumes to be c. 4 km at the time of magma emplacement. This is based on the basaltic lava flows in Leitch Bjerg and Kap MacKenzie on NE Geographical Society Ø, north of Traill Ø (Fig. 2.2) that are of equivalent age with the intrusions emplaced into the host rock. At this depth, host rocks are well consolidated, therefore sill intrusions in these sequences are being dominated by brittle emplacement structures, as the host rocks were too cemented and mechanically strong to behave in a ductile manner.

In addition, features typical for sills propagating in non-brittle rocks, such as fingers and lobes, have not been observed, indicating that the intrusions have propagated into well-consolidated sediments. Structures related to non-brittle host rocks are most common when sills are emplaced closer to the surface (Hansen and Cartwright 2006, Schofield et al. 2012b, Magee et al. 2016).

From the work presented in the results, host rock lithology plays an important role in sill morphology and emplacement of intrusions. Numerous other studies have shown that sill emplacement is dependent on host rock properties (e.g. Thomson 2007, Schofield et al. 2012b, Eide et al. 2017). Sill intrusions are emplaced along the stratigraphy along the entire outcrop. They seem to prefer some stratigraphic intervals more than others (Fig. 5.8b), and within each stratigraphic interval they prefer specific horizons. There are five intervals where the intrusions are emplaced: Interbedded sandstone, mudstone and coal in the Traill Ø Group (Carboniferous), carbonates and evaporites in Foldvik Creek Group (Permian), interbedded sandstone and mudstone in the Wordie Creek Formation (Triassic), Jurassic and Triassic

homogenous sandstone and Cretaceous mudstone. How and why the intrusions are emplaced into one or several levels along the outcrop are discussed below.

Permian:

The intrusions emplaced into the Permian succession prefer the lowermost part of the succession, directly above the Huledal Formation, and intrusions follow this interval as long as it is emplaced into the Permian succession. This interval is the Kartstryggen Formation, which is mainly composed of limestone and in some places gypsum along the East Greenland Margin (Surlyk 1990). In one area, this intrusion within the Triassic Karstryggen Formation behaves differently (Fig. 5.10b). This behavior is hard to explain, but it may be due to the presence of gypsum. A previous study by Schofield et al. (2014), shows evidence that magma has the ability to heat hydrous salts and make it flow. Gypsum is a hydrous salt, and will start to melt between 100 and 150°C (Schofield et al. 2014), but since there is no evidence of non-brittle emplacement structures such as perperite or magma fingers in this interval (Schofield et al. 2012b, Schofield et al. 2014), the intrusions are presumable not intruded directly into a pure gypsum succession. However, it could be that the interval contains at least some amount of gypsum, and it is therefore easier for the intrusions to be emplaced within this specific interval.

Triassic and Carboniferous:

The intrusions within the Triassic Wordie Creek interval have been emplaced into several different levels along the outcrop, in contrary to the Permian interval. The Triassic deposits consist of interbedded sandstone and mudstone. Therefore, intrusions will be emplaced in different levels, wherever the host rock is a bit weaker, commonly within a mudstone layer. Laterally emplaced intrusions are known to exploit mudstone horizons (Mudge 1968), because they can act as zones of weakness. However, it seems that the intrusions have not followed the most homogenous mudstone layers within the Triassic. Rather, it appears that sills are preferentially emplaced where there are thin sandstone and thin mudstone layers interbedded.

Broken bridges are only seen in the Triassic deposits. According to Hutton (2009), bridges are typically composed of sandstone/siltstone with thin shaley layers and lamina. Pure shale bridges are very rare, but are observed in small-scale by Schofield et al. (2016). This is consistent with the bridges along the outcrop at Traill Ø, because they are dominated by sandstone interbedded with mudstone. The fact that bridges only are found within the Triassic unit, might indicate that the lithological contrast between units within the Triassic is low, and there is weak anisotropy of the host rock. This can lead to propagation of magma in several different intervals within this unit, which might lead to the formation of bridges when the vertically offset of minor sills coalesce as they grow (c.f. Fig. 6.1).

Similar to the Triassic, the Carboniferous succession consists of interbedded sandstone and mudstone. However, the sills in the Carboniferous succession only account for 2,4 % of the entire interval, and intrusions are only exposed near the top of the outcrop, leaving a large part of the Carboniferous un-intruded. The intrusions show common splays, and stepping up in the stratigraphy. This can be due to strongly interbedded alternating sandstone and mudstone leading to strong anisotropy between the different layers.

Jurassic and Triassic (Pingo Dal Group):

Within the more homogenous sandstone units, the sills have no preferred interval and they transgress out of the interval over short distances as dykes (See Fig. 5.7, Dyke B). This suggests that intrusions do not prefer sandstone intervals and lack of strong lithological contrasts to follow or exploit. The sills emplaced into homogenous sandstone described from Jameson Land are also transgressing out of the sandstone interval over short distances (Eide et al. 2017).

Cretaceous

Within the Cretaceous mudstone interval only one intrusion is emplaced along the outcrop, and the proportion of intrusions within Cretaceous deposits is large (Fig 5.8b). The intrusion makes up almost 50 % of the entire Cretaceous interval, and the intrusion occurs right above the Base Cretaceous Unconformity. This is in agreement with Parson et al. (2017), which state that the thickest sills on Traill Ø occur above the Base Cretaceous Unconformity and the intrusions within this interval can reach thicknesses of 300 meters. These thick sills are rarely

observed in field, however the Ferrar dolerite sills from the McMurdo Dry Valley, Antarctica can reach thicknesses of 500 meter (Hersum et al. 2007). It has been widely reported that sills have a tendency to prefer mudstone horizons (Pollard et al. 1975, Thomson 2007, Magee et al. 2014, Eide et al. 2017), because mudstone has a strong anisotropy and it is easier for intrusions to follow the mudstone layers in the horizontal plane than the vertical (Mudge 1968). It seems that generally thick sills are emplaced into extensive mudstone succession.

6.1.4 Connectivity of sill complexes

Sill complexes have recently been shown to play a more important role in magma ascent through basins than previously believed (Cartwright and Hansen 2006, Schofield et al. 2015, Magee et al. 2016). These networks are typically dominated by mafic, relatively thin (<100 m thick) sills (Magee et al. 2016, Smallwood et al. 2002, Schofield et al. 2015), while more viscous magma in intermediate to felsic magma systems tends to form thick laccoliths and plutons (Johnson and Pollard 1973). The thick mafic sills observed in Trail Ø can however indicate that also thicker sills may play a major role in these mafic sill complexes. The intrusions within the studied outcrop show some connectivity with climbing sills and dykes transferring magma to higher levels within the outcrop, but most of the sill intrusions are flat over large distances. This is in agreement with work done on other deeply emplaced intrusions (Hutton 2009, Eide et al. 2017).

Observations from the Svinhufvuds Bjerge outcrop indicate that the dykes are a minor component of the entire outcrop. Other field observation, also support this observation (Leat 2008, Muirhead et al. 2014, Eide et al. 2017). It is therefore presumable to believe that sills mainly accommodate magma transport through the outcrop.

Along the outcrop, two dykes follow the only two reverse faults in the outcrop. How these reverse faults originate are not certain, however they can be a result of compression as the pluton on Kap Simpson was emplaced (e.g. Parsons et al. 2017, c.f. Traill Ø geological map Fig. 2.2). In this case, these dykes will have to be younger than the rest of the intrusions. They may thus be related to the second magmatic period on Traill Ø, which formed smaller volumes of alkaline dykes and the two large syenite complexes around c. 36 Ma (Price et al. 1997, see Section 2.3). There have been no dating of these dykes, therefore one cannot say for certain

what age these dykes are. Walker et al. (2017) observed a relationship between reverse faults cutting sills in the San Rafael subvolcanic field in Utah in an overall extensional system, and suggested that sill geometry provides an indication of regional stress during emplacement, and not all sill geometry is the response of bedding. Crosscutting relationships in this area provide evidence for sill emplacement during horizontal shortening in a tectonically inert or extensional system (Walker et al. 2017).

6.1.5 Effect of pre-magmatic faults on primary intrusive geometry

It can sometimes be hard to explain why intrusions follow one specific layer; however, it can seem that intrusions exploit weaknesses within the host rock, whether it is a mechanical weak layer (see Discussion 6.1.3) or a fault. Pre-existing faults can exert a major influence on magma flow pathways and emplacement of intrusions as they can offer paths of least resistance to magma intruding through a basin (Gaffney et al. 2007, Magee et al. 2013).

Along the outcrop, one well-exposed intrusion follows a large-scale fault for part of its length, but leaves the fault at some point during its vertical ascent (see Fault 12 in Fig. 5.2 and Dyke C in Fig. 5.7). The intrusion originates from below the outcrop. The few other pre-magmatic faults along the outcrop (Fault 1,2,9 and 13 in Fig. 5.2) have not been exploited by intrusions. Where the intrusions crosscut through a fault (Fault 1, 9 and 13 in Fig. 5.2), it is possible that the reason for the lack of exploitation of faults, is mechanically similar lithologies at each side of the fault, or related to the magma propagation direction in relation to the fault plane (Magee et al. 2013). Magee et al. (2013) suggested that sills that approach a fault from the footwall side will continue to crosscut the fault, while if the sill approaches from the hangingwall side it is more likely to exploit the fault plane (Fig. 6.2).

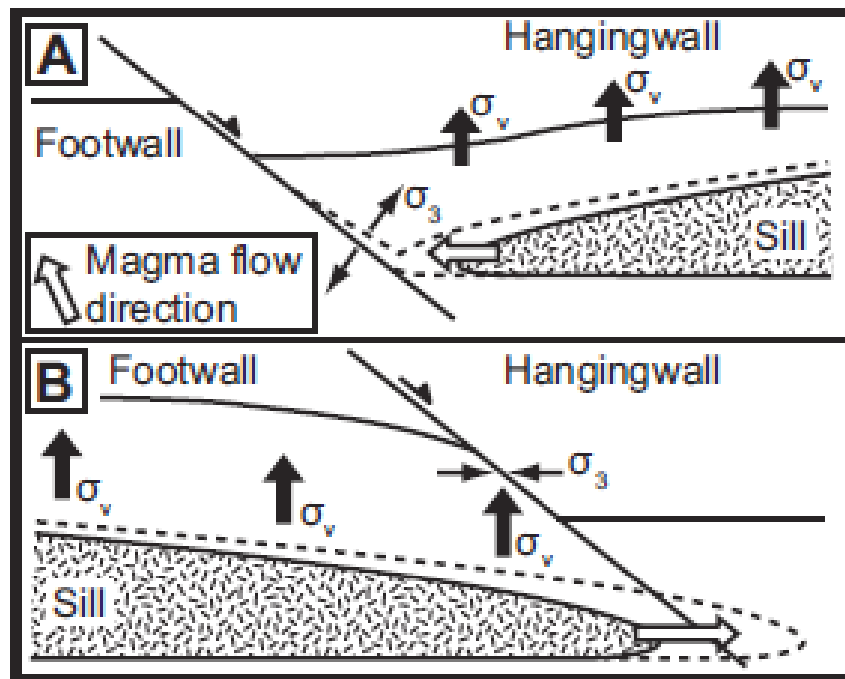


Figure 6.2: The difference in sill propagation pathways when sills are emplaced into the A) hangingwall and the B) footwall of a fault. Arrows show magma propagation direction. σ_3 is the minimum principal stress and σ_v are the vertical stresses. From Magee et al. 2013.

Intrusions in the Solsikke seismic survey also show this trend of intrusions following faults (Fig. 5.15a-c). The sills seem to have been emplaced either at the base of the faults in the seismic data, because no faults are imaged below these deep intrusions, or they are emplaced and have exploited faults. The outcrop data is only in 2D, however studies on intrusions following faults in seismic data can lead to a better understanding of the movement of magma as the movement of magma can be studied in 3D.

From these data and a number of studies done on interaction between faults and intrusions in seismic data (Gaffney et al. 2007, Thomson and Schofield 2008, Magee et al. 2013), the presence of faults can modify the geometry of intrusions. Sills can climb fault planes and exploits faults where it is possible. In many cases, sills exploit inclined dips of the beds between faults, but in other cases, they cut straight trough. Sill intrusions can also exploit the edge of tilted fault blocks to climb to stratigraphically higher levels (Thomson and Schofield 2008).

6.2 Comparison between outcrop and modelled seismic

In this section, the discussion of how the synthetic seismic data relates to the outcrop model is presented. Synthetic seismograms can generally reproduce the geometry of the input intrusion model quite well, but it depends on seismic frequency and lateral resolution.

Studies on sill intrusions in seismic data have helped our understanding of sill complexes within sedimentary basin (e.g Hansen and Cartwright 2006, Schofield et al. 2015, Magee et al. 2016). However, interpretation of sills in seismic data depends on comparison with field analogues to interpret intrusion morphologies and features. The key problems associated with seismic data are the limitation in resolution. This resolution problem can be addressed by using seismic modelling to image the features with both high and low frequencies, which makes it easier to compare to the real seismic data (see Section 6.3).

As seen from the results, the seismic expression of different sill intrusions can vary in response to changes in frequency, thickness of the sills and the presence of interbedded strata. Frequencies above 20 Hz used in this study, generally reproduce the outcrop with a good amount of details. The host rocks in this case are homogenous and the individual sill geometries are particularly well defined. However if 10 Hz is used many of the small details are not preserved and there are a lot of tuning effects and interference between different reflectors. The variation in amplitude of the reflectors correspond to interference between the upper and lower reflections. This tuning response occurs below the limit of resolution/seperability, and is influenced by the sill thickness and frequency of the seismic data (Smallwood et al. 2002). The impedance contrast between sill intrusions and host rock and other sill intrusions can lead to interference, and lower or higher seismic amplitude of sill reflectors.

Figure 6.3 shows how the seismic modelling result (Section 5.3) relates and compares to the original outcrop on Traill Ø, by combining the modelled seismic in 20 Hz on top of the reflectivity model. The first thing to notice is that top and base sill reflectors interfere with each other, but in the case of thicker sills, the top and base of an intrusion are imaged (Fig. 6.3). Another observation is that the amplitude of sill reflectors seems to vary in strength along the outcrop. This can be due to constructive or destructive interference between i.e. thin sills

and a thicker main sill or between stratigraphy and sill reflectors (Fig. 6.3). This interference pattern seems to be related to the geometry of the sills and the spacing between individual sills. Figure 6.3 shows how two sills, one thin sill on top of a thicker sill, interfere with each other creating a reflector with a low amplitude compared to the other sills. It also shows constructive interference between a base sill reflection and top Permian reflection resulting in a strong amplitude. At frequencies above 20 Hz, it is possible to observe 5 m thin individual sills as tuned reflectors. However if these thin sills are close to another sill, they will not be imaged as individual reflectors, but interfere with the other sill.

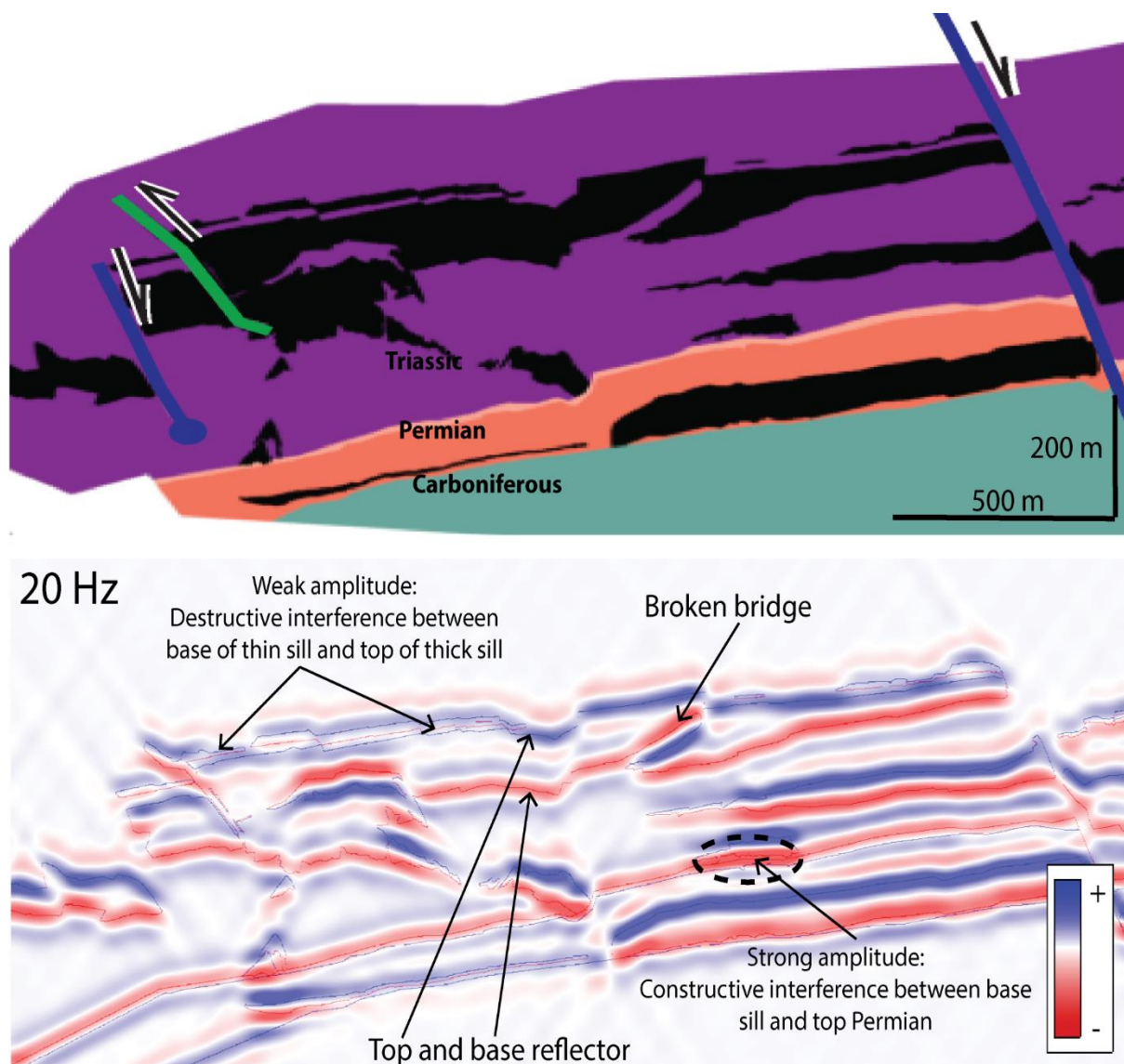


Figure 6.3 Modelled seismic overlain the reflection model. Upper figure showing outcrop with stratigraphy, sill intrusions and faults. Lower figure showing a combination of the modelled seismic data with a frequency of 20 Hz and the reflectivity model represented by thin lines. Note the variation in amplitude strength. The variations in amplitude strength are mostly due to constructive and destructive interference between different reflectors.

Broken bridges are well imaged and easy to recognize at this scale and frequency. However, the sill intrusions on Traill Ø and in the Theron Mountains (Hutton 2009) are thick, and the broken bridges are large compared to other settings, e.g. Jameson Land and San Rafael Swell (Eide et al. 2017, Walker et al. 2017). Since the intrusions on Traill Ø are much thicker than the sills in the other localities, broken bridges within them can be imaged more easily in seismic data. The broken bridge in Figure 6.3 consists of host rock and is shown as a downward decrease in seismic energy from the interface between the sill and the broken bridge. The broken bridge is therefore imaged as a red slightly dipping reflector below the top sill reflector (Fig. 6.3).

Magee et al. (2015) demonstrated that stratigraphic reflections from layered rocks could interfere with reflections generated at the intrusive contact of sills and may produce seismic artifacts that could be misinterpreted as real features imaged in seismic datasets. This can lead to apparent steps (pseudosteps) in climbing sills and dykes. In the layered model presented in Section 5.3.3, there is no evidence of such pseudosteps. There could be several reasons for this: (1) The acoustic impedance contrast is lower between the layers in the model presented in this thesis, (2) the ratio between sandstone and mudstone is much lower or (3) the use of 2D convolution instead of the 1D convolution used in Magee et al. (2015). However, another difference seen from the outcrop layered modelled is that intrusions may be influenced by destructive interference from the changing stratigraphic layering. The destructive interference seen in Figure 5.19 can be misinterpreted to represent a gap in the intrusion. Different sills may cause similar reflection geometries, but have quite different expression in outcrop data.

Pseudosteps can be important in some cases, e.g. when the contrast between the intrusions and the host rock is low. However, in this study, realistic velocities from well data have been used, and the result and the layered model show that the contrast between the dolerite sills and the sediments is too high, that the layering should be of much consequence.

6.3 Comparison between seismic modelling and real seismic data

In the previous section, the seismic modelling was compared with the outcrop model. This following section will examine the relationship between observation from outcrop, the

modelled seismic and the real seismic data from the Solsikke area in the Møre Basin. The target host rocks in the Møre Basin consist mostly of shales, while on Traill Ø there is a large variety in the stratigraphy in the area. This can also influence the geometry and morphology of sills. Post-magmatic faulting is more common in the Traill Ø area and they cut through the sill intrusions in the outcrop. Such post-magmatic faults are not observed in the Solsikke area.

Synthetic seismic can help and guide interpretation of different geological features in the subsurface. Not many other seismic studies have compared features seen in intrusions in real seismic with seismic imaging. Magee et al. (2015) have done a study on controls on expression of igneous sills in seismic by using 1D convolution modelling to image hypothetical cases of interaction between sills and host rock, and then comparing these synthetic seismograms with real seismic data. Other studies have compared intrusions in field directly with seismic observation (Schofield et al. 2012a, Magee et al. 2016).

In Figure 6.4, three examples of comparisons between features in modelled seismic and real seismic data are shown. The first example shows how an intrusion can follow a fault (Fig. 6.4a). Intrusions climbing faults are well known from the literature (Gaffney et al. 2007, Magee et al. 2013, Schofield et al. 2015). The outcrop at Traill Ø shows one of these intrusions that follow a pre-magmatic fault. The dyke is almost impossible to see in the modelled seismic even at high frequencies. In real seismic data, intrusions seem to follow fault as well. Sometimes the intrusions show a low amplitude, and it is therefore not easy to recognize some of these dykes in the seismic. Dykes that are obliquely dipping are normally not well imaged in seismic. This is due to the limitation in lateral resolution and the illumination angle (e.g. Lecomte et al. 2016). Dykes are normally too thin and steeply dipping to be imaged in seismic data (Planke et al. 2014). However, some of the intrusions are quite well imaged in the Solsikke data. This can be due to irregularities on the dykes margins, making it easier to image. It is reasonable to presume that many dykes that follow faults and dykes in general, are not imaged in the seismic, because of limitation in seismic resolution and illumination (Smallwood et al. 2002, Thomson 2007).

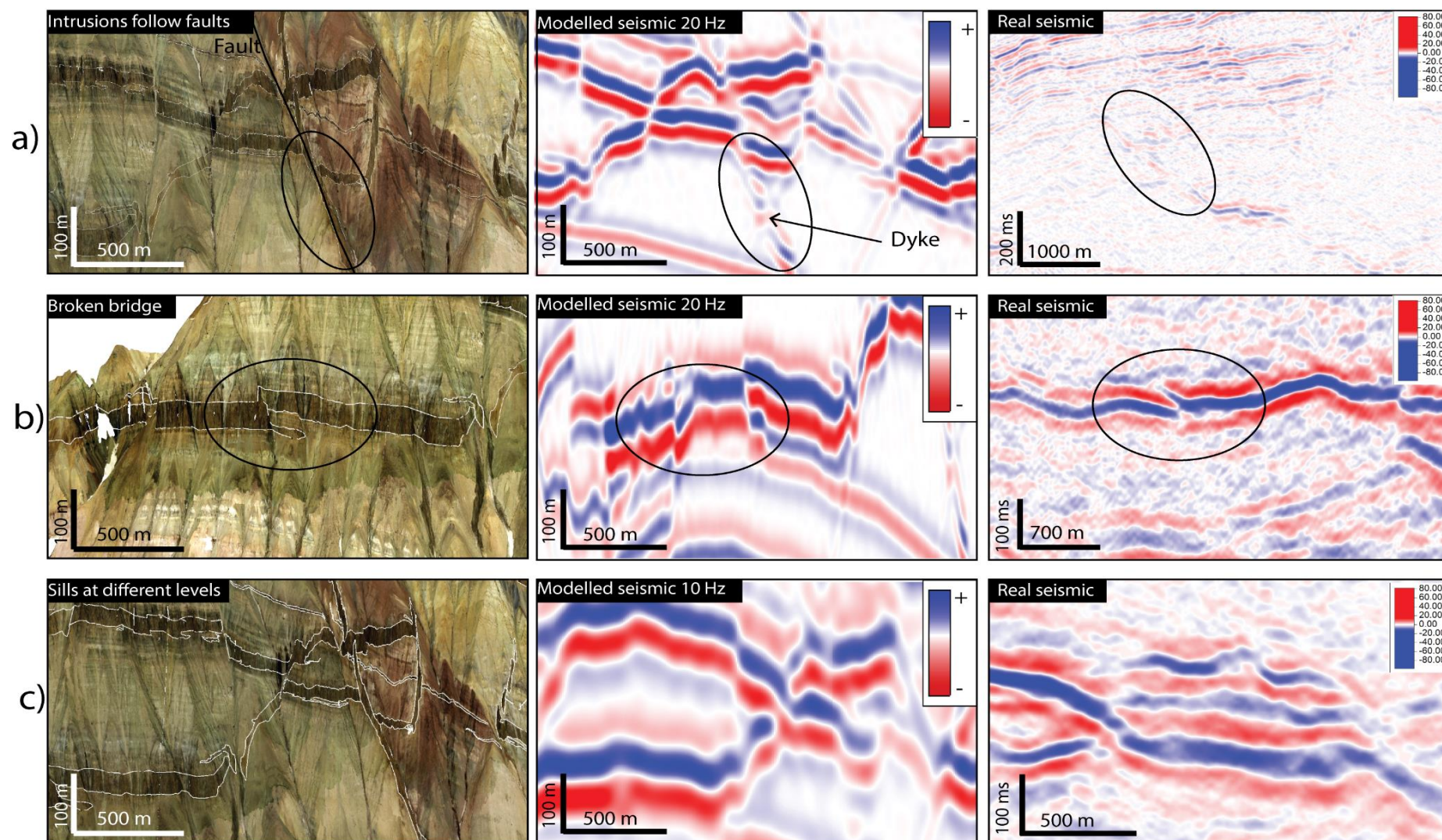


Figure 6.4: Comparison between intrusions in the outcrop data, the expression in synthetic seismic and seismic data from the Møre Basin. Examples of a) intrusion following a fault, b) broken bridge in seismic data and c) sills at different levels and complex interaction between sill intrusions.

The next example shows a broken bridge imaged at a frequency of 20 Hz (Fig. 6.4b). The sill reflector from a broken bridge in seismic shows a slight offset, that may resemble a small fault. This feature is also seen some places in the Møre seismic. Broken bridges imaged in seismic, are characterized by distinct separate magma lobes in regions away from the magma source, but closer to the source, the distinct magma lobes coalesce into a single reflection showing steps (Schofield et al. 2012a). In the Solsikke seismic, this trend is also shown a couple of places, when two distinct reflectors coalesce into one. From the modelled seismic, there is only observed either two distinct reflectors not connected or totally connected reflectors without the stepped appearance.

Broken bridges in mudstone are very rare (Hutton 2009), but are observed in small scale from Isle of Skye (Schofield et al. 2016). However, several broken bridges are observed in the seismic data from the Solsikke area, which are dominated by mudstone and siltstone. These bridges might indicate coarser grained areas within the mudstone. Since the broken bridges are imaged well in the synthetic seismic and in the seismic data, it is reasonable to assume that the intrusions in the Møre Basin have the same thickness as the intrusions on Traill Ø.

The last example shows how intrusions at different stratigraphic levels are imaged, and how intrusions may form complex network of sills (Fig 6.4b). In the modelled seismic with a frequency of 10 Hz, it is apparent that the actual complexity within the area is not preserved. The thinner sills are not imaged, and the main sills are imaged as tuned reflectors. By comparing this with real seismic from the Møre Margin, there is a possibility that also the real complexity of this network of sills is not well represented in the seismic either.

6.3.1 Resolution and detectability of sill intrusions

There are numerous rules of thumb for determining seismic detectability, and these will predict different thickness for the thinnest layer that may be imaged. Planke et al. (2005) suggested that the seismic detectability for sill intrusions is represented by $\lambda/10$. However, Sheriff and Geldart (1995) suggested that low impedance sands with a reasonable data quality could already be imaged at $\lambda/20$ to $\lambda/30$. It follows from this that due to the higher impedance contrast between host-rock and intrusions, intrusions can be imaged at lower thicknesses than of normal sandstone beds. In reality, there is no simple rule of thumb when it comes to seismic

detectability, because the seismic detectability depends on several factors: signal to noise-ratio in the data, acquisition, processing, and the acoustic impedance contrast between layers.

If the seismic detectability according to Planke et al. (2005) is used, the deep sills in the seismic data from the Møre Margin have a calculated detectability of c. 48 m and a vertical resolution of c. 120 m (see Section 5.2.2 for calculation). This detectability limit is significantly lower than other seismic studies done on sills, since most studies have focused on shallow sills. In the Solsikke 3D seismic survey on the Mid-Norwegian Margin (c.f. Section 5.2), all sills are imaged as tuned reflectors. It is therefore safe to assume that none of the sills are thicker than the resolution limit of 120 meters, and that the observed reflectors are above the detectability limit. In the published literature, the top and base reflectors of sill intrusions are very rarely observed. To my knowledge only laccoliths which typically are thicker than sills (Cruden et al. 2017), are observed to show both top and base reflector in seismic data (Jackson et al. 2013).

Intrusions along the Traill Ø outcrop make up 13 % of the outcrop. Even though sills generally are thick along the outcrop, by using the detectability limit of 48 m, only some of the sills in the area would be imaged in the subsurface at depths of c. 3 km. In the synthetic seismic generated however, some of the thin reflectors (often down to 5 m) are also imaged in seismic with frequencies of 10 and 20 Hz as weak reflectors. The modelling method used in this thesis does not show any acquisition noise, and it will not lose frequencies below the intrusions. Therefore, thin intrusions with a high impedance contrast can be imaged. This depends on the seismic quality of the data, and if the quality is good, intrusions below the detectability limit suggested by Planke et al. (2005), which is $\lambda/10$, can be imaged because of the high impedance contrast.

Intrusions can also mask reflections of deeper sills, causing deeper sills with thicknesses above the vertical resolution to not be imaged. Bore hole data have suggested that as much as c.80 % of intrusions are not imaged in seismic as they are below the limit of detectability in seismic data (Schofield et al. 2015). This implies that the deeply emplaced sill intrusions observed in the Møre Basin are only a small part of the entire volume of sill intrusions.

7 Conclusions and further work

7.1 Conclusions

This thesis has presented exceptionally well-exposed intrusions along a virtual outcrop at Traill Ø, East Greenland, and used it as an analogue for seismic data from the Møre Margin. A better understanding of the controls on deeply emplaced intrusions and the expression of thick sill complexes in seismic data has been achieved by using outcrop data and seismic modelling. The result and discussion in this thesis have led to the following conclusions.

- 1) Lithology has an important control on the emplacement mechanisms of sill intrusions, and the Traill Ø outcrop shows a large range of different lithologies. Sills preferentially exploit extensive thick mudstone units, where they commonly form thick intrusions, or thinly bedded sandstone and mudstone units. They also seem to prefer carbonate/evaporite units. Sills do not prefer homogenous sandstone as sill intrusions transgress out of sandstone units over short distances.
- 2) Deep sill intrusions are mostly emplaced along stratigraphic layers and show mainly planar parallel sill geometries. Features like broken bridges and steps show that the intrusions are emplaced into a brittle host rock.
- 3) Pre-existing faults can exert a major influence on the emplacement mechanism of sill intrusions, and intrusions can exploit faults as they can offer least resistance paths through sedimentary basins.
- 4) Deeply emplaced intrusions have propagated by elastic tensile fracture, as magma propagation is accommodated by host-rock uplift with no or minor deformation.
- 5) Comparison between outcrop data and synthetic seismic can improve mapping of intrusions in seismic data significantly.
- 6) Sill intrusions are often well imaged in seismic data even when they are below the resolution, due to strong impedance contrast between intrusions and host rock. The detectability limit for intrusions are much higher than for siliciclastic rocks as the impedance contrast on intrusions are generally high.

- 7) Thin sills and steeply dipping intrusions are commonly not imaged in seismic, and it can be difficult to know their presence in seismic data, which can lead to the underestimation of sills in the subsurface.

This thesis has shown the importance of the emplacement and geometry of deep sill intrusions in sedimentary basins on volcanic rifted margins. By understanding host rock lithology, pre-existing structures and the emplacement mechanisms, it is possible to predict the sill intrusion geometry and expression in seismic data. The limited seismic coverage of deep sill complexes in the subsurface can be strengthened by correlation between outcrop, synthetic seismic and seismic data.

7.2 Further work

Igneous sill complexes have a high degree of complexity, and this thesis is a contribution to the understanding of these. However, the following future work ideas could improve and extend the study of sill intrusions on Traill Ø, and improve knowledge on sill complexes in general.

- Fieldwork and stratigraphic logging of the host rock in the study area would lay more confidence into the interpretation, and make the connection between host rock and emplacement morphology clearer.
- Study small-scale intrusions structures and deformation on the sill margins. It would be interesting to observe how these relates to the linear elastic fracture model for sill emplacement and the large-scale geometry of the sills.
- Dating of the two dykes crosscutting the sills, in order to constrain their age, and find out if they are related to the first or second period of magmatism.
- Seismic modelling of sill complexes with generally thin sills, and comparing this with this study on thick sill intrusions.
- More focus on understanding deep sill intrusions in seismic data, as most of the work done in seismic data until now focuses on shallow sills.

References

- Abdelmalak, M. M., R. Mourgues, O. Galland & D. Bureau (2012) Fracture mode analysis and related surface deformation during dyke intrusion: Results from 2D experimental modelling. *Earth and Planetary Science Letters*, 359-360, 93-105.
- Berger, D. & W. Jokat (2008) A seismic study along the East Greenland margin from 72°N to 77°N. *Geophysical Journal International*, 174, 733-748.
- Bjerager, M., L. Seidler, L. Stemmerik & F. Surlyk (2006) Ammonoid stratigraphy and sedimentary evolution across the Permian–Triassic boundary in East Greenland. *Geological Magazine*, 143, 635-656.
- Blakey, R. 2012. <https://deeptimemaps.com/europe-series-thumbnails/>. (Accessed 04.01.17)
- Brekke, H. (2000) The tectonic evolution of the Norwegian Sea Continental Margin with emphasis on the Voring and More Basins. *Geological Society, London, Special Publications*, 167, 327-378.
- Brekke, H. & A. Nøttvedt (2000) The tectonic evolution of the Norwegian Sea continental margin with emphasis on the Voring and More basins. *Geological Society Special Publications*, 167, 327-378.
- Brooks, C. K. (2011) The East Greenland rifted volcanic margin. *Geological Survey of Denmark and Greenland Bulletin*, 24, 1-96.
- Bryan, S. E. & L. Ferrari (2013) Large igneous provinces and silicic large igneous provinces: Progress in our understanding over the last 25 years. *The Geological Society of America Bulletin*, 125, 1053-1078.
- Buckley, S., J. Vallet, A. Braathen & W. Wheeler (2008) Oblique helicopter-based laser scanning for digital terrain modelling and visualisation of geological outcrops. *International Archives of the Photogrammetry, Remote Sensing and Spatial Information Sciences*, 37.
- Buckley, S. J., T. H. Kurz, J. A. Howell & D. Schneider (2013) Terrestrial lidar and hyperspectral data fusion products for geological outcrop analysis. *Computers & Geosciences*, 54, 249-258.
- Bugge, T., J. Ringas, D. Leith, G. Mangerud, H. Weiss & T. Leith (2002) Upper Permian as a new play model on the mid-Norwegian continental shelf: Investigated by shallow stratigraphic drilling. *AAPG bulletin*, 86, 107-127.
- Cartwright, J. & D. M. Hansen (2006) Magma transport through the crust via interconnected sill complexes. *Geology*, 34, 929-932.
- Chevallier, L. & A. Woodford (1999) Morpho-tectonics and mechanism of emplacement of the dolerite rings and sills of the western Karoo, South Africa. *South African Journal of Geology*, 102, 43-54.
- Christiansen, F., S. Piasecki, L. Stemmerik & N. Telnæs (1993) Depositional environment and organic

- geochemistry of the Upper Permian Ravnefjeld Formation source rock in East Greenland. *AAPG Bulletin*, 77, 1519-1537.
- Cruden, A., K. McCaffrey & A. Bungler. 2017. Geometric scaling of tabular igneous intrusions: Implications for emplacement and growth. In *Advances in Volcanology*.
- Dalland, A., D. Worsley & K. Ofstad. 1988. *A Lithostratigraphic scheme for the Mesozoic and Cenozoic succession offshore mid- and northern Norway*. Oljedirektoratet.
- Domenico, S. N. (1984) Rock lithology and porosity determination from shear and compressional wave velocity. *Geophysics*, 49, 1188-1195.
- Eide, C. H., N. Schofield, D. A. Jerram & J. A. Howell (2017) Basin-scale architecture of deeply emplaced sill complexes: Jameson Land, East Greenland. *Journal of the Geological Society*, 174, 23.
- Gaffney, E. S., B. Damjanac & G. A. Valentine (2007) Localization of volcanic activity: 2. Effects of pre-existing structure. *Earth and Planetary Science Letters*, 263, 323-338.
- Galland, O., S. Burchardt, E. Hallot, R. Mourgues & C. Bulois (2014) Dynamics of dikes versus cone sheets in volcanic systems. *Journal of Geophysical Research: Solid Earth*, 119, 6178-6192.
- Hald, N. & C. Tegner (2000) Composition and age of tertiary sills and dykes, Jameson Land Basin, East Greenland: relation to regional flood volcanism. *LITHOS*, 54, 207-233.
- Hansen, D. M. & J. Cartwright (2006) Saucer-shaped sill with lobate morphology revealed by 3D seismic data: implications for resolving a shallow-level sill emplacement mechanism. *J. Geol. Soc.*, 163, 509-523.
- Hansen, J., D. A. Jerram, K. McCaffrey & S. R. Passey (2009) The onset of the North Atlantic Igneous Province in a rifting perspective. *Geol. Mag.*, 146, 309-325.
- Herron, D. A. 2011. *First steps in seismic interpretation*. Society of Exploration Geophysicists.
- Hersum, T. G., B. D. Marsh & A. C. Simon (2007) Contact Partial Melting of Granitic Country Rock, Melt Segregation, and Re-injection as Dikes into Ferrar Dolerite Sills, McMurdo Dry Valleys, Antarctica. *Journal of Petrology*, 48, 2125-2148.
- Holford, S. P., N. Schofield, C. A. L. Jackson, C. Magee, P. F. Green & I. R. Duddy. 2013. Impacts of igneous intrusions on source and reservoir potential in prospective sedimentary basins along the western Australian continental margin. In *West Australian Basins Symposium. Proceedings of the Petroleum Exploration Society of Australia Symposium, Perth, WA*, 1-12.
- Hutton, D. (2009) Insights into magmatism in volcanic margins: bridge structures and a new mechanism of basic sill emplacement - Theron Mountains, Antarctica. *Petrol. Geosci.*, 15, 269-278.
- Jackson, C. A. L., N. Schofield & B. Golenkov (2013) Geometry and controls on the development of igneous sill-related forced folds: A 2-D seismic reflection case study from offshore southern Australia. *Geological Society of America Bulletin*, 125, 1874-1890.

- Japsen, P., P. F. Green, J. M. Bonow, T. F. D. Nielsen & J. A. Chalmers (2014) From volcanic plains to glaciated peaks: Burial, uplift and exhumation history of southern East Greenland after opening of the NE Atlantic. *Global and Planetary Change*, 116, 91-114.
- Johnson, A. M. & D. D. Pollard (1973) Mechanics of growth of some laccolithic intrusions in the Henry mountains, Utah, I: Field observations, Gilbert's model, physical properties and flow of the magma: Field observations, Gilbert's model, physical properties and flow of the magma. *Tectonophysics*, 18, 261-309.
- Kavanagh, J. L., T. Menand & K. A. Daniels (2013) Gelatine as a crustal analogue: Determining elastic properties for modelling magmatic intrusions. *Tectonophysics*, 582, 101-111.
- Larsen, H. C. & C. Marcussen (1992) Sill-intrusion, flood basalt emplacement and deep crustal structure of the Scoresby Sund region, East Greenland. *Geological Society, London, Special Publications*, 68, 365-386.
- Larsen, L., A. Pedersen, C. Tegner & R. Duncan (2014) Eocene to Miocene igneous activity in NE Greenland: northward younging of magmatism along the East Greenland margin. *Journal of the Geological Society*, 171, 539.
- Larsen, P. & H. Bengaard (1991) Devonian basin initiation in East Greenland - A result of sinistral wrench faulting and caledonian extensional collapse. *J. Geol. Soc.*, 148, 355-368.
- Leat, P. T. (2008) On the long-distance transport of Ferrar magmas. *Geological Society, London, Special Publications*, 302, 45-61.
- Lecomte, I. (2008) Resolution and illumination analyses in PSDM: A ray-based approach. *The Leading Edge*, 27, 650-663.
- Lecomte, I., H. Gjøystdal & Å. Drottning. 2003. Simulated Prestack Local Imaging: a robust and efficient interpretation tool to control illumination, resolution, and time-lapse properties of reservoirs. In *SEG Technical Program Expanded Abstracts 2003*, 1525-1528. Society of Exploration Geophysicists.
- Lecomte, I., P. L. Lavadera, I. Anell, S. J. Buckley, D. W. Schmid & M. Heeremans (2015) Ray-based seismic modeling of geologic models: Understanding and analyzing seismic images efficiently. *Interpretation*, 3, SAC71-SAC89.
- Lecomte, I., P. L. Lavadera, C. Botter, I. Anell, S. J. Buckley, C. H. Eide, A. Grippa, V. Mascolo & S. Kjoberg (2016) 2 (3) D convolution modelling of complex geological targets beyond-1D convolution. *First Break*, 34, 99-107.
- Magee, C., C. A. L. Jackson & N. Schofield (2013) The influence of normal fault geometry on igneous sill emplacement and morphology. *Geology*, 41, 407-410.
- Magee, C., C. L. Jackson & N. Schofield (2014) Diachronous sub-volcanic intrusion along deep-water margins: insights from the Irish Rockall Basin. *Basin Research*, 26, 85-105.
- Magee, C., S. Maharaj, T. Wrona, C. Jackson & C. Magee (2015) Controls on the expression of igneous intrusions in seismic reflection data. *Geosphere*, 11, 1024-1041.

- Magee, C., J. Muirhead, A. Karvelas, S. Holford, C. Jackson, I. Bastow, N. Schofield, C. Stevenson, C. McLean, W. McCarthy & C. Magee (2016) Lateral magma flow in mafic sill complexes. *Geosphere*, 12, 809-841.
- Mjelde, R., A. Breivik, T. Raum, E. Mittelstaedt, G. Ito & J. Faleide (2008) Magmatic and tectonic evolution of the North Atlantic. *Journal of the Geological Society*, 165, 31-42.
- Mjelde, R., T. Raum, P. Digranes, H. Shimamura, H. Shiobara & S. Kodaira (2003) Vp/Vs ratio along the Vøring Margin, NE Atlantic, derived from OBS data: implications on lithology and stress field. *Tectonophysics*, 369, 175-197.
- Mudge, M. R. (1968) Depth Control of Some Concordant Intrusions. *Geological Society of America Bulletin*, 79, 315-332.
- Muirhead, J. D., G. Airoidi, J. D. L. White & J. V. Rowland (2014) Cracking the lid: Sill-fed dikes are the likely feeders of flood basalt eruptions. *Earth and Planetary Science Letters*, 406, 187-197.
- Olesen, O., J. Ebbing, E. Lundin, E. Mauring, J. R. Skilbrei, T. H. Torsvik, E. K. Hansen, T. Henningsen, P. Midtbøe & M. Sand (2007) An improved tectonic model for the Eocene opening of the Norwegian–Greenland Sea: Use of modern magnetic data. *Marine and Petroleum Geology*, 24, 53-66.
- Parsons, A. J., A. G. Whitham, S. R. A. Kelly, B. P. H. Vautravers, T. J. S. Dalton, S. D. Andrews, C. S. Pickles, D. P. Strogen, W. Braham, D. W. Jolley & F. J. Gregory (2017) Structural evolution and basin architecture of the Traill Ø region, NE Greenland: A record of polyphase rifting of the East Greenland continental margin. *Geosphere*.
- Peron-Pinvidic, G., G. Manatschal & P. T. Osmundsen (2013) Structural comparison of archetypal Atlantic rifted margins: A review of observations and concepts. *Marine and Petroleum Geology*, 43, 21.
- Planke, S., T. Rasmussen, S. S. Rey & R. Myklebust. 2005. Seismic characteristics and distribution of volcanic intrusions and hydrothermal vent complexes in the Vøring and Møre basins. 833-844.
- Planke, S., H. Svensen, R. Myklebust, S. Bannister, B. Manton & L. Lorenz. 2014. Geophysics and Remote Sensing. In *Advances in Volcanology*, 1-16. Berlin, Heidelberg: Springer Berlin Heidelberg.
- Planke, S., P. A. Symonds, E. Alvestad & J. Skogseid (2000) Seismic volcanostratigraphy of large-volume basaltic extrusive complexes on rifted margins. *Journal of Geophysical Research: Solid Earth*, 105, 19335-19351.
- Pollard, D. D. (1973) Derivation and evaluation of a mechanical model for sheet intrusions. *Tectonophysics*, 19, 233-269.
- Pollard, D. D., O. H. Muller & D. R. Dockstader (1975) The Form and Growth of Fingered Sheet Intrusions. *Geological Society of America Bulletin*, 86, 351-363.
- Price, S., J. Brodie, A. Whitham & R. Kent (1997) Mid-tertiary rifting and magmatism in the Traill O region, East Greenland. *J. Geol. Soc.*, 154, 419-434.

- Rickwood, P. (1990) The anatomy of a dyke and the determination of propagation and magma flow directions. *Mafic dykes and emplacement mechanisms*. Balkema, Rotterdam, 81, 100.
- Rubin, A. M. (1993) Tensile fracture of rock at high confining pressure: implications for dike propagation. *Journal of Geophysical Research: Solid Earth*, 98, 15919-15935.
- Schlindwein, V. & W. Jokat (1999) Structure and evolution of the continental crust of northern east Greenland from integrated geophysical studies. *Journal of Geophysical Research: Solid Earth*, 104, 15227-15245.
- Schmiedel, T., S. Kjoberg, S. Planke, C. Magee, O. Galland, N. Schofield, C. A.-L. Jackson & D. A. Jerram (2017) Mechanisms of overburden deformation associated with the emplacement of the Tulipan sill, mid-Norwegian margin. *Interpretation*, 5, SK23-SK38.
- Schofield, N., I. Alsop, J. Warren, J. Underhill, R. Lehné, W. Beer & V. Lukas (2014) Mobilizing salt: Magma-salt interactions. *Geology*, 42, 599.
- Schofield, N., L. Heaton, S. Holford, S. Archer, C. Jackson & D. Jolley (2012a) Seismic imaging of 'broken bridges': linking seismic to outcrop-scale investigations of intrusive magma lobes. *Journal of the Geological Society*, 169, 421-426.
- Schofield, N., S. Holford, J. Millett, D. Brown, D. Jolley, S. Passey, D. Muirhead, C. Grove, C. Magee, J. Murray, M. Hole, C. Jackson & C. Stevenson (2015) Regional Magma Plumbing and emplacement mechanisms of the Faroe-Shetland Sill Complex: Implications for magma transport and petroleum systems within sedimentary basins. *Basin Research*.
- Schofield, N., D. A. Jerram, S. Holford, S. Archer, N. Mark, A. Hartley, J. Howell, D. Muirhead, P. Green, D. Hutton & C. Stevenson. 2016. Sills in Sedimentary Basins and Petroleum Systems. In *Advances in Volcanology*, 1-22. Berlin, Heidelberg: Springer Berlin Heidelberg.
- Schofield, N., C. Stevenson & T. Reston (2010) Magma fingers and host rock fluidization in the emplacement of sills. *Geology*, 38, 63.
- Schofield, N. J., D. J. Brown, C. Magee & C. T. Stevenson (2012b) Sill morphology and comparison of brittle and non-brittle emplacement mechanisms. *Journal of the Geological Society of London*, 169, 127-141.
- Senger, K., J. Millett, S. Planke, K. Ogata, C. H. Eide, M. Festøy, O. Galland & D. A. Jerram (in press) Effect of igneous intrusions on the petroleum system: a review. *First Break*, 35.
- Senger, K., S. Roy, A. Braathen, S. J. Buckley, K. Bælum, L. Gernigon, R. Mjelde, R. Noormets, K. Ogata, S. Olausen, S. Planke, B. O. Ruud & J. Tveranger (2013) Geometries of doleritic intrusions in central Spitsbergen, Svalbard: an integrated study of an onshore-offshore magmatic province with implications for CO₂ sequestration.
- Sheriff, R. E. & L. P. Geldart. 1995. *Exploration seismology*. Cambridge university press.
- Simm, R., M. Bacon & M. Bacon. 2014. *Seismic Amplitude: An interpreter's handbook*. Cambridge University Press.
- Skilling, I., J. White & J. McPhie (2002) Peperite: a review of magma-sediment mingling. *Journal of*

- Volcanology and Geothermal Research*, 114, 1-17.
- Skogseid, J. (2001) Volcanic margins: geodynamic and exploration aspects. *Marine and Petroleum Geology*, 18, 457-461.
- Skogseid, J., T. Pedersen, O. Eldholm & B. T. Larsen (1992) Tectonism and magmatism during NE Atlantic continental break-up: the Voring Margin. *Geological Society, London, Special Publications*, 68, 305-320.
- Skogseid, J., S. Planke, J. I. Faleide, T. Pedersen, O. Eldholm & F. Neverdal (2000) NE Atlantic continental rifting and volcanic margin formation. *Geological Society, London, Special Publications*, 167, 295-326.
- Smallwood, J. R., J. Maresh, D. W. Jolley & B. R. Bell (2002) The properties, morphology and distribution of igneous sills; modelling, borehole data and 3D seismic from the Faroe-Shetland area. *Geological Society Special Publications*, 197, 271-306.
- Spacapan, J. B., O. Galland, H. A. Leanza & S. Planke (2016) Igneous sill and finger emplacement mechanism in shale-dominated formations; a field study at Cuesta del Chihuido, Neuquen Basin, Argentina. *Journal of the Geological Society of London*, 174, 422-433.
- Stemmerik, L., F. Christiansen, S. Piasecki, B. Jordt, C. Marcussen & H. Nøhr-Hansen. 1993. Depositional history and petroleum geology of the Carboniferous to Cretaceous sediments in the northern part. In *Arctic Geology and Petroleum Potential: Proceedings of the Norwegian Petroleum Society Conference, 15-17 August 1990, Tromsø, Norway*, 66. Elsevier.
- Stemmerik, L., J. Vigran & S. Piasecki (1991) Dating of Late Paleozoic Rifting Events in the North Atlantic: New Biostratigraphic Data from the Uppermost Devonian and Carboniferous of East Greenland. *Geology*, 19, 218.
- Stoker, M. S., M. A. Stewart, P. M. Shannon, M. Bjerager, T. Nielsen, A. Blischke, B. O. Hjelstuen, C. Gaina, K. McDermott & J. Ólavsdóttir (2016) An overview of the Upper Palaeozoic–Mesozoic stratigraphy of the NE Atlantic region. *Geological Society, London, Special Publications*, SP447.2.
- Surlyk, F. (1990) Timing, style and sedimentary evolution of Late Palaeozoic-Mesozoic extensional basins of East Greenland. *Geological Society, London, Special Publications*, 55, 107-125.
- Surlyk, F. (2003) The Jurassic of Denmark and Greenland: The Jurassic of East Greenland: a sedimentary record of thermal subsidence, onset and culmination of rifting. *Geological Survey of Denmark and Greenland Bulletin*, 01, 657-722.
- Surlyk, F. & N. Noe-Nygaard (2001) Cretaceous faulting and associated coarse-grained marine gravity flow sedimentation, Traill Ø, East Greenland. *Norwegian Petroleum Society Special Publications*, 10, 293-319.
- Talwani, M. & O. Eldholm (1977) Evolution of the Norwegian-Greenland Sea. *Geological Society of America Bulletin*, 88, 969-7606-88-7-969-17460.
- Therkelsen, J. (2016) Diagenesis and reservoir properties of Middle Jurassic sandstones, Traill Ø, East Greenland: The influence of magmatism and faulting. *Marine and Petroleum Geology*, 78,

196-221.

- Therkelsen, J. & F. Surlyk (2004) The fluviatile Bristol Elv Formation, a new Middle Jurassic lithostratigraphic unit from Traill Ø, North-East Greenland. *The Jurassic of North-East Greenland. Geological Survey of Denmark and Greenland Bulletin*, 5, 19-29.
- Thomson, K. (2007) Determining magma flow in sills, dykes and laccoliths and their implications for sill emplacement mechanisms. *Official Journal of the International Association of Volcanology and Chemistry of the Earth's Interior (IAVCEI)*, 70, 183-201.
- Thomson, K., P. Green, A. Whitham, S. Price & J. Underhill (1999) New constraints on the thermal history of North-East Greenland from apatite fission-track analysis. *Geological Society of America Bulletin*, 111, 1054-1068.
- Thomson, K. & N. Schofield (2008) Lithological and structural controls on the emplacement and morphology of sills in sedimentary basins. *Geological Society, London, Special Publications*, 302, 31-44.
- Upton, B. G. J., C. H. Emeleus, D. C. Rex & M. F. Thirlwall (1995) Early Tertiary magmatism in NE Greenland. *Journal of the Geological Society*, 152, 959-964.
- Vigran, J. O., L. Stemmerik & S. Piasecki (1999) Stratigraphy and Depositional Evolution of the Uppermost Devonian-Carboniferous (Tournaisian-Westphalian) Non-Marine Deposits in North-East Greenland. *Palynology*, 23, 115-152.
- Vosgerau, H., P. Alsen, I. D. Carr, J. Therkelsen, L. Stemmerik & F. Surlyk (2004) The Jurassic of North-East Greenland: Jurassic syn-rift sedimentation on a seawards-tilted fault block, Traill Ø, North-East Greenland. *Geological Survey of Denmark and Greenland Bulletin*, 05, 09-18.
- Walker, R., D. Healy, T. Kawanzaruwa, K. Wright, R. England, K. McCaffrey, A. Bubeck, T. Stephens, N. Farrell & T. Blenkinsop (2017) Igneous sills as a record of horizontal shortening: The San Rafael subvolcanic field, Utah. *Geological Society of America Bulletin*, B31671. 1.
- Whitham, A. G. & S. P. Price (1997) Exhumed hydrocarbon traps in East Greenland: Analogs for the Lower-Middle Jurassic play of Northwest Europe. *AAPG Bulletin*, 81, 196-221.
- Whitham, A. G., S. P. Price, A. M. Koraini & S. R. A. Kelly (1999) Cretaceous (post-Valanginian) sedimentation and rift events in NE Greenland (71-77N). *Petroleum Geology of Northwest Europe: Proceedings of the 5 th Conf*, 325-336.
- Ziegler, P. A. (1992) North Sea rift system. *Tectonophysics*, 208, 55-75.

<http://factpages.npd.no/factpages/> (Accessed 20.02.2017)